`

INVESTIGATION OF THERMOPHYSICAL PROPERTIES OF NANOFLUIDS WITH CRYOGENS AS BASE FLUID TO BE USED IN FUTURISTIC HTS CABLES

Dissertaion-2

Submitted in partial fulfillment of the requirement for the award of degree

of

MASTER OF TECHNOLOGY

in

MECHANICAL ENGINEERING

by

Priyanka Anand

(11507993)

Under the guidance of

Gaurav Vyas

(17703)

DEPARTMENT OF MECHANICAL ENGINEERING
LOVELY PROFESSIONAL UNIVERSITY
PUNJAB
2016-2017

`

CERTIFICATE

I, hereby certify that the work being presented in the dissertation entitled "**Investigation of Thermophysical Properties of Nanofluids with Cryogens as base fluid to be used in futuristic HTS cables**" in partial fulfillment of the requirement of the award of the degree of Master of Technology and submitted to the Department of Mechanical Engineering of Lovely Professional University, Phagwara, is an authentic record of my own work carried out under the supervision of (Gaurav Vyas, Assistant Professor) Department of Mechanical Engineering, Lovely Professional University. The matter embodied in this dissertation has not been submitted in part or full to any other University or Institute for the award of any degree.

(Date) Priyanka Anand

11507993

This is to certify that the above statement made by the candidate is correct to the best of my knowledge.

(Date) Mr. Gaurav Vyas

(17703)

COD (ME)

The external viva-voce examination of the student was held on successfully _____

Signature of Examiner

`

ACKNOWLEDGEMENT

In completion of this research work, many individual have supported and I am very grateful that they give their precious time and support. So, I would like to extend my sincere gratitude to all of them.

I am deeply obliged to my dissertation supervisor, Assistant Prof. **Gaurav Vyas,** co-guide **Dr. Raja Sekhar Dondapati** for their respectable guidance, support, encouragement and constant supervision as well as for providing necessary information regarding my thesis. This dissertation would not have been accomplished without their valuable advice and support.

I am also thankful to **Mr. Gurpreet Singh Phull**, (HOS) and **Mr. Sudhanshu Dogra** (HOD) School of Mechanical Engineering, Lovely Professional University, Punjab

I would like to thank all the staff members of School of Mechanical engineering who have been very patient and co-operative with us.

I would also like to extend my gratitude to my seniors Mr. Mohit Kalisa, Mr. Abhinav Kumar, Mr. Venkata Ramana Uppada, Mr. Rajesh Gadekula and Ms. Neelam Verma who always encouraged and supported me in this thesis work.

I would like to thank **Lovely Professional University** for giving me opportunity to use their resource and work in such a challenging environment. I am grateful to the individuals whom contributed their valuable time towards my thesis.

Nonetheless, I am very thankful to my family, friends and classmates for their endless support, love and encouragement. Acknowledging the parents support is foremost in achieving what I am now.

Priyanka Anand

(11507993)

`

NOMENCLATURE

T_C	Critical Temperature
ρ	Density of fluid (kg/m^3)
m	Mass (kg)
V	Volume (m^3)
Q	Heat transfer (W)
C_p	Specific Heat (kJ/kgK)
ΔT	Change in temperature (K)
τ_{wall}	Shear stress at wall
μ	Viscosity of fluid (Pa-s)
k	Thermal Conductivity (W/mK)
v_{avg}	Average velocity of fluid (m/s)
D	Diameter of piper (m)
A	Area of pipe (m^2)
Ø	Volume concentration
HTS	High Temperature Superconductors
BF	Base fluid
NP	Nanoparticle
NF	Nanofluid
k_{eff}	Effective thermal conductivity
μ_{eff}	Effective viscosity

`

TABLE OF CONTENTS

`

`

`

List of Figures

`

`

`

`

ABSTRACT

The concept of Nano fluids is the recent advancement in the field of nanotechnology which provides vast scope for research. Nano fluid is a fluid which provides better heat transfer effect and thermophysical properties. Due to its better heat transfer characteristics and enhanced thermophysical properties, Nano fluids are used in various fields. They are used for engine cooling in automobile sector, transformer and generator cooling, also used as coolant in machining and welding. Moreover, they are used in double pipe heat exchangers, solar heating for power generation and in refrigeration. Nano fluids are mixed with base fluid for the evaluation of thermophysical properties. Base fluid can be water, oil, any refrigerant or cryogens. Cryogens are the gases in the liquid form stored under extremely low temperature. Commonly used cryofluids or cryogens are liquid helium, liquid nitrogen and liquid oxygen.

In the proposed research work, two different cryogens namely liquid nitrogen and liquid oxygen having boiling point 77.35K and 90.19K respectively are considered and mixed. The mixing is done at various composition and the thermophysical properties such as density, viscosity, specific heat and thermal conductivity are evaluated. For this evaluation the standard database- NIST SUPERTRAPP is used. The temperature and pressure range of 70-100K and 0.9-1.3MPa is taken into consideration. After this, the Nano fluid is added with the mixed cryogen and again the thermophysical properties are calculated. The obtained result is then used for computational analysis in the software called as Ansys (Fluent). In Ansys (Fluent), geometry of corrugated pipe with dimensions of 1m length and 5mm diameter is designed and meshed. The mixed cryogen with Nano fluid is allowed to flow through the pipe. Then the appropriate boundary conditions are implemented. The properties obtained from NIST SUPERTRAPP are applied under given temperature range. Thus, the expected outcomes and results give the pressure drop in the pipe. From the obtained results, it can be also concluded that how effective is the heat transfer in the cryogen mixed with Nano fluid.

Keywords: Cryogens, Nanoparticles, Thermophysical properties and HTS cables.

`

CHAPTER-I

1 INTRODUCTION

Electricity, nowadays, is the most important source of energy. It is the basis of all day-to-day work. From the starting of an ordinary fan to the functioning of large industries, electricity is needed everywhere. The required electricity is provided by power plants with the help of high extension wires. However, these wires do not transfer the total amount of electricity and exhibits power losses. More than 30% of power loss occurs in the form of heat loss ($Q = i^2Rt$). So, to overcome this challenge, the new technology of HTS cables is developed which provides the minimum heat loss.

HTS cables, being application of superconductivity requires cryogenic temperature for functioning. For incorporation of superconductivity efficient coolants are required. And for effective power transmission dispersion of nanoparticles can be done in coolants. Various metallic and metal oxides nanoparticles are available with various characteristics. These nanoparticles enhance the thermophysical properties of Nanofluids.

`

CHAPTER-II

2 TERMINOLOGY

2.1 Superconductivity

A Dutch Physicist, in 1911, Professor H Kammerlingh Onnes conducted experiment. While researching for the properties of mercury, he decreases the temperature up to certain limits which shows the changes in properties of mercury. On further decreasing temperature at 4.2K superconductivity is attained for pure mercury.

Superconductivity is defined as “during the flow of current in the conductor, resistance is zero at the absolute zero temperature”. It means at critical temperature (T_c), resistance becomes zero.

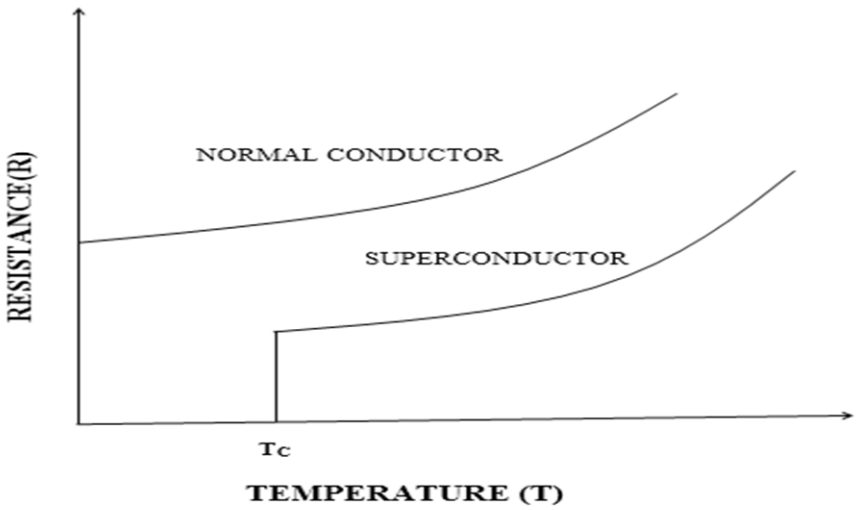

Figure 1 Resistance vs Temperature for normal conductor and superconductor

Initially the power transmission and distributions is done with conventional cables like copper and aluminum. The power produced is not used fully due to losses occur in the form of heat through these conventional cables. The power loss in the form of heat dissipation is also increasing the atmosphere’s temperature. So, to overcome this challenge a technology is developed which is loss free and eco-friendly.

2.2 High Temperature Superconductor (HTS)

High Temperature Superconductors is a wire device used to transmit large electric current. These transmission cables can transmit 5 to 10 times more power than traditional copper or aluminum wires/cables. These cables consist of corrugated steel pipe which carries coolant. The HTS tapes carries current and insulated by thermal insulation wire. Also, these HTS cables are coated with dielectric and cable shield.

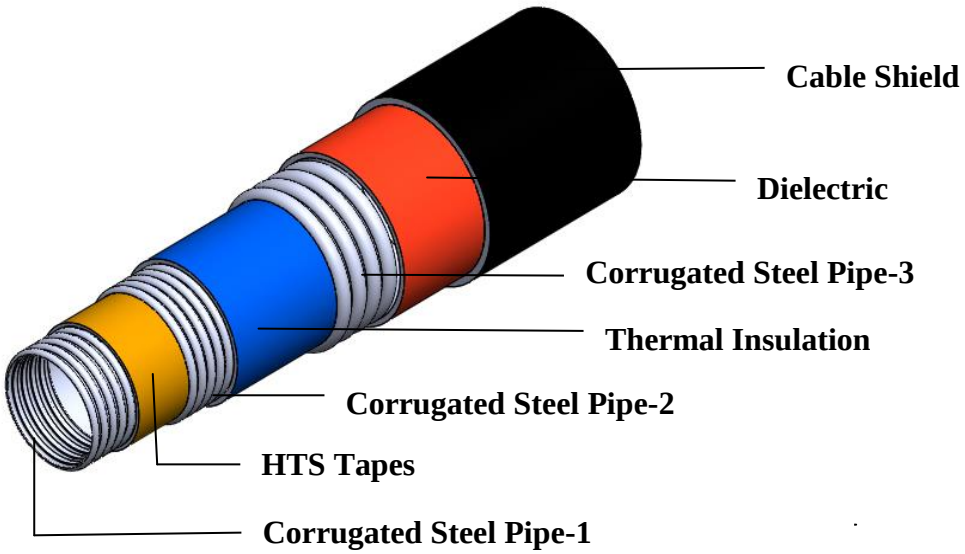

Figure 2 HTS cables.

2.3 Nano-Fluids

A Nano fluid is the combination of base fluid and Nano particles. When an appropriate proportion of Nano particles are suspended into base fluid, Nano fluid is formed. The Nano fluids contain very small sized (Nano-sized) particles called as Nano particles. These nanoparticles are available in the form of metals, carbides and oxides. Commonly used base fluids are water, oil, ethylene glycol. The suspended Nano particles in the base fluids enhance thermophysical properties convective heat transfer coefficient and thermal conductivity of the fluid. Nano-fluids, basically, have two phase i.e. solid nanoparticles and liquid base fluids.

`

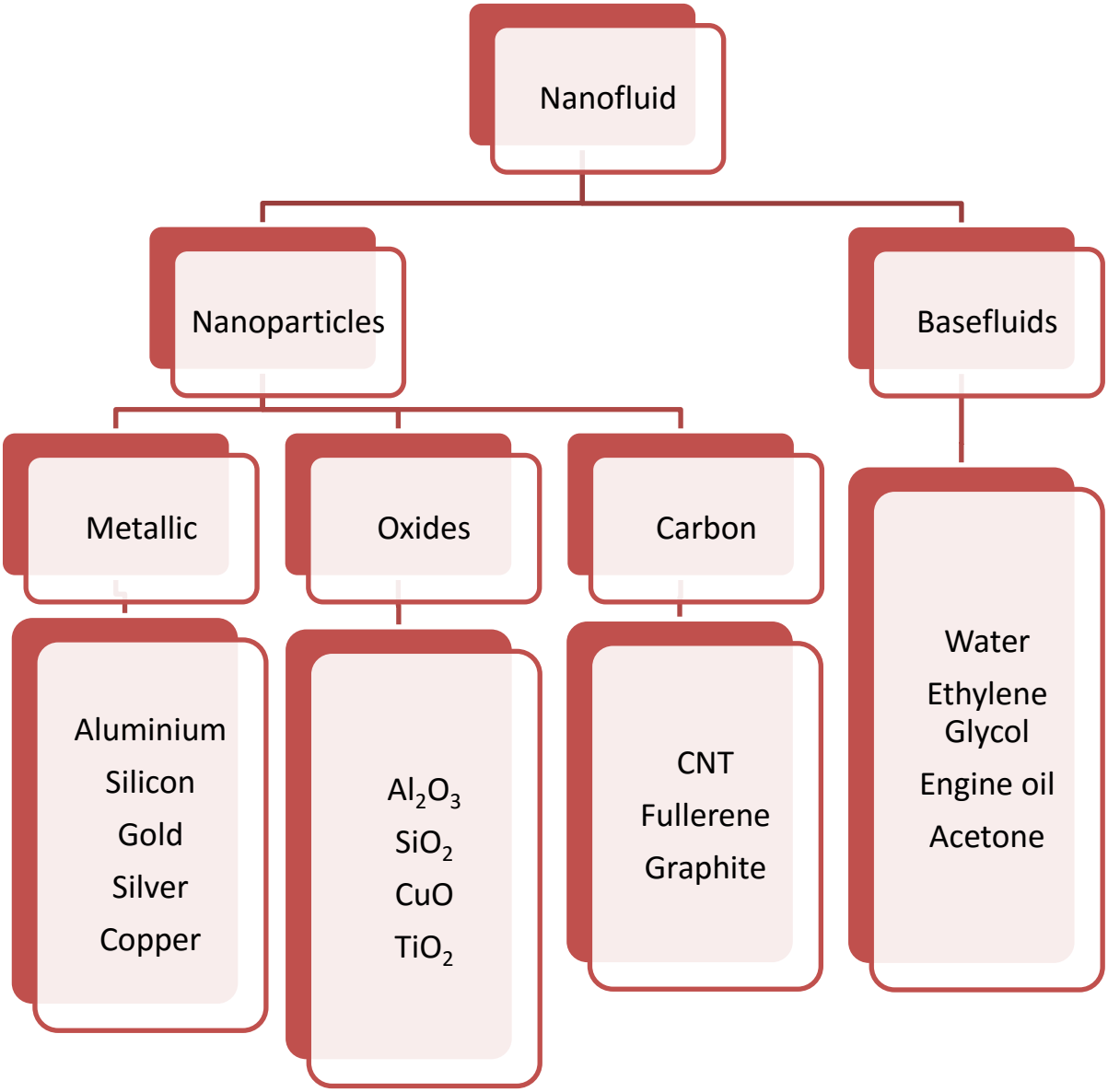

Figure 3Classifications of Nano fluids

2.3.1 Advantages of Nano fluids

Before use of Nano fluids, the conventional method of cooling used was dispersing of water. However, Nano fluids proved to be more effective over conventional techniques. Following are the advantages of Nano fluids over conventional cooling techniques:

- ❖ Nanoparticles have high surface areas more heat transfer surface is possible between particles and base fluids.

`

- ❖ Stability of dispersed nanoparticles in basefluid is high with the predominant Brownian motion in particles.
- ❖ Clogging of particles is reduced, hence provides miniature system set-up.
- ❖ Properties like thermal conductivity, surface wettability are easily adjustable, by varying concentration of particles for different applications.

2.4 Preparation Method of Nano fluids

2.4.1 Two Step Preparation Method

This is a two-step method; in the first step nanoparticles used are produced in dry powder form by physical, mechanical or chemical method such as milling, grinding, sol-gel and vapor phase method. Then, in the second step, these Nano sized dry powders are dispersed in the base fluid with the help of intensive magnetic force agitation, ultrasonic agitation, homogenization and ball milling. Surfactants are used in Nano fluids to enhance the stability.

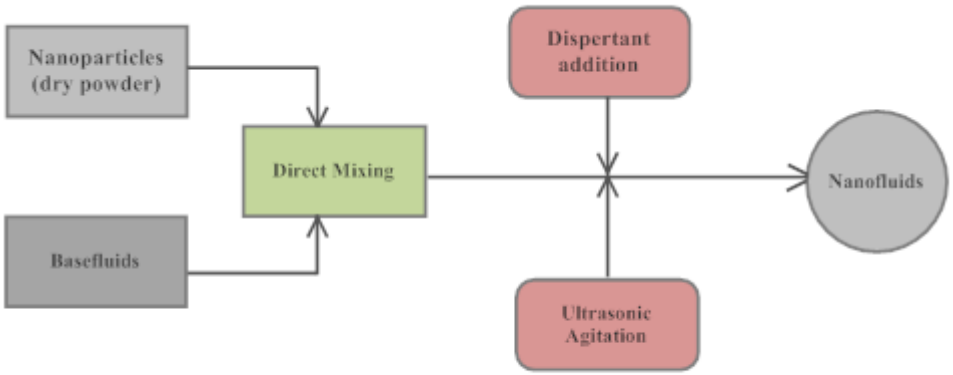

Figure 4 Two Step Method for preparation of Nano fluid

2.4.2 One Step Preparation Method

One step preparation method came into existence due to difficulty in preparing stable Nano fluids by two step preparation method. In this method, simultaneous making and

`

dispersing of particles is done in the fluid which reduces the agglomeration of particles. Also the process of drying, storage, transportation is avoided to minimize the agglomeration. However, the major disadvantage of one step method is that the reactants residuals are left in the Nano fluids due to incomplete reaction.

Another method for preparing the nanoparticles is vacuum submerged arc nanoparticles synthesis system (vacuum-SANSS) by using different dielectrics. The nanoparticles formed are in polygon, square and circular shapes. Mineral oil-silver Nano fluids, Copper Nano fluids and Ethylene-silver Nano fluids are prepared by using this method.

2.4.3 Other Novel Method

Preparation of Nano fluids depends on the structure and shape of nanoparticles. This method provides the better solubility and controllability of nanoparticles in the base fluids. During the chemical reaction, continuous synthesis of nanoparticles is done by varying the temperature, ultrasonic irradiation, concentration of reactants and additives, acidity. Thus enhancement in the thermal conductivity is achieved by this chemical reaction. Gold, silver, copper, platinum based water and kerosene Nano fluids are prepared by this method.

2.5 Nanoparticle and its classifications

The size of nanoparticle ranges from 1 to 100 nanometers. Based on the diameter, nanoparticles are categorized as ultrafine, fine and coarse. Ultrafine has the size from 1 to 100nm, fine has 100 to 2500nm and coarse has size from 2500 to 10000nm. The synthesis of nanoparticles can be done in three phase, that is liquid phase, vapor phase and gas phase.

2.5.1 Metallic Nanoparticle

Nano sized metals having certain dimension within range of 1 to 100nm is called as metallic nanoparticle. They are categorized as metallic nanoparticle (zero dimension), metallic nanowires and rods (one dimensional), metallic Nano sheets and platelets (two dimensional) and metallic nanostructures (three dimensional). List of metallic nanoparticles are gold (Au), silver (Ag), Aluminum (Al), Copper (Cu) and Silicon (Si). However, commonly used metallic nanoparticles are gold (Au) and silver (Ag).

`

2.5.2 Carbon Nanoparticle

Carbon is a non-metal abundantly available in the universe. It is placed in block P, period 2 in the periodic table. Carbon nanoparticles are spherical in shape and appear as black powder. Fullerene and graphite are used as carbon nanoparticles. Graphite is the most stable carbon under standard conditions.

2.5.3 Oxide Nanoparticle

Metallic nanoparticles in its oxide form are oxide nanoparticles. Aluminum oxide (Al_2O_3) nanoparticle is highly flammable and is available in the powder form. Also, it increases strength, thermal conductivity. Copper oxide (CuO) is available in the form brownish-black powder. When it comes in contact with hydrogen or carbon mono oxide under high temperature, metallic copper is formed. It affects human and aquatic life. Zinc oxides antibacterial, antifungal and anti-corrosive and helps in UV filtering.

2.6 Cryogenics and Applications

Cryogenics, in physics, is the study of material's behavior and its production at very low temperature. The word cryogenics has its etymology from Greek words 'cryos' meaning 'cool' and 'genic' meaning "produce". To be specific, a low temperature environment is known as the cryogenic environment. So a cryogenic environment has the temperature range below the point at which the gases start to liquefy that is below -150^0C or 123K.

2.6.1 Space

The space science deals with the use of cryogenics broadly in two fields. First the space science mission and second the space transportation infrastructure or propulsion of rockets.

- The cryogenic engines in space vehicle are mechanized by cryogenic propellants.
- Liquid Hydrogen as a fuel and Liquid Oxygen as an oxidizer is used to propel the rocket.
- In cooling of Infra-Red detectors, cold probes, telescopes also the cryogenic fluids are used.

`

2.6.2 Mechanical Field

Cryogenics, in the field of Mechanical Engineering has endless applications. Starting from the magnetic separation to heat treatment and recycling of materials all can be done by cryogenics.

- Superconducting Magnets are used for the separation of materials. This technique is implemented in enhancing the brightness of kaolin and the quality of quartz.
- Cryogenics heat treatment enhances the lives of tools, die castings and their dies, jigs and fixtures etc.
- Mostly Poly Vinyl Chloride (PVC) and rubbers are subjected to cryogenics recycling which turns the scrap into raw materials by supervising these scraps to cryogenics temperatures.

2.6.3 Medical Field

With the advancement and research in field of cryogenics, its application can also be seen in the field of medicine and surgery. The cryosurgery, cell and blood preservation and also food storage is made only possible with the help of cryogenics engineering.

- Cryosurgery is a unique approach in which the harmful tissues are destroyed by freezing them to cryogenic temperature.
- It is generally applied to patient with skin disorder, retinal problems or kidney cancer.
- The preservation of blood cells, plasma cells, human and animal organs can also be done by maintaining cryogenic temperature.
- Liquid nitrogen is used for long time preservation of sea food, milk, meat at cryogenic temperature.

2.6.4 Gas Industry

The gas industries use cryogenic fluids to modify the physical properties or to maintain the temperature during working process. Also cryogenics helps in liquefaction, separation and storage of gases.

- The gases are transported in liquid state which can only be achieved by cryogenics.

`

- Steel industry uses oxygen for the production of steel. Basic oxygen furnace uses oxygen rather than air.
- In chemical, metallurgical and welding industries, nitrogen and argon are used to contribute the inert environment.

2.6.5 Superconductivity

Superconductivity is the ability of materials to conduct electricity or electric current at practically zero resistance. This superconductivity is applied in real life science like in NMR, MRI, maglev trains, transformers and generators, HTS Cables

- The Nuclear Magnetic Resonance (NMR) is used in pharmaceutical industry for the study of molecular structure in which a superconducting magnet of 10T~25T is imposed.
- The Magnetic Resonance Imaging (MRI) is used for body scanning. The superconducting magnets in this are cooled by liquid helium.
- Maglev Trains works on the principle of electromagnetic forces between the superconducting magnets on the vehicle and coils on the ground. This results in no friction.

Superconducting generators and transformers are maintained at low temperature through cryogenics.

2.7 Cryogens

Cryogens are liquefied gases stored under very low temperature. The low temperature liquefies the atmospheric gases like nitrogen, oxygen, helium, hydrogen, argon, methane and neon. These gases are condensed, collected, distilled and then separated. After all the processes these liquefied gases can be used as a cryogen. Every cryogen has its unique characteristics and usage. Commonly used cryogens are liquid nitrogen (LN2), liquid oxygen (LO2), liquid hydrogen (LH2), liquid helium (LHe).

2.7.1 Liquid Nitrogen

- It has two isotopes: N14 and N15.
- It is used to provide inert atmosphere in chemical and metallurgical industries.
- Also used in preservation of blood, food.

`

2.7.2 Liquid Oxygen

- It is slightly magnetic in nature and exits in three isotopes: O16, O17 and O18.
- It is broadly used in steel and iron manufacturing industries.
- Oxidizer propellants are used for spacecraft rocket application.

2.7.3 Liquid Hydrogen

- It has three isotopes namely hydrogen, deuterium, tritium.
- It is used as propellant in cryogenics engine.
- Some automobiles use liquid hydrogen as fuel.
- Closed cycle working cryocooler uses liquid hydrogen as fuel.

2.7.4 Liquid Helium

- It is an inert gas and exists in monatomic state.
- Liquid helium was analyzed by Kammerlingh Onnes for superconductivity

2.7.5 Liquid Methane

- It can be used as a rocket fuel.
- Also in the form of Compressed Natural Gas (CNG).

2.7.6 Liquid Argon

- It is inert, non-toxic gas and has three isotopes: Ar35, Ar38 and Ar40.
- It is used to suppress molds in casting industry.
- It provides inert atmosphere for welding stainless steel, aluminum, titanium.

2.7.7 Liquid Neon

- It is commercially used as refrigerant.
- It is compact, inert and less expensive.

2.7.8 Liquid Air

- It is considered as mixture of 78% nitrogen, 21% oxygen, 1% argon and other gases.
- It was earlier used as precoolant for low temperature application.

`

- It is mainly used in production of pure nitrogen, oxygen and rare gases.

2.8 Thermophysical Properties

Material properties that vary with temperature without altering the materials chemical properties are called as thermophysical properties. These properties can be classified as below:

2.8.1 Density

Density is the property of material which tells how much space the mass occupies. The mass per unit volume is termed as density. It is denoted by 'ρ'. Mathematically, it is expressed as

$$\rho = \frac{m}{V}$$

Where ρ is density, m is mass and V is volume. Unit of density is kg/m^3.

2.8.2 Specific Heat

Specific Heat is another type of physical property. The amount of heat required to raise the temperature of unit mass by one degree Celsius is specific heat. It is denoted by 'c'. Mathematically, it is expressed as

$$Q = mc\Delta T$$

Where Q is heat, m is mass, c_p is specific heat and ΔT is temperature difference. Unit of specific heat is kJ/kgK.

2.8.3 Viscosity

Viscosity is the measure of fluid's resistance to gradual deformation. It is the property arises due to collision of two neighboring fluid particles that are moving with two different velocities. It is denoted by 'μ'. Mathematically, can be expressed as

$$\tau = \mu \frac{du}{dy}$$

Where, τ is shear stress which is force per unit area, μ is viscosity and $\frac{du}{dy}$ is velocity gradient. Unit of viscosity is Pa-s.

`

2.8.4 Thermal Conductivity

The property of material to conduct heat per unit area and per unit time is thermal conductivity. Materials with low thermal conductivity have lesser heat transfer whereas the materials with high thermal conductivity transfer more heat comparatively. Thermal conductivity follows the Fourier law of heat conduction. It is denoted by 'k'. Mathematically expressed as

$$q = -k\frac{dT}{dx}$$

Where q is heat conduction, k is thermal conductivity and $\frac{dT}{dx}$ is temperature gradient. Unit of thermal conductivity is W/mK.

2.9 Thermohydraulic Properties

The properties which can be seen due to the flow of fluid are the thermohydraulic properties. All these properties can only be measured only when flow happens.

2.9.1 Pressure Drop

The change or difference in pressure between two locations during the fluid flow is pressure drop. The pressure drop occurs due to friction, vertical elevation in pipes and change in kinetic energy.

$$\Delta p = \frac{fLv_{avg}^2}{2\rho D}$$

Where, Δp is pressure drop (Pa), f is friction factor, v_{avg} is average velocity (m/s).

2.9.2 Frictional Loss

The effect of viscosity of fluid near the surface of pipe results in loss of pressure is frictional loss. This is given by equation

$$f = \frac{8\tau_{wall}}{\rho v_{avg}^2}$$

Where f is friction factor, τ_{wall} is shear stress at wall.

`

2.9.3 Heat Transfer

When two bodies are at different temperature heat flows from high temperature to low temperature. This is called heat transfer. Conduction, convection and radiation are three modes of heat transfer.

For convection heat transfer is given as

$$q = hA\Delta T$$

Where, h is heat transfer coefficient.

2.10 Dimensionless Numbers

2.10.1 Reynolds's Number

The ratio of the inertia force and the viscous force of the fluid is Reynolds's Number. It is denoted by R_e. Mathematically expressed as

$$R_e = \frac{\rho VD}{\mu}$$

Where ρ is density of fluid, V is velocity of Fluid, μ is viscosity of fluid and D is diameter of pipe.

2.10.2 Prandtl Number

The ratio of momentum diffusivity and thermal diffusivity is termed as Prandtl Number. It is denoted by 'Pr'. Mathematically expressed as

$$\Pr = \frac{\mu C_p}{k}$$

Where μ is dynamic viscosity, C_p is specific heat and k is thermal conductivity.

2.10.3 Nusselt Number

The ratio of convective heat transfer to conductive heat transfer is termed as Nusselt Number. It is denoted by 'Nu'. Mathematically expressed as

$$Nu = \frac{hL}{k}$$

`

Where h is convective heat transfer, L is characteristic length and k is thermal conductivity.

Relationship between Reynold's Number, Prandtl Number and Nusselt Number

$$Nu = C\,\mathrm{Re}^{m}\,\mathrm{Pr}^{n}$$

C, m and n are constants.

`

CHAPTER-III

3 SCOPE OF STUDY

Now-a-days electrical energy is important need of every individual. From ceiling fan to mobile phones everything runs on electricity. For the transmission of these electricity power transmission devices such as aluminum wires, power girds are required. However conventional power transmitting device exhibits higher losses, hence high temperature superconducting (HTS) cables proved to be more efficient power transmitting device. These HTS cables, works on the principle of superconductivity. The superconductivity is the resistance offered by conductor when the flow of current is zero at absolute zero temperature. Superconducting motors, generators, SMES devices, maglev trains are the various applications of superconductivity. As superconductivity works on very low temperature, hence the need of cryogenics fluid arises. Cryogenic fluids or cryogens are used as coolants. Liquid nitrogen, liquid oxygen, liquid helium, liquid hydrogen is few commonly used cryogens. Cryogenics is used in space industry for rocket propulsion, space simulation and also for magnetic separation and heat treatment in mechanical field. Cryogenics is applied cryosurgery, cell preservation, food preservation and in gas industry for liquefaction, separation and storage. The thermophysical properties such as density, viscosity, thermal conductivity and specific heat are considered which helps in evaluating pressure drop and heat transfer coefficient.

Nanoparticles are nanometer sized particles which enhances the thermophysical properties of base fluids. Base fluids are fluids in which nanoparticles are mixed. Water, ethylene glycol, refrigerants and cryogens are few base fluids in which aluminum oxide; zinc oxide, silicon dioxide and titanium oxide nanoparticles can be added. Since nanoparticles enhances the thermophysical properties, so it can be used in the field of engine cooling, heating and cooling of buildings, cooling of welding and electronics, refrigeration, defense and biomedical.

`

CHAPTER-IV

4 OBJECTIVE OF THE STUDY

In the present research work, thermophysical properties such as density, viscosity, thermal conductivity and specific heat of mixed cryogen i.e. liquid nitrogen and liquid oxygen are evaluated. The operating pressure and temperature range are considered to be 0.9-1.3MPa and 70-100K.These thermophysical properties are investigated for futuristic HTS cables. Mixed cryogen is used as coolant in these HTS cables.

Further the nanoparticles like Al_2O_3 and CuO are suspended in base fluid (mixed cryogens) at operating pressure and temperature of 0.9MPa and 70-100K. The volume concentration nanoparticles are taken to be from 1% to 5%. Further, again the thermophysical properties such as effective thermal conductivity, effective viscosity, effective specific heat and effective density are evaluated using theoretical or experimental correlation for Nanofluids (base fluid+ nanoparticles).

Moreover, Computational Fluid Dynamics (CFD) analysis using ANSYS® (FLUENT) is done for investigating the thermohydraulic performance of the Nanofluid. Pressure drop, heat transfer and Nusselt number at varying mass flow rate of 20g/s to 60g/s are calculated at operating pressure of 0.9MPa and 70K. Geometry of corrugated steel pipe is considered and relevant boundary conditions are given for obtaining the appropriate results.

`

CHAPTER-V

5 REVIEW OF LITERATURE

Baojie Wei et al. [1] investigated on Diathermic oil has high boiling point, low vapor pressure and low pour point, so it was widely used as heat carrier in heat transfer systems. It has been reported that increasing, thermal conductivity of SiC/TiO2 nanofluids is higher than SiC or TiO2 nanofluids and maximum of thermal conductivity enhancement was obtained.

Su Sik et al. [2] introduced modeling and simulation of HTS cables which were inadequate for high frequency analysis. This paper also concluded the effects of cable-to-connector in order to minimize error between simulated and measured data under ambient and superconductive conditions. Furthermore, based on the proposed modeling and simulation technique, S-parameters of long-distance HTS cables can be exactly derived in vast range of frequency.

Gabriela Huminic, Angel Huminic [3] researched heat transfer and fluid flow characteristics in curved tube using conventional fluids and Nanofluids as working fluids. The curved tubes was divided into three group helically coiled tubes spirally coiled tubes and other curved tubes according to the configurations of the tube curvature.

Raja Sekhar Dondapati et al. [4] proposed the research where HTS cables were to be cooled below the critical temperature of superconductors used in making cable which will regain its superconductivity. Supercritical Nitrogen (SCN) was used as feasible coolant to achieve the required cooling. It was concluded that temperature dependent analytical functions were developed for thermophysical properties of SCN. Also it is useful in predicting thermohydraulic performance (pressure drop, pumping power and cooling capacity). The results were compared with liquid nitrogen (LN2) and found that circulating pumping power required to pump SCN was significantly smaller than that to pump LN2.

Yi Liu et al. [5] developed a boiling model by Computational Fluid Dynamics (CFD) code to calculate the source term of a cryogenic liquid spill. The model includes the effect of the changing ground temperature on the vaporization rate of the cryogenic liquid. Also, the

`

model includes the effect of the changing ground temperature on thevaporization rate of cryogenic liquid. Eventually, model development was still necessary to improve the prediction of the nucleate boiling regime.

Gaurav Vyas, Raja Sekhar Dondapati [6] investigated High Temperature Superconducting (HTS) cable used for efficient power transmission. Additionally, AC losses in HTS cable due to self-field with various parameters were calculated and validated. It was concluded the major AC losses arise due to self-field in the HTS cable and losses can be obtained by approximated Norris equation. Also two different superconducting cables- one with BSCCO and other with YBCO tapes were examined for the analysis.

Myung Chang et al. [7] designed and tested for superconducting magnets cooled at 20–30 K by a cryocooler. Metallic parts were fabricated for thermal connection between cold head and six magnet bobbins in hexagonal array and assembled with bolt joints. The result showed that all six bobbins were uniformly cooled down to 13 K under no load and maintained at20–30 K under additional thermal load of 26–60 W.

Meibo Xing et al. [8] investigated thermophysical properties of water-based single-walled carbon nanotubes Nanofluids (SWCNTs-Nanofluids) experimentally. The effect of mass concentration varying from 0.1 to 1% weight on thermal conductivity, viscosity and density of Nanofluids were investigated at the temperatures range of 10-60°C. It was found that thermophysical properties such as thermal conductivity increase whereas the viscosity and density decreases with increase in the temperature.

Sadanori Iwai et al. [9] introduced the cryogen-free 25 T superconducting magnet using a ReBCO insert coil that generates 11.5 T in 14 T background field of outer low-temperature superconducting (LTS) coils. The conclusion drawn was two GM cryocoolers cool a circulating helium gas through heat exchangers and gas is transported over a long distance to cold stage located on ReBCO insert coil, in order to protect cryocoolers from the leakage field of high magnetic fields.

Raja Sekhar Dondapati, V.V Rao [10] examined liquid nitrogen (LN2) is used for effective power transmission in the high temperature superconducting (HTS) cables which were internally cooled. The HTS cable at operating temperature receives heat flux from different sources such as the leads and AC losses through superconductor and the heat-in-leak insulation. Conclusions obtained were that pressure drop and heat transfer analyses

were carried out for different flow rates of LN2 to obtain friction factor, pumping power and heat transfer rate. This analysis was useful in characterizing operating flow regime and safe operating temperature range in HTS cables.

Madhusree Kole, T.K. Dey [11] proposed the stable and well dispersed Cu-gear oil Nanofluids having Cu nanoparticles of volume concentration between 0.11 to 2% and were prepared with oleic acid surfactant. It was observed that the formation of interfacial layer at the nanoparticles liquid boundary and ballistic transport of phonons across the percolating aggregates were believed to be responsible for observed thermal conductivity enhancement. Additionally, thermal conductivity enhancement of 24% was observed with 2% volume of Cu nanoparticle loading at room temperature is obtained.

F.S.Javadi et al. [12] improved heat exchanger's performance by increasing overall heat transfer and minimizing pressure drop. Nanoparticles such as SiO2, TiO2 and Al2O3 were applied in a plate heat exchanger and the effects on thermophysical properties and heat transfer characteristics were compared with the base fluid. The highest overall heat transfer coefficient was achieved by Al2O3 Nanofluid, which is 308.69 W/m2.Kin 0.2% nanoparticle concentrations as result.

Jung-Bin Song, Haigun Lee [13] introduced a cooling system employing solid cryogen (SC) such as solid nitrogen (SN2) for high-temperature superconducting (HTS) applications. Also, thermal contact between SC and HTS was degraded by repeated over current runs resulting in ‘thermal dry-out’. Novel cryogens with small amounts of liquid cryogen had been used to overcome the problem. Cryogens such as solid–liquid nitrogen, solid argon–liquid nitrogen, and solid nitrogen–liquid neon were used.

R. Saidur, KY Leong [14] introduced the various applications of nanofluids in research field. Recent researches indicated that substitution of conventional coolants by nanofluids appears advantageous. Specific application of nanofluids in engine cooling, solar water heating, cooling of electronics, cooling transformer oil, improving diesel generator efficiency. It had been found that nanofluids have higher and strongly temperature-dependent thermal conductivity at very low particle concentration.

Yongliang Li et al. [15] used cryogen as an energy carrier with the focus on thermodynamic aspects and cryogenic energy extraction. It was shown that cryogens have higher energy density than other commonly used thermal energy storage media. And,

`

concluded that if there was only ambient and/or low grade heat source, a combination of direct expansion and Rankine cycle was more attractive due to its low power consumption in the compression process.

Higashikaw et al. [16] investigated cooling performance of a hybrid refrigerant of solid nitrogen. This paper discusses the phase state as well as the quantity of neon required for such improvement. Nitrogen gas was introduced into a sample chamber through a mass flow controller and then was liquefied. From these results it was concluded that introducing neon can be liquefied and it was the best way to make the most of the potential of hybrid refrigerant.

Yujin Hwang et al. [17] proposed the homogenous mixing of nanoparticles and physical treatment techniques based on two-step method including stirrer, ultrasonic disruptor, ultrasonic bath and high-pressure homogenizer was systematically tested. Results obtained were long-term stable silicon oil-based fluid and average diameter of Ag nanoparticles was found to be ~3 nm. Also modified magnetron sputtering system was an effective one-step method to prepare Nanofluids that were stable. Silicon oil thin film were employed to prepare Nanofluids with nanoparticles of much lesser quantity.

Cristina V. Iancu et al. [18] investigated the principal resolution limitation in electron cryomicroscopy of frozen-hydrated biological samples were due to radiation damage. Results obtained were tomographic reconstructions produced with total doses between 10 and 350 e¡/Å2 showed better results at 82K than 12K for every dose tested. Thus cooling with liquid helium was actually disadvantageous for cryotomography.

Yoshiaki Suzuki et al. [19] proposed subcooled liquid nitrogen a good cooling medium of high temperature superconducting (HTS) electric power systems such as electric power line and a power transformer. As per the required result one system of HTS power transformer was tested in distribution power line and in each case the temperature of the cold head of the cryocooler was kept at 64 K little above nitrogen freezing temperature.

L.J Masur et al. [20] provided an update on development of performance and application of first and second generation high temperature superconductor (HTS) wires fabricated at American Superconductor (AMSC). First generation, multifilamentary composite wire was available commercially today in different viable product forms. Conclusion drawn from

this paper was a product differentiation with a view on the application of HTS wire in the electric power sector can be provided.

Jürgen Keller's et.al [21] investigated that the production of HTS wire for power applications were increasingly elaborating into industrial dimensions. The most widely considered manufacturing method for this conductor was the BSCCO-2223-OPIT route used internationally by many organizations including American Superconductor. Due to their compactness, these motors were less expensive to manufacture compared with conventional motors and will be more energy efficient according to results obtained.

Victor Anton et.al [22] investigated the density, refractive indices kinematic viscosities for 1-propylpyridinium tetrafluoroborate with water mixtures at the temperatures of 293.15, 303.15, 313.15 and 323.15K and pressure of 99.0 kPa. Several properties and its deviations are obtained and further correlated from experimental data. These properties are discussed taking considering energetic and structural factors. Results indicate that interactions ionic liquids with water are weaker in comparison to those operating for pure compounds

Yimin Xuan et.al [23] proposed mixing of nanoparticle into liquid which can be metallic or nonmetallic in nature. These ultra fine particles are suspended in liquid which exhibits effective enhancement in properties of heat transfer. Assumptions are made that Nanofluid behaves like fluid not like solid liquid mixture. Two approaches are used for deriving correlation for heat transfer. Transport property and thermal dispersion of Nanofluid are included.

Y.B. Tao et.al [24] in present research used anisotropic porous media model in pulse tube refrigerator (PTR) for generation of mesh regenerator. Effects of geometric parameters, operating pressure and cryogenic temperature are considered for permeability coefficient. Mesh geometries and properties of materials are taken into account for heat transfer and fluid flow. Increase in specific heat increases the cooling power of pulse tube regenerator. Also as depth of penetration increases, density is found to be decreasing. Thus better heat transfer performance is obtained.

Haisheng Chen et.al [25] conducted experiment on behavior of ethylene glycol (EG) based on titanate nanotubes (TNT) Nanofluids at 20-60°C with 0.5, 1.0, 2.0, 4.0 and 8.0 wt. %

`

Results depicts influences on particle concentration and temperature with zero shear viscosity (ZSV) and high shear viscosity (HSV).

Yi Jin et.al [26] proposed a methodology for analyzing the effective thermal conductivity for nanoparticles dispersed in based on rheology which uses data to conclude microstructures of nanoparticles .Hamilton–Crosser equation is used to predict effective thermal conductivity for Nanofluids. Validation using four types of Nanofluids such as titania nanoparticles and titanate nanotubes with water and ethylene glycol is done. And later modified Hamilton–Crosser equation is used to predicted effective thermal conductivity for Nanofluids.

Kazem Mahanpour et.al [27] determined effective thermal conductivity and viscosity for both experimental and theoretical for aluminum oxide with water Nanofluid for microwave for distilled water by sonic device with volume concentration of 0.15 to 3%. Properties are measured at constant temperature Al2O3 Nano particles in water show Newtonian behavior. Theoretical models estimate thermal conductivity and viscosity using Hamilton Crosser of Nanofluids.

M.F. Nabil et.al [28] proposed novel research on hybrid Nanofluids and hybrid nanolubricants by dispersing two or more dissimilar nanoparticles either in mixture or composite form in basefluid. The main objective is to improve thermal properties or rheological properties that are better than conventional Nanofluids. This review provides research on thermo-physical properties of hybrid Nanofluids including methods of preparation and performance in terms of heat transfer and pressure drop.

Naheed Begum et.al [29] investigated the effect of variable thermophysical properties of Nanofluid on boundary layer flow for uniformly heated cone. The governing equations used are in non-dimensional form with continuous transformations further solved using implicit finite difference method. It is found that thermophysical properties of fluid are likely to promote the rate of heat transfer as compared to fluid with constant properties.

P.Lu et.al [30] investigated thermophysical properties of under cooled liquid Ni-Zr for molecular dynamics simulation with Finnis-Sinclair potential, including melting point temperature, density, excessive volume and thermal expansion. The melting temperatures

`

is achieved by evolution of crystal-liquid-crystal model where exist low differences of 4.14% for alloy.

Munish Gupta et.al [31] summarizes the important results for improvement of thermophysical properties of Nanofluids. The influence of parameters such as particle's loading, material size and shape, type of base fluid, temperature, additives and pH value is considered. Further advantages of Nanofluids in solar collectors and also as coolants in automotive heat exchangers is shown.

Gabriela Huminic et.al [32] experimentally investigated thermo-physical properties of SiC/water Nanofluids. Thermal conductivity, viscosity and also surface tension Nanofluids are measured for concentrations of 0.5 and 1.0 wt% of nanoparticles at range of 20 °C to 50°C. The surface tension Nanofluids increases with increase of weight concentrations of nanoparticles. However results having concentration 0.5 wt%, surface tension is lesser than surface tension of water.

Janki Shah et.al [33] investigated the properties of Nanofluids as absorber due to smaller size of nanoparticles which cover surface area largely, increase heat transfer. Thermophysical properties are increased due to increase in surface area of nanoparticles. Thermal conductivity is enhanced by Brownian motion, interface resistance of nanoparticles In this review paper, synthesis of Nanofluids by various methods of stabilization, thermal conductivity and heat transfer properties are summarized.

I.M Mahabubul et.al [34] proposed the study to determine heat transfer and pressure drop for Al2O3-R141b nanorefrigerants at various volume concentrations. The experimental conditions considered are constant mass flux of 100 kgm^2/s, vapor qualities from 0.2 to 0.7, temperature at 25°C and pressure of 0.078535 MPa. Heat transfer and Pressure drop increases with enhancement of volume concentrations of nanoparticle.

Yihuan Xu et.al [35] used evacuated tube to provide vacuum condition so that HTS Maglev can run at ultrahigh speed. The low-pressure environment is maintained inside tube which reduces air friction to be resistance of Maglev. Liquid nitrogen (LN2) is used as coolant to attain superconductor bulk.

`

Xu Bin [36] investigated experimentally, the pressure drop of liquefied natural gas during flow boiling in vertical micro-fin tube. The effect of mass flux, inlet pressure and heat flux on pressure drop for multi-phase flow for liquefied natural gas is analyzed. Results show that pressure drop increases as heat flux and also mass flux increases but decreases as inlet pressure increases.

Yang Hun Kim et.al [37] discussed about application of cryogenics on HTS cables. HTS power cable system of 22.9 kV/50 MVA AC specification and 410 m length is considered at the constant temperature. This paper summarizes design of cryogenic system and grid operations.

Dongmin Kim et.al [38] investigated on HTS power cables that are cooled by forced circulation of liquid nitrogen in sub cooled state to reduce heat loss and maintain cryogenic environment. This paper represents transient thermo-hydraulic performance of HTS cable refrigeration system as per variable heat load. Design directions of pressure in build-up tank and controlled algorithm are obtained.

A. Demko et.al [39] demonstrated HTS cable of 100m. Compact and efficient cooling technique is achieved using counter flow of cooling arrangements on (1G) BSCCO wire. HTS cable is studied for numerical model to obtain thermal hydraulic characteristics of cable with both AC and the thermal losses.

Raja Sekhar Dondapati et.al [40] studied dual channel for CICC using Computational Fluid Dynamics analysis to get complex behavior of flow. Two dimensional axi-symmetric models is generated and then meshed in GAMBIT. The effects of mass flow rate from 6 g/s to 10 g/s for Supercritical helium is analyzed and further used as coolant, in CICC for pressure gradient and velocity gradient analysis.

O.Maruyama et.al [41] studied the flow characteristic of pressure drop of LN2 in long length HTS cable and also heat transfer characteristics, AC loss, and also heat leak from cryostat-pipes. As a result, volumetric flow increases with maximum distance to be transmitted and discharge pressure also.

Raja Sekhar Dondapati et.al [42] studied the thermohydraulic performances for porous medium in dual channel CICC for International Thermonuclear Experimental Reactor. Results estimate that mass flow between the two channels

and also the pumping power required. Further CFD analysis gives clear phenomena of flow and the heat transfer in ultra complex geometries.

Jung-Bin Song and Haigun Lee [43] used the mixed cryogen in HTS applications. This paper provides a description and also summary for recent activities at Korea University for cooling systems used in mixed cryogens such as solid with liquid nitrogen, solid nitrogen with liquid and neon solid argon with liquid nitrogen.

Handry Afrianto et.al [44] numerically studied liquid natural gas (LNG) flow and its heat transfer for heat exchanger at pressure of 0.6 MPa. Computational fluid dynamics (CFD) code using FLUENT to simulate the flow and heat transfer Furthermore, optimization of mass flow rate for vaporization process is studied.

Raja Sekhar Dondapati et.al [45] investigated a three dimensional model for dual channel CICC which is generated in GAMBIT-2.1 and thus solved in solver FLUENT-6.3.26 module. Also influence of mass flow rate on the Turbulent Kinetic Energy is studied. The computational results for pressure drop are validated with relevant experimental data results.

Ho-Myung Chang et.al [46] proposed a new concept for cryogenic cooling in long-length of HTS cables. This research provides integrating refrigerator with liquid nitrogen of circulation to eliminate the cryogenic pumps. The modified dual-pressure cycle as cooled with the expander stream is found to be better for long HTS cables.

Gabriela Huminic et.al [47] summarizes enhancement of the effective heat transfer for heat exchanger devices with use of Nanofluids. Both experimental and theoretical results are compared and viscosity also Nusselt number is calculated.

Thomas M. Kochenburgera et.al [48] used mixed refrigerant for cooling of high-temperature superconductors at temperature range 55K to70 K. Process have pre-cooling and low-temperature where pre cooling is 120K. Simulated results for pre-cooling stage are validating with experimental data.

Jisung Lee et.al [49] investigated on mixed refrigerant Joule–Thomson (MR JT) refrigerator for good performance at refrigeration temperatures of 80K and above For HTS cable cooling neon–nitrogen (pre cooled) MR JT refrigerator is used at

`

70K. The coefficient of performance is achieved to be 0.058 at temperature of 70K with optimum design variables. Further, COP is improved to 0.064 by enhancing efficiency of pre cooling cycle.

Yoshiaki Suzuki et.al [50] used the subcooled liquid nitrogen as coolant in high temperature superconducting (HTS) power systems. Cryocooler is used to produce the subcooled liquid nitrogen by circulation pump. The pressure is maintained at 0.108 MPa and operating temperature of 68K. The temperature of cold head of cryocooler is taken at temperature of 64K.

`

CHAPTER-VI

6 RESEARCH METHODOLOGY

After literature review and according to the objective of present research work, following methodologies are considered

Selection of mixed cryogen (base fluid)
Selection of nanoparticles with suitable volume concentration
Operating pressure and temperature range
Selection of HTS cables

Commonly used nanoparticles Al_2O_3 and CuO are dispersed in the base fluid i.e. mixed cryogen (LN_2+LO_x). The composition is taken to be from 10%-90% (LN_2-LO_x) to 90%-10% (LN_2-LO_x) according to molecular weight. In order to achieve the performance of HTS cables thermophysical properties such as density, viscosity, thermal conductivity and specific heat are studied for mixed cryogen with and without nanoparticles.

6.1 Study of thermophysical properties of mixed cryogen without nanoparticles

Using NIST database standard 4 (SUPERTRAPP®) versions 3.2.1, desired thermophysical properties are obtained for 10gm of mixed cryogen (LN_2+LO_x) operating under the pressure range of 0.9MPa-1.3MPa and temperature range of 70K-100K.

6.2 Study of thermophysical properties of mixed cryogen with various nanoparticles

Various theoretical and experimental models, from literature are used. However these models with specified correlations are applicable for limited base fluids such as water, oil and ethylene glycol with nanoparticle. These correlations when used with mixed cryogen with volume concentration of 1% to 5% provide approximate desired results.

6.2.1 Density

In this research work effective density is calculated as function of volume concentration from 1% to 5% of nanoparticle, at operating pressure of 0.9MPa and temperature range of 70K-100K, after every 6K.

`

$$\rho_{NF} = (1 - \emptyset)\rho_{BF} + \emptyset\rho_{NP}$$

ρ_{NF} is the effective density of Nanofluid (*NF*) with volume concentration (*Ø*) of Nanoparticle (*NP*) and ρ_{BF} is the density of base fluid (*BF*).

6.2.2 Specific Heat

Specific Heat of Nanofluid is measured as the function of volume concentration of nanoparticle, at operating pressure of 0.9MPa and temperature range of 70K-100K, after every 6K.

$$C_{pNF} = \frac{(1 - \emptyset)(\rho C_p)_{BF} + \emptyset(\rho C_p)_{NP}}{(1 - \emptyset)\rho_{BF} + \emptyset\rho_{NP}}$$

C_{pNF} is the effective specific heat of Nanofluid (*NF*) with volume concentration (*Ø*) of Nanoparticle (*NP*), C_p is specific heat and ρ_{BF} is the density of base fluid (*BF*) i.e. mixed cryogen.

6.2.3 Thermal Conductivity

Thermal Conductivity is considered as the function of volume concentration of nanoparticles at operating pressure of 0.9MPa and temperature range of 70K-100K, at every 6K. From the theoretical model for liquid and solid suspension, Maxwell correlation is used to measure effective thermal conductivity of Nanofluid.

$$\frac{k_{eff}}{k_f} = \frac{k_p + 2k_f + 2\emptyset(k_p - k_f)}{k_p + 2k_f - \emptyset(k_p - k_f)}$$

k_{eff} is the effective thermal conductivity of Nanofluid with volume concentration (*Ø*) using k_f as thermal conductivity of basefluid and k_p is thermal conductivity of nanoparticles.

6.2.4 Viscosity

For the present Nanofluid, viscosity is considered as function of volume concentration of nanoparticles at operating pressure of 0.9MPa and temperature range of 70K-100K, at every 6K. Einstein (theoretical) model for infinitely dilute suspension of spheres and Drew and Passman (experimental) model for volume concentration less than 5% is used. However both the models depict same correlation for calculation.

$$\frac{\mu_{eff}}{\mu_f} = 1 + 2.5\emptyset$$

`

μ_{eff} is the effective viscosity of Nanofluid with volume concentration ($\varnothing$) and μ_f is the viscosity of basefluid.

6.3 Computational Evaluation of Thermohydraulic Performance of HTS cables

6.3.1 Mathematical Method

For HTS cable, geometry of corrugated pipe is taken into account. And simultaneously three governing equations namely, conservation of mass, momentum and energy are solved.

Equation for Mass Conservation

$$\frac{\partial \rho}{\partial t} + \nabla . \rho \vec{v} = S_m$$

Where S_m is the source term of mass.

Equation for Momentum Conservation

$$\frac{\partial}{\partial t}(\rho \vec{v}) + \nabla . (\rho \vec{v} \vec{v}) = -\nabla p + \nabla . \tau + \rho \vec{g} + \vec{F}$$

Equation for Energy Conservation

$$\frac{\partial}{\partial t}(\rho E) + \nabla . \left(\vec{v}(\rho E + p)\right) = -\nabla . \sum_j h_j J_j + S_h$$

6.3.2 Computational Method

FLUENT module of ANSYS® workbench version 15 is been used in order to achieve Thermohydraulic characteristics such as pressure drop, heat transfer and Nusselt number for given composition and mass flow rates.

6.3.2.1 Geometry

Figure shows the geometry of corrugated pipe for HTS cables. Diameter of pipe is 40mm, corrugation pitch is 60mm and length is 1000mm.

`

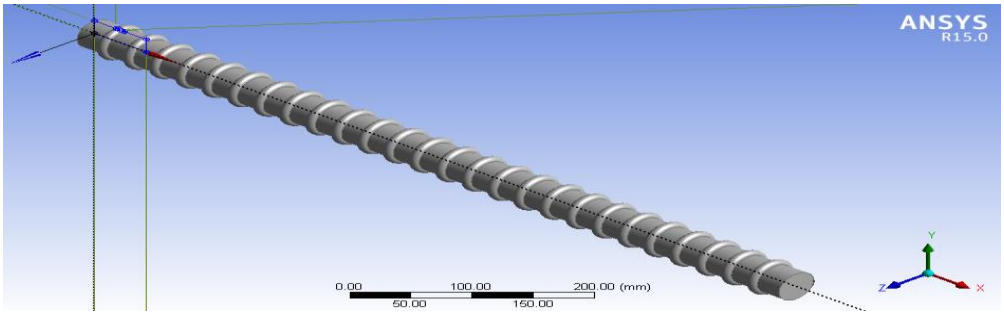

Figure 5 Corrugated steel pipe geometry

6.3.2.2 Meshing

Auto generated mesh is considered with prescribed named selection of inlet, wall and outlet. Uniform inlet and wall temperature is maintained.

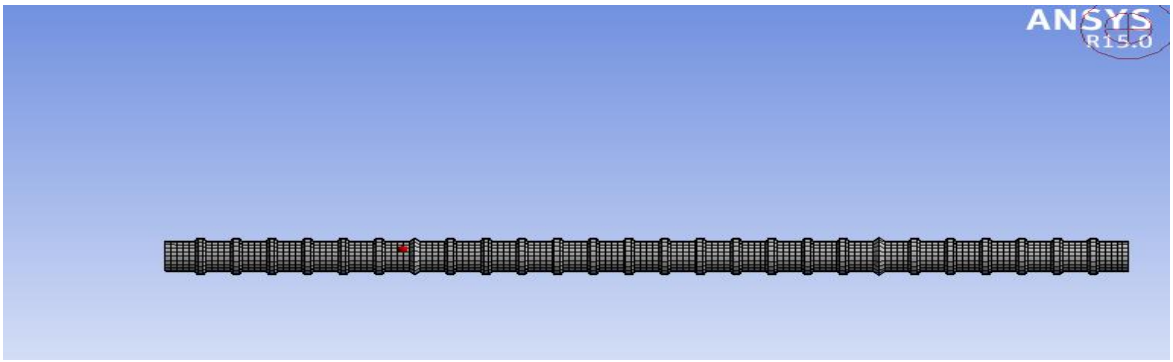

Figure 6 Meshing of geometry

6.3.2.3 Boundary Conditions

Inlet temperature of 70K and wall temperature of 290K is maintained at operating pressure of 0.9MPa. The fluid is flowing with mass flow rate from 20g/s - 60g/s. k-€ energy model is used.

6.3.2.4 Solution

Using FLUENT solver, the descritized model is being solved under 0.001 residuals with finite number of iterations. Hybrid initialization is done for solution initialization.

6.3.2.5 Post Processing

Results are obtained and represented in form of graphs, vectors, contours and various profiles

`

CHAPTER-VII

7 RESULT AND DISCUSION

7.1 Thermophysical Properties of Mixed Cryogen

7.1.1 Thermophysical properties of mixed cryogen at varying pressure

The pressure range of 0.9MPa to 1.3MPa is considered under the temperature limit of 70K to100K and thus thermophysical properties such as specific heat, density, viscosity and thermal conductivity is evaluated.

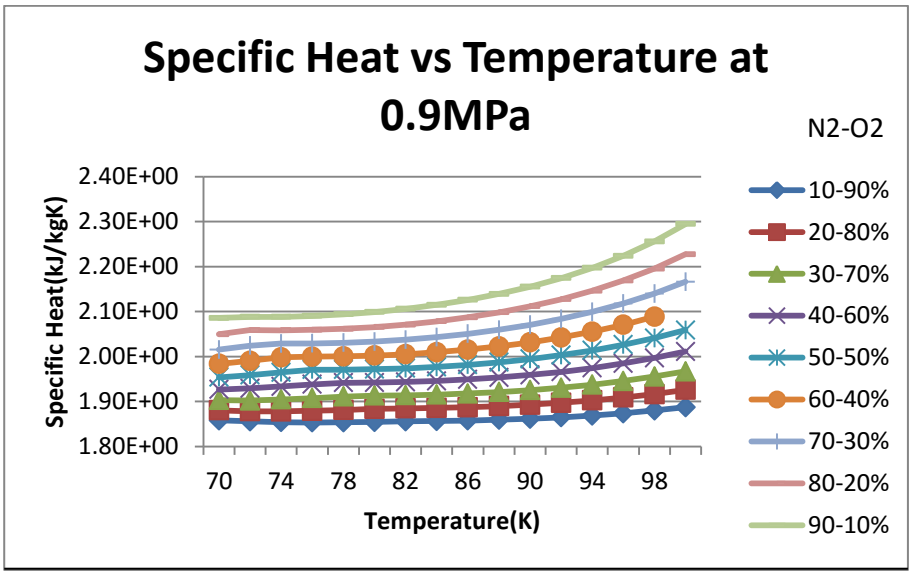

Figure 7Specific Heat vs Temperature at 0.9MPa

Figure7 shows the variation of specific heat as the function of temperature at a pressure of 0.9MPa with varying composition of N2-O2. It is observed that with the increase in temperature, specific heat is found to be increasing. It can also be seen with increase of N2 and decrease of O2 in composition, specific heat increases.

`

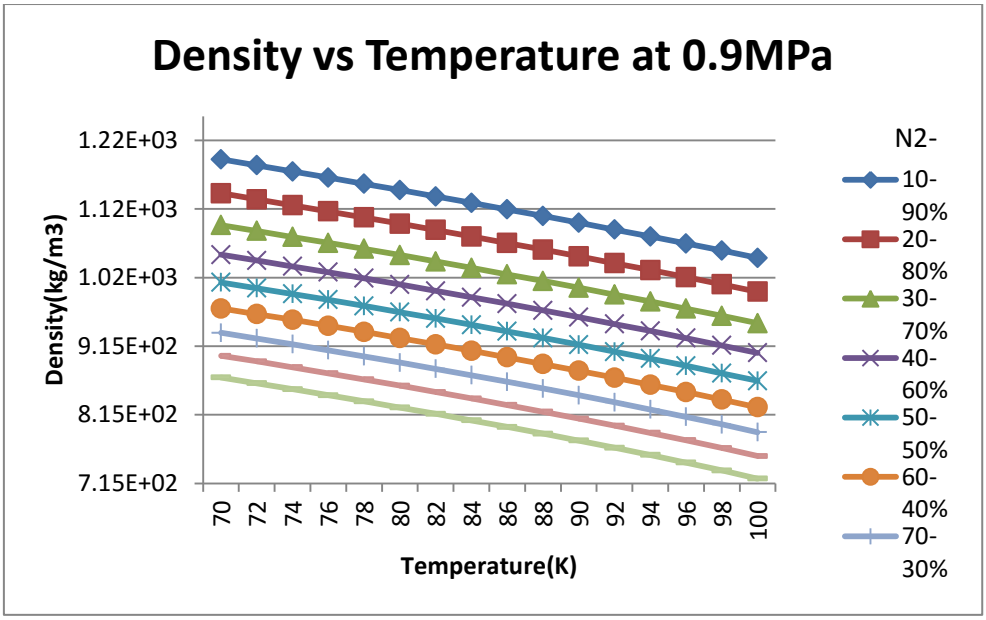

Figure 8Density vs Temperature at 0.9MPa

Figure8 shows the variation of density with respect to temperature at a pressure of 0.9MPa with varying composition of N2-O2. It is observed that with the increase in temperature, density is decreasing gradually. It is observed that with increase of N2 and decrease of O2 in composition, density deceases at a significant rate.

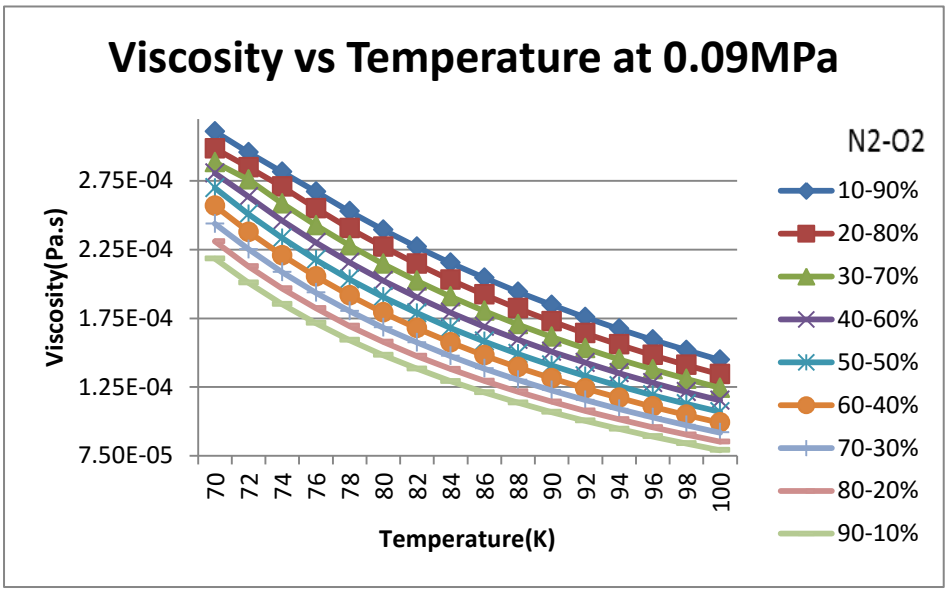

Figure 9Viscosity vs Temperature at 0.09MPa

Figure9 shows the variation of viscosity as the function of temperature at a pressure of 0.9MPa with varying composition of N2-O2. It is observed that with the increase in

temperature, viscosity decreases. It is also observed that with increase of N2 and decrease of O2 in composition, there is a gradual decrease in viscosity.

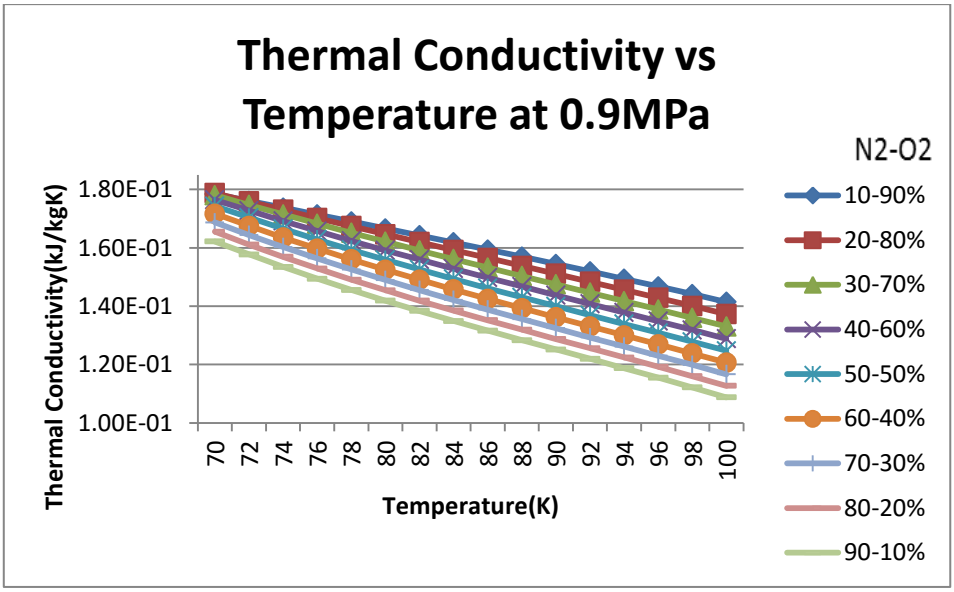

Figure 10 Thermal Conductivity vs Temperature at 0.9MPa

Figure10 shows the variation of thermal conductivity as the function of temperature at a pressure of 0.9MPa with varying composition of N2-O2. It is observed that with the increase in temperature, thermal conductivity decreases. It is observed that with increase of N2 and decrease of O2 in composition, thermal conductivity decreases.

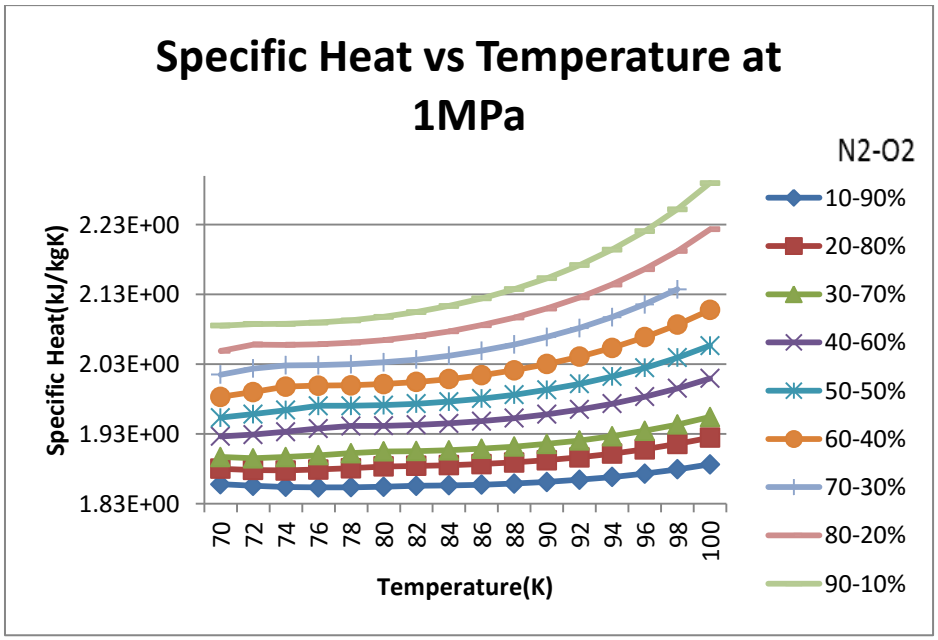

Figure 11Specific Heat vs Temperature at 1MPa

`

Figure11 shows the variation of specific heat as the function of temperature at a pressure of 1.0MPa with varying composition of N2-O2. It is observed that with the increase in temperature, specific heat is found to be increasing. It can also be seen with increase of N2 and decrease of O2 in composition, specific heat increases.

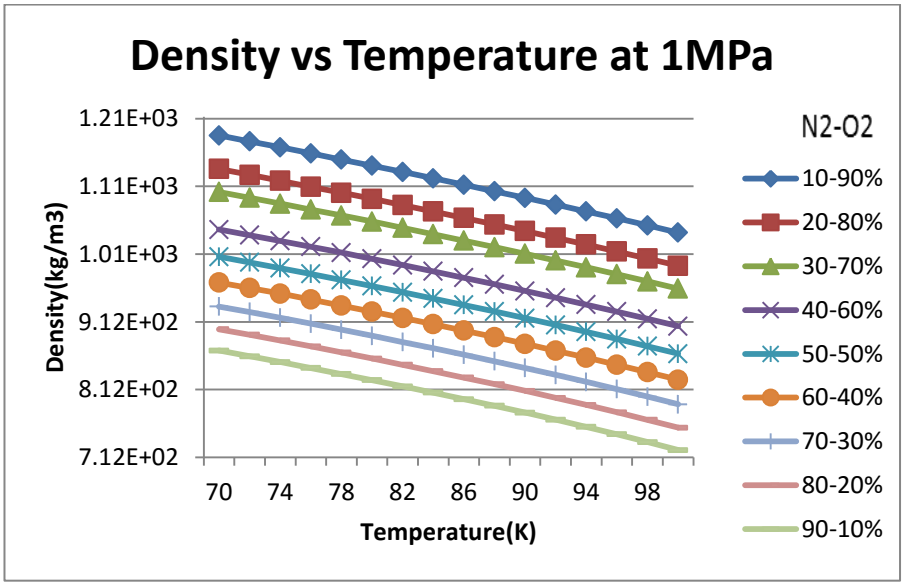

Figure 12Density vs Temperature at 1MPa

Figure12 shows the variation of density with respect to temperature at a pressure of 1.0MPa with varying composition of N2-O2. It is observed that with the increase in temperature, density is decreasing gradually. It is observed that with increase of N2 and decrease of O2 in composition, density deceases at a significant rate.

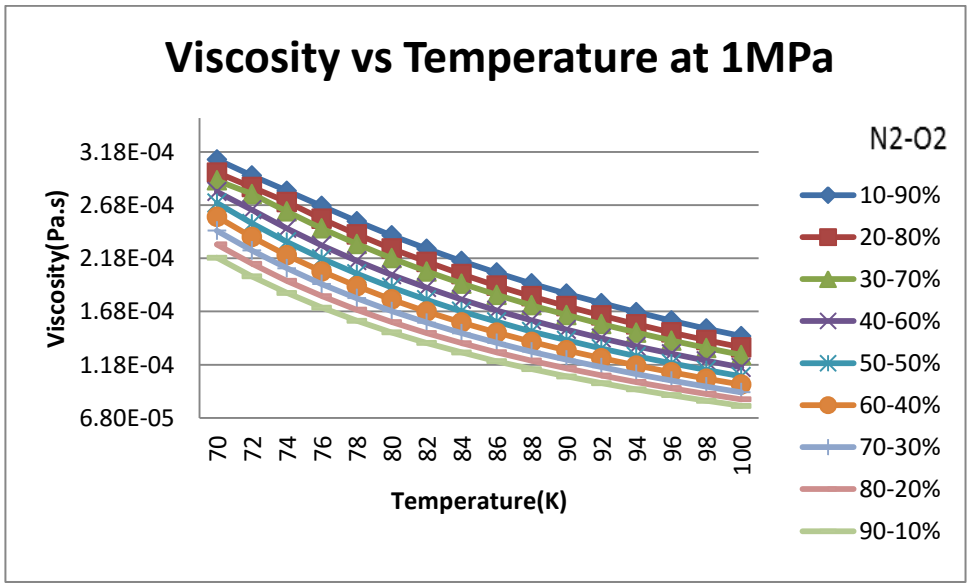

Figure 13Viscosity vs Temperature at 1MPa

`

Figure13 shows the variation of viscosity as the function of temperature at a pressure of 1.0MPa with varying composition of N2-O2. It is observed that with the increase in temperature, viscosity decreases. It is also observed that with increase of N2 and decrease of O2 in composition, there is a gradual decrease in viscosity.

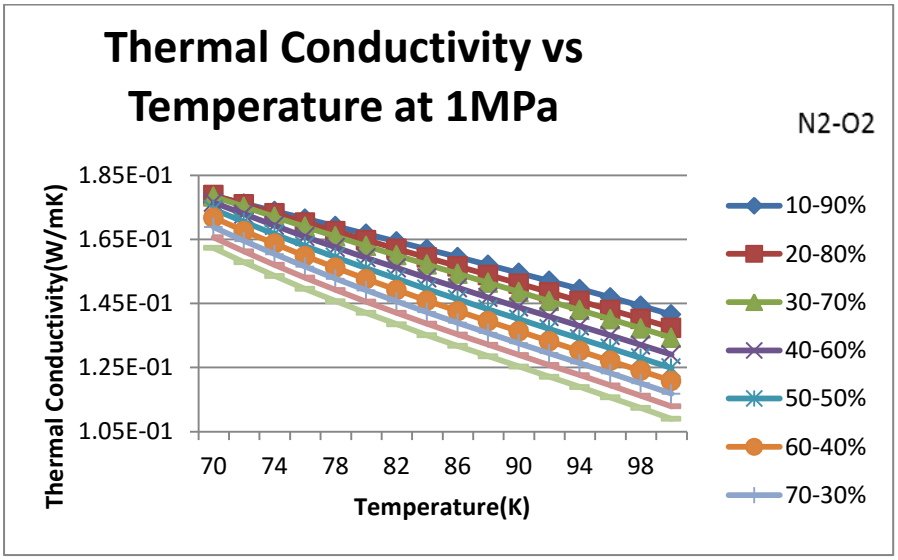

Figure 14Thermal Conductivity vs Temperature at 1MPa

Figure14 shows the variation of thermal conductivity as the function of temperature at a pressure of 1.0MPa with varying composition of N2-O2. It is observed that with the increase in temperature, thermal conductivity decreases. It is observed that with increase of N2 and decrease of O2 in composition, thermal conductivity deceases.

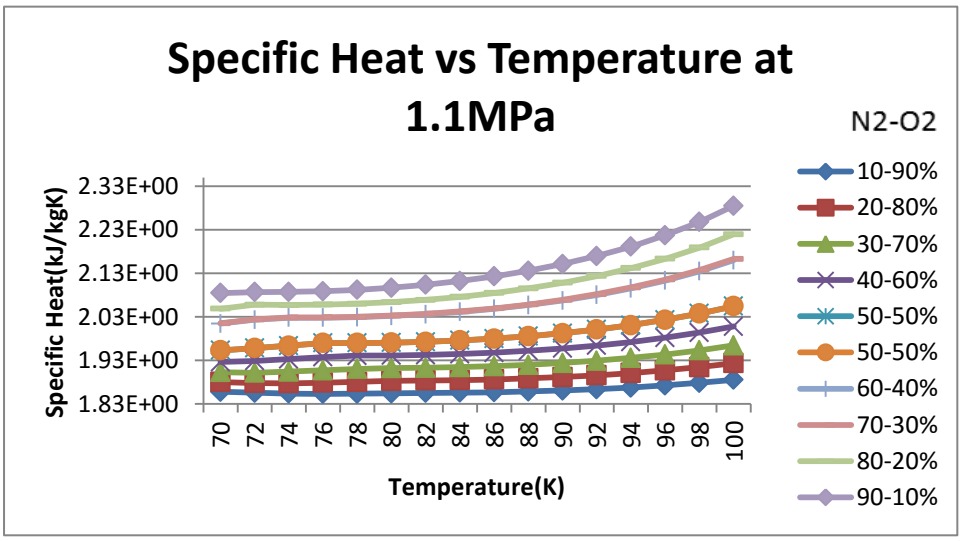

Figure 15Specific Heat vs Temperature at 1.1MPa

`

Figure15 shows the variation of specific heat as the function of temperature at a pressure of 1.1MPa with varying composition of N2-O2. It is observed that with the increase in temperature, specific heat is found to be increasing. It can also be seen with increase of N2 and decrease of O2 in composition, specific heat increases.

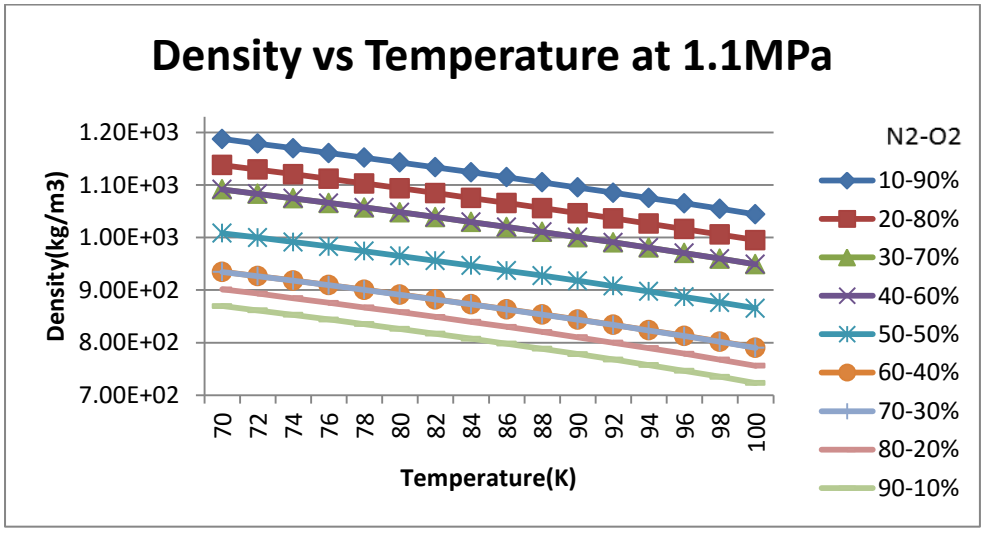

Figure 16Density vs Temperature at 1.1MPa

Figure16 shows the variation of density with respect to temperature at a pressure of 1.1MPa with varying composition of N2-O2. It is observed that with the increase in temperature, density is decreasing gradually. It is observed that with increase of N2 and decrease of O2 in composition, density deceases at a significant rate.

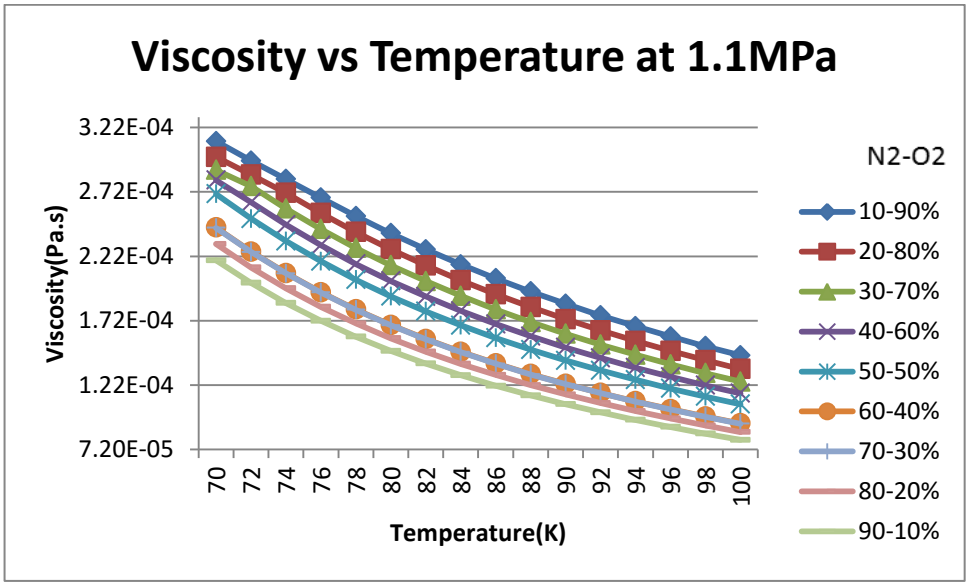

Figure 17Density vs Temperature at 1.1MPa

`

Figure17 shows the variation of viscosity as the function of temperature at a pressure of 1.1MPa with varying composition of N2-O2. It is observed that with the increase in temperature, viscosity decreases. It is also observed that with increase of N2 and decrease of O2 in composition, there is a gradual decrease in viscosity.

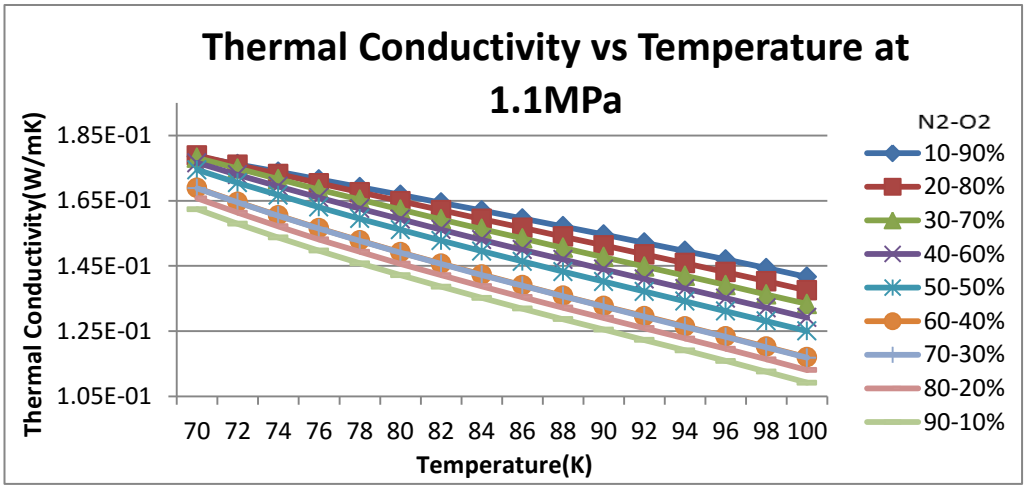

Figure 18 Thermal Conductivity vs Temperature at 1.1MPa

Figure18 shows the variation of thermal conductivity as the function of temperature at a pressure of 1.1MPa with varying composition of N2-O2. It is observed that with the increase in temperature, thermal conductivity decreases. It is observed that with increase of N2 and decrease of O2 in composition, thermal conductivity decreases.

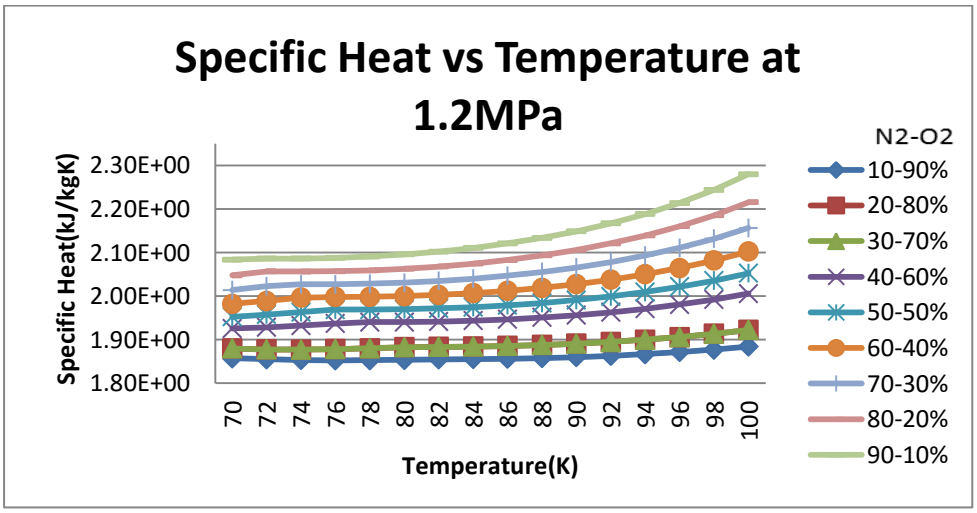

Figure 19Specific Heat vs Temperature at 1.2MPa

`

Figure19 shows the variation of specific heat as the function of temperature at a pressure of 1.2MPa with varying composition of N2-O2. It is observed that with the increase in temperature, specific heat is found to be increasing. It can also be seen with increase of N2 and decrease of O2 in composition, specific heat increases.

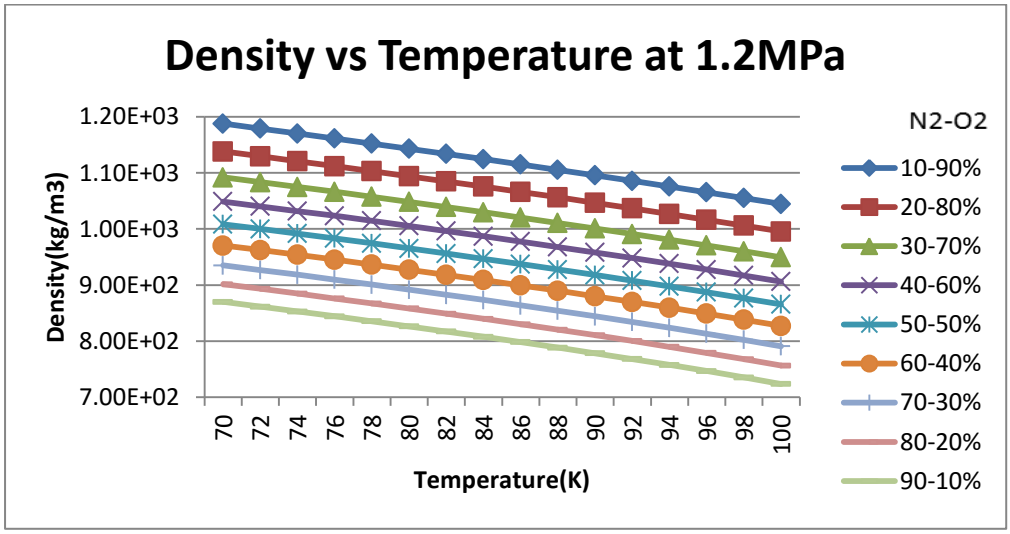

Figure 20Density vs Temperature at 1.2MPa

Figure20 shows the variation of density with respect to temperature at a pressure of 1.2MPa with varying composition of N2-O2. It is observed that with the increase in temperature, density is decreasing gradually. It is also observed that with increase of N2 and decrease of O2 in composition, density deceases at a significant rate.

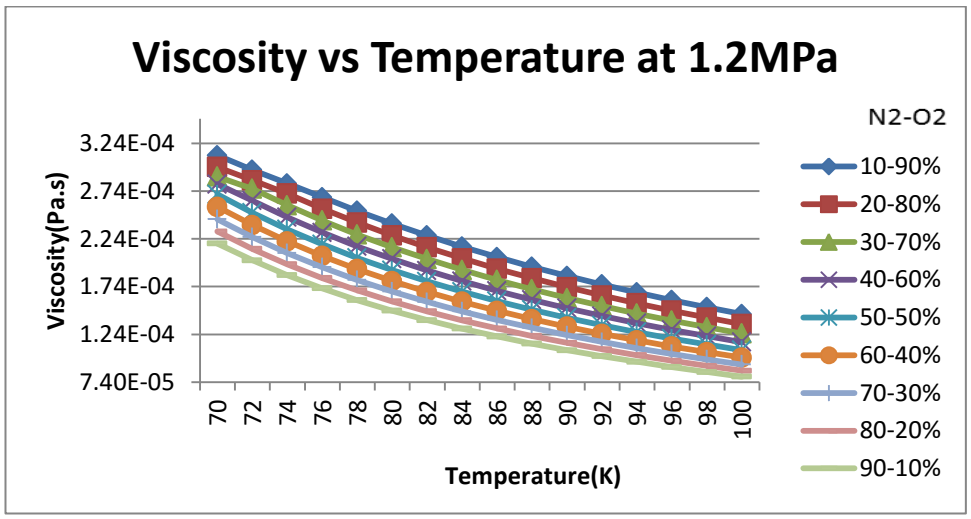

Figure 21Viscosity vs Temperature at 1.2MPa

Figure21 shows the variation of viscosity as the function of temperature at a pressure of 1.2MPa with varying composition of N2-O2. It is observed that with the increase in

temperature, viscosity decreases. It is also observed that with increase of N2 and decrease of O2 in composition, there is a gradual decrease in viscosity.

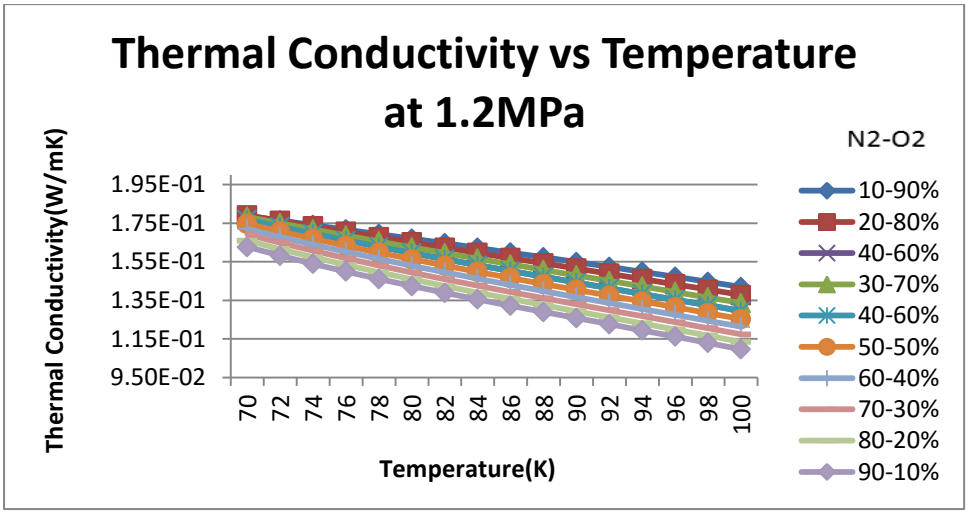

Figure 22Thermal Conductivity vs Temperature at 1.2MPa

Figure22 shows the variation of thermal conductivity with temperature at a pressure of 1.2MPa with varying composition of N2-O2. It is observed that with the increase in temperature, thermal conductivity decreases. It is also seen that with increase of N2 and decrease of O2 in composition, thermal conductivity decreases.

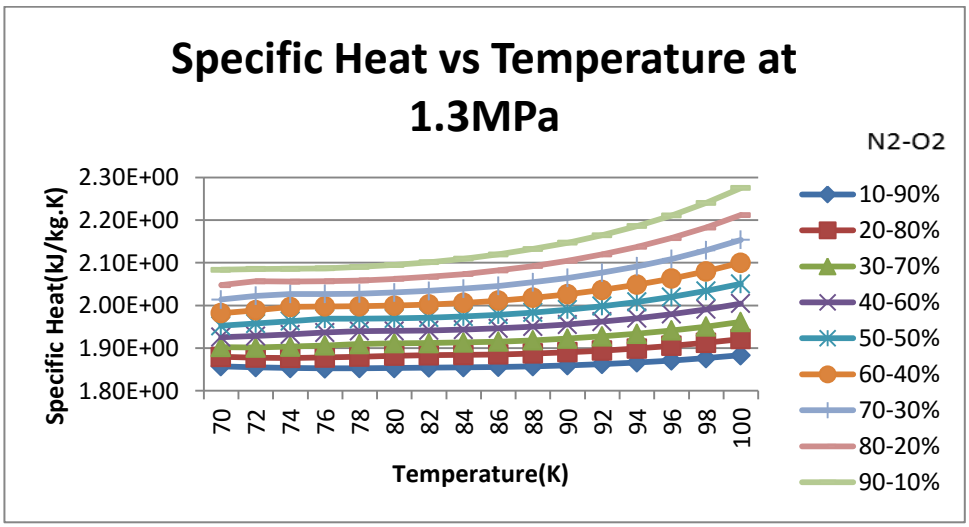

Figure 23Specific Heat vs Temperature at 1.3MPa

Figure23 shows the variation of specific heat as the function of temperature at a pressure of 1.3MPa with varying composition of N2-O2. It is observed that with the increase in

`

temperature, specific heat is found to be increasing. It can also be seen with increase of N2 and decrease of O2 in composition, specific heat increases.

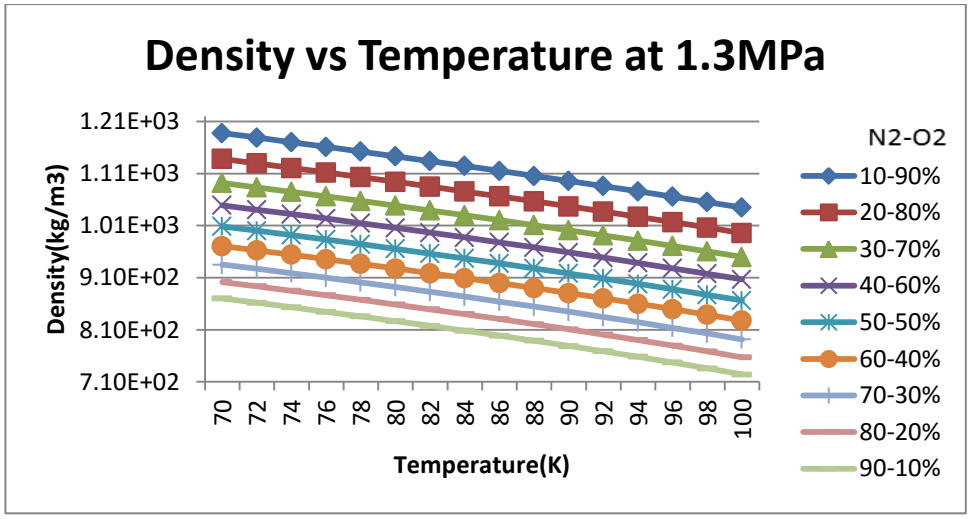

Figure 24Density vs Temperature at 1.3MPa

Figure24 shows the variation of density with respect to temperature at a pressure of 1.2MPa with varying composition of N2-O2. It is observed that with the increase in temperature, density is decreasing gradually. It is also observed that with increase of N2 and decrease of O2 in composition, density deceases at a significant rate.

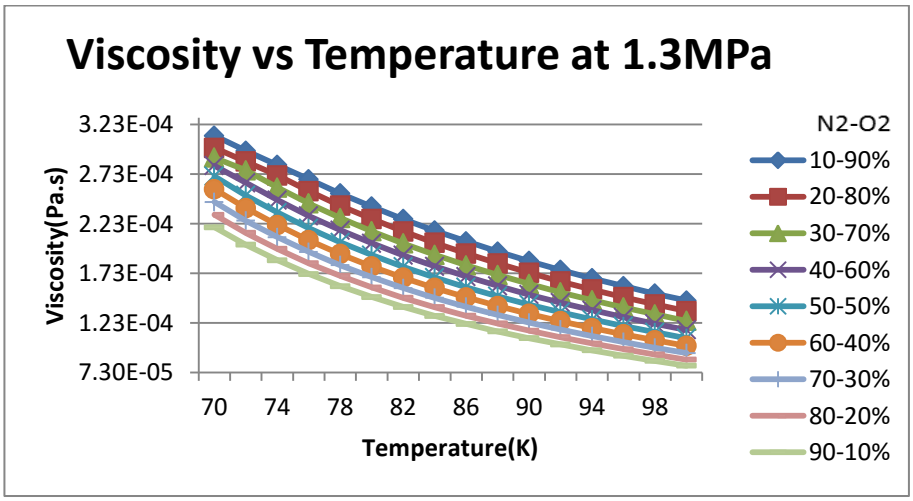

Figure 25Viscosity vs Temperature at 1.3MPa

Figure25 shows the variation of viscosity as the function of temperature at a pressure of 1.3MPa with varying composition of N2-O2. It is observed that with the increase in temperature, viscosity decreases. It is also observed that with increase of N2 and decrease of O2 in composition, there is a gradual decrease in viscosity.

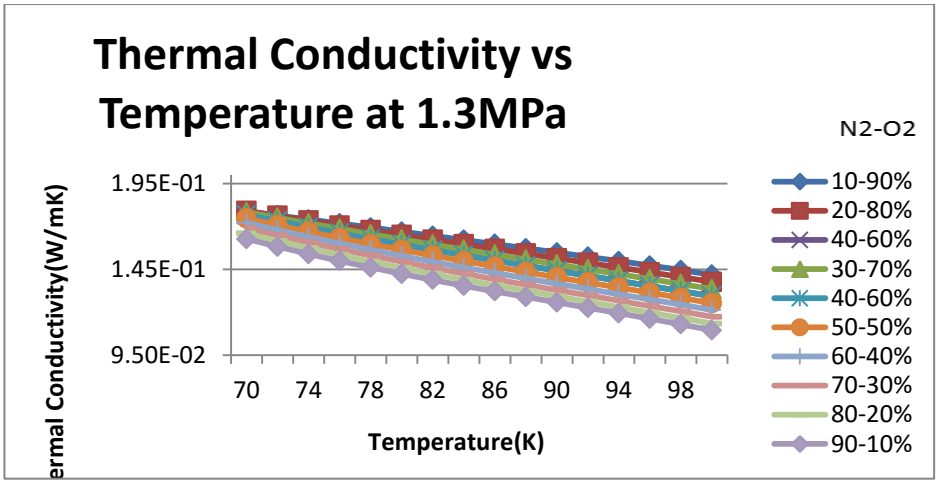

Figure 26Thermal Conductivity vs Temperature at 1.3MP

Figure26 shows the variation of thermal conductivity with temperature at a pressure of 1.3MPa with varying composition of N2-O2. It is observed that with the increase in temperature, thermal conductivity decreases. It is also seen that with increase of N2 and decrease of O2 in composition, thermal conductivity decreases.

7.1.2 Thermophysical properties of mixed cryogen at various composition

Liquid nitrogen and liquid oxygen are mixed in different composition and under same temperature range of 70K-100K thermophysical properties are evaluated.

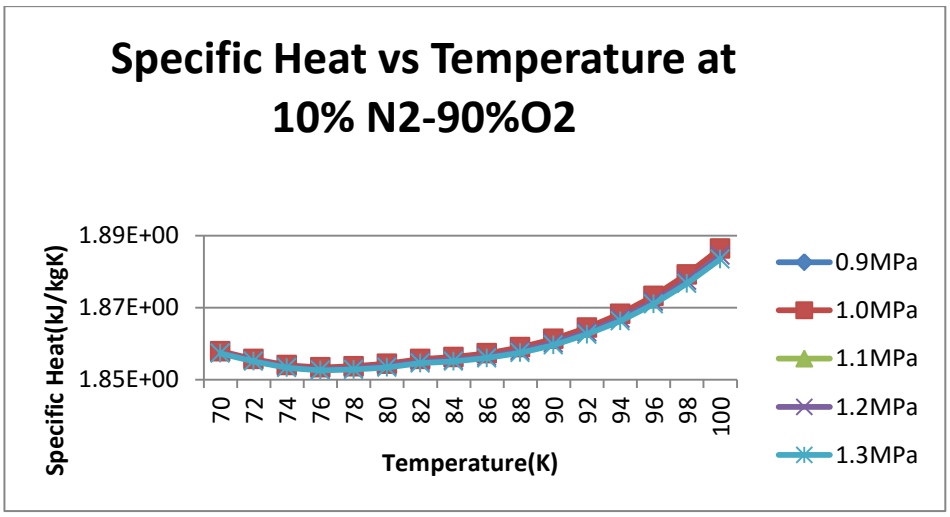

Figure 27Specific Heat vs Temperature at 10% N2-90%O2

`

Figure27 represents the variation of specific heat as the function of temperature at various pressures. It is observed that as temperature increases, specific heat also increases. It is also observed with increase in pressure, there is no significant change in specific heat.

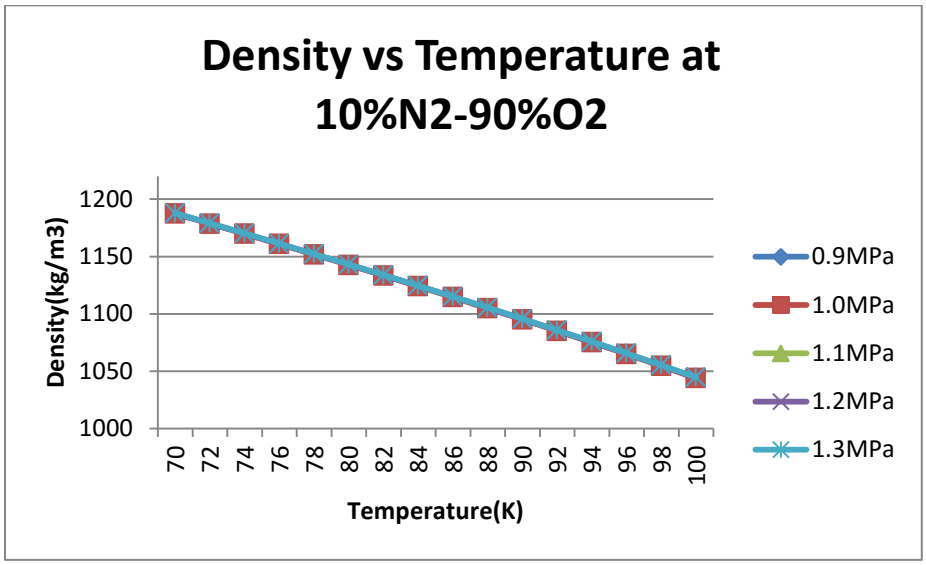

Figure 28Density vs Temperature at 10%N2-90%O2

Figure28 represents the variation of density with respect to temperature at various pressures. It is observed that with the increase in temperature, density decreases gradually. It is also seen that with increase in pressure, there is no significant change in density.

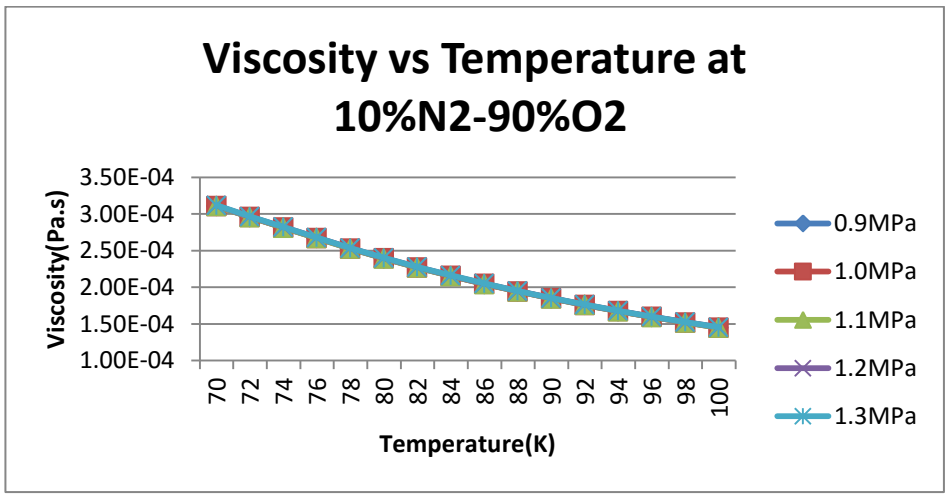

Figure 29Viscosity vs Temperature at 10%N2-90%O2

Figure29 represents the variation of viscosity as the function of temperature at various pressures. It is observed that viscosity decreases with the increase in temperature. It is also seen that there is no significant change in viscosity with the increase in pressure.

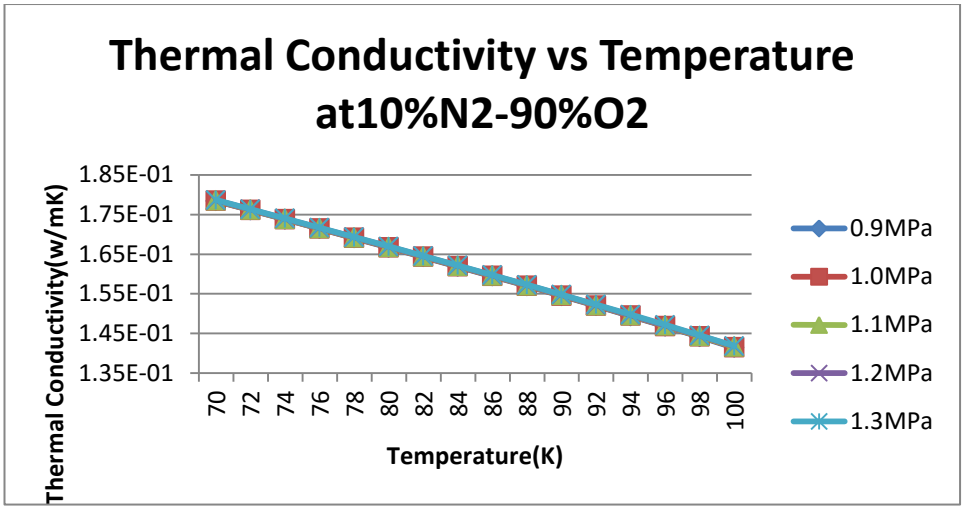

Figure 30Thermal Conductivity vs Temperature at10%N2-90%O2

Figure30 represents the variation in thermal conductivity with respect to temperature at various pressures. It is observed that with the increase in temperature, thermal conductivity decreases. It is also observed that there is no significant change in thermal conductivity with the increase in pressure.

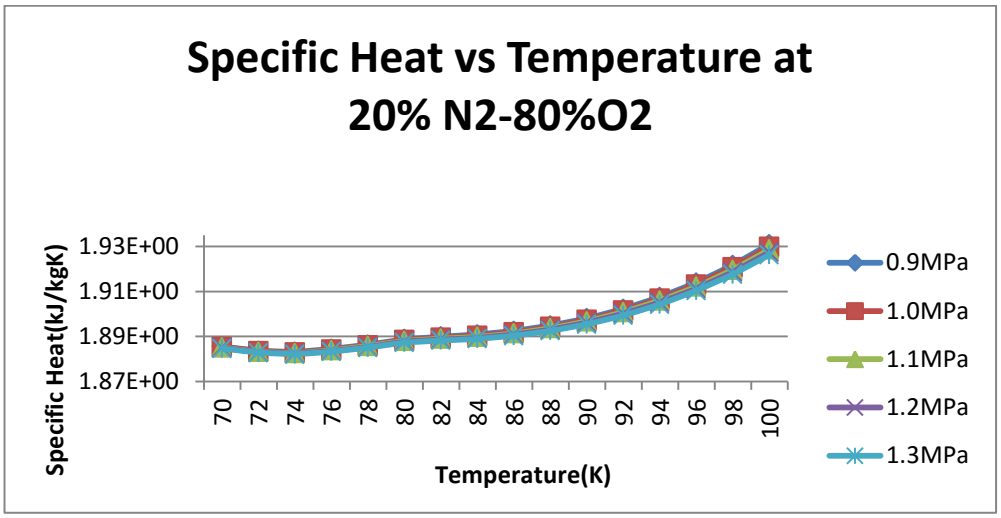

Figure 31Specific Heat vs Temperature at20% N2-80%O2

Figure31 represents the variation of specific heat as the function of temperature at various pressures. It is observed that as temperature increases, specific heat also increases. It is also observed with increase in pressure, there is no significant change in specific heat.

`

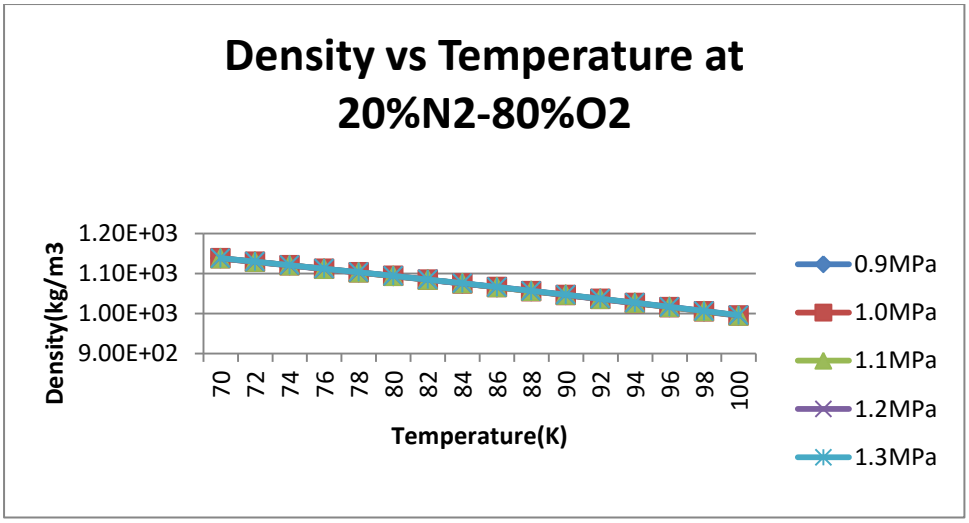

Figure 32Density vs Temperature at 20%N2-80%O2

Figure32 represents the variation of density with respect to temperature at various pressures. It is observed that with the increase in temperature, density decreases gradually. It is also seen that with increase in pressure, there is no significant change in density.

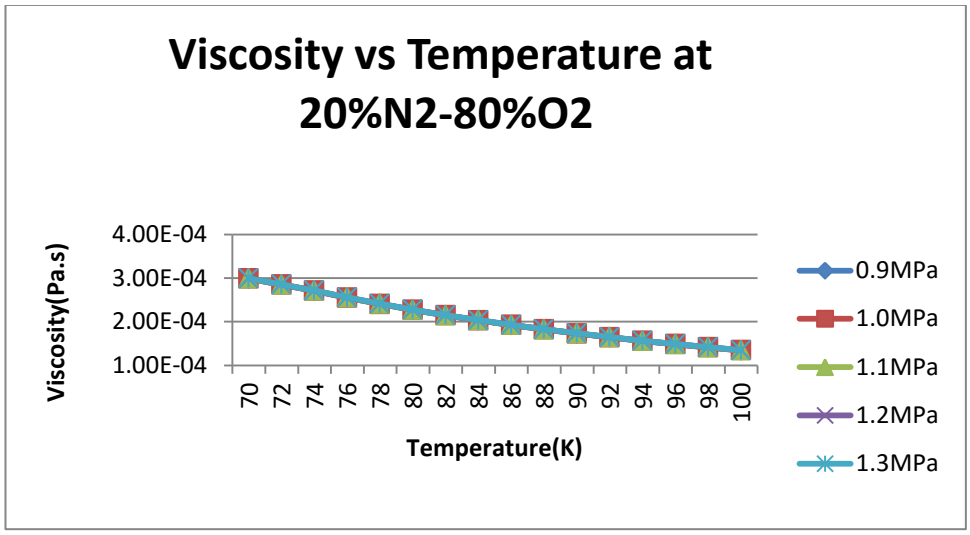

Figure 33Density vs Temperature at 20%N2-80%O2

Figure33 represents the variation of viscosity as the function of temperature at various pressures. It is observed that viscosity decreases with the increase in temperature. It is also seen that there is no significant change in viscosity with the increase in pressure.

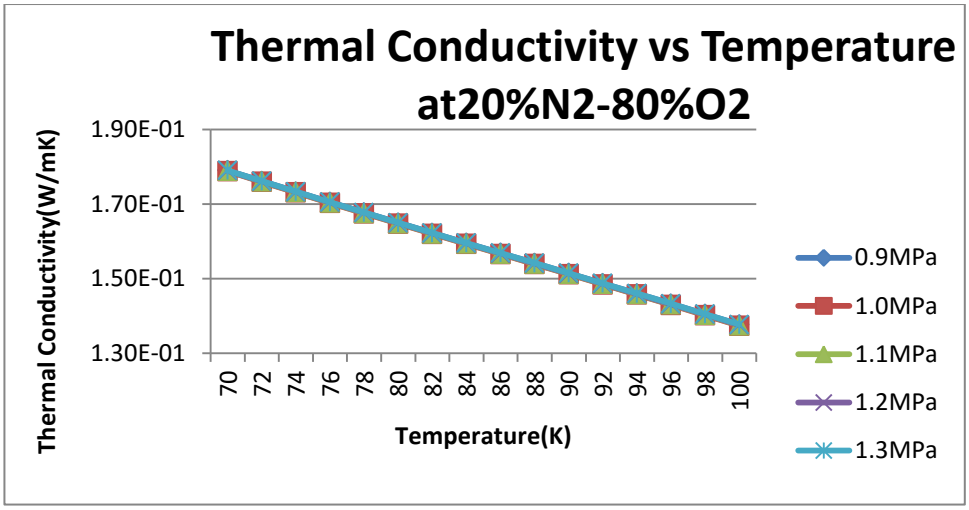

Figure 34Thermal Conductivity vs Temperature at 20%N2-80%O2

Figure34 represents the variation in thermal conductivity with respect to temperature at various pressures. It is observed that with the increase in temperature, thermal conductivity decreases. It is also observed that there is no significant change in thermal conductivity with the increase in pressure.

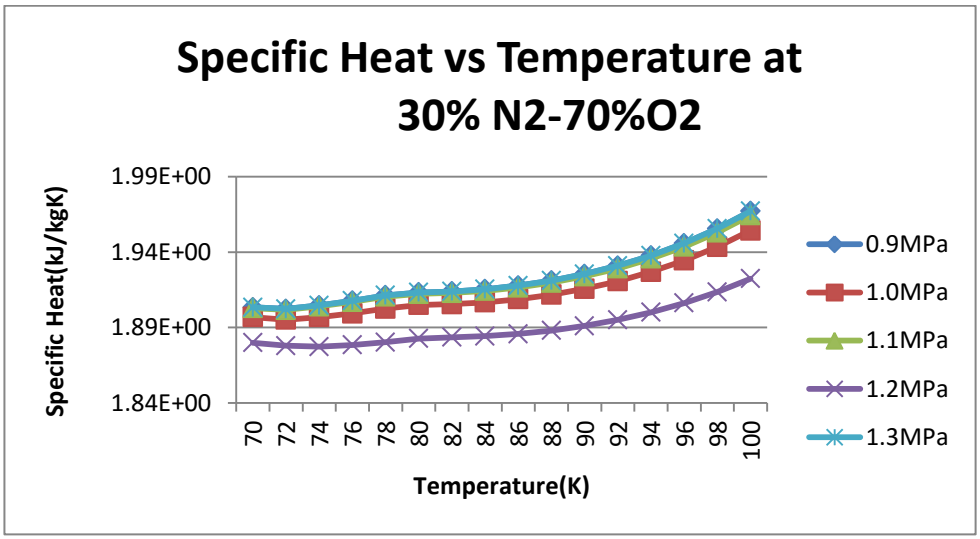

Figure 35Specific Heat vs Temperature at 30% N2-70%O2

Figure35 represents the variation of specific heat with to respect temperature at various pressures. It is observed that as temperature increases, specific heat also increases. It is also observed with increase in pressure, the specific heat at 1.2 MPa is lowest.

`

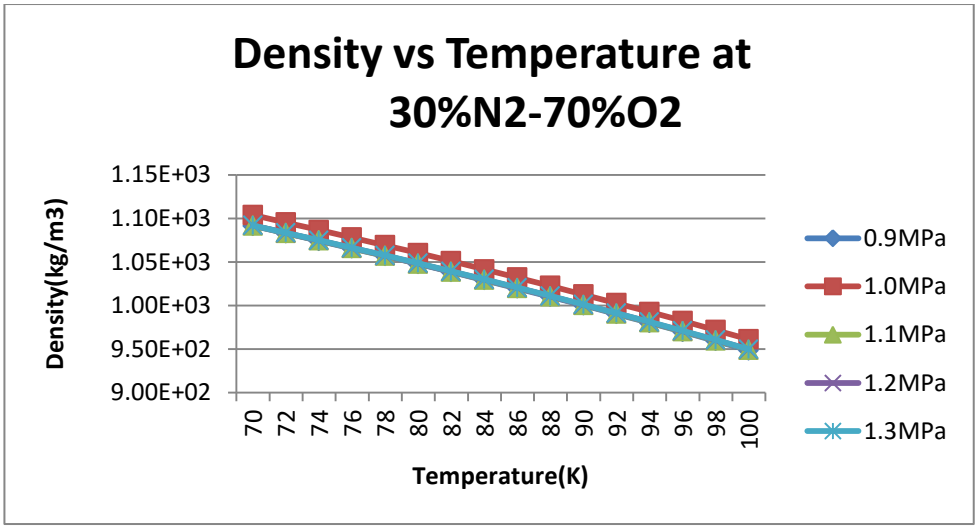

Figure 36Density vs Temperature 30%N2-70%O2

Figure36represents the variation of density with respect to temperature at various pressures. It is observed that with the increase in temperature, density decreases gradually. It is also seen that with increase in pressure, density changes.

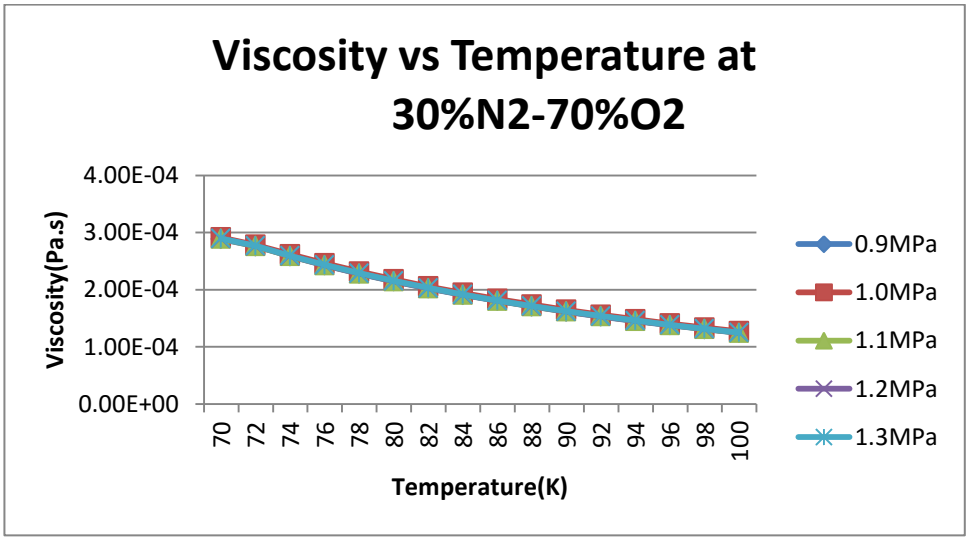

Figure 37Viscosity vs Temperature at 30%N2-70%O2

Figure37 represents the variation of viscosity with respect to temperature at various pressures. It is observed that viscosity decreases with the increase in temperature. It is also seen that there is no significant change in viscosity with the increase in pressure.

`

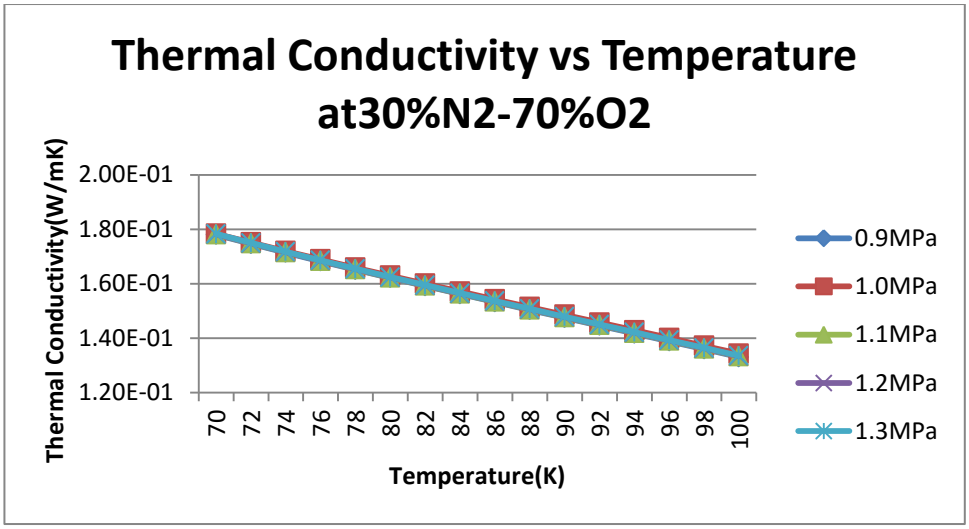

Figure 38Thermal Conductivity vs Temperature at 30%N2-70%O2

Figure38 represents the variation in thermal conductivity with respect to temperature at various pressures. It is observed that with the increase in temperature, thermal conductivity decreases. It is also observed that with the increase in pressurethere is no significant change in thermal conductivity.

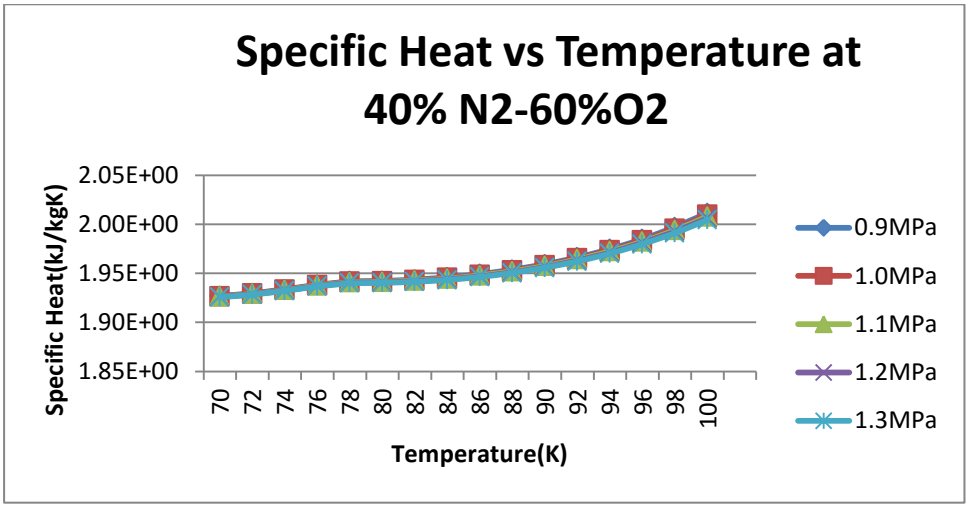

Figure 39Specific Heat vs Temperature at 40% N2-60%O2

Figure39 represents the variation of specific heat as the function of temperature at various pressures. It is observed that as temperature increases, specific heat also increases. It is also observed with increase in pressure, there is no significant change in specific heat.

`

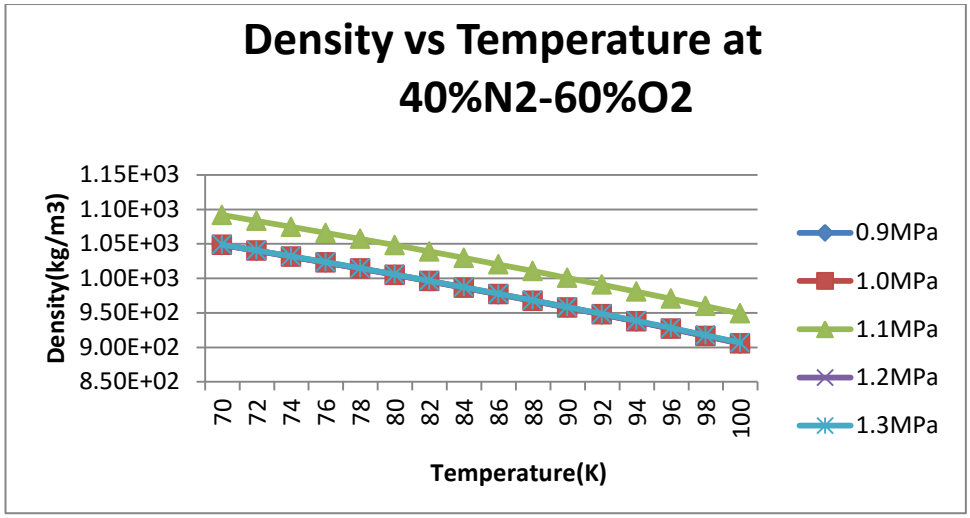

Figure 40Density vs Temperature at 40%N2-60%O2

Figure40 represents the variation of density with respect to temperature at various pressures. It is observed that with the increase in temperature, density decreases gradually. It is also seen that with increase in pressure, density changes.

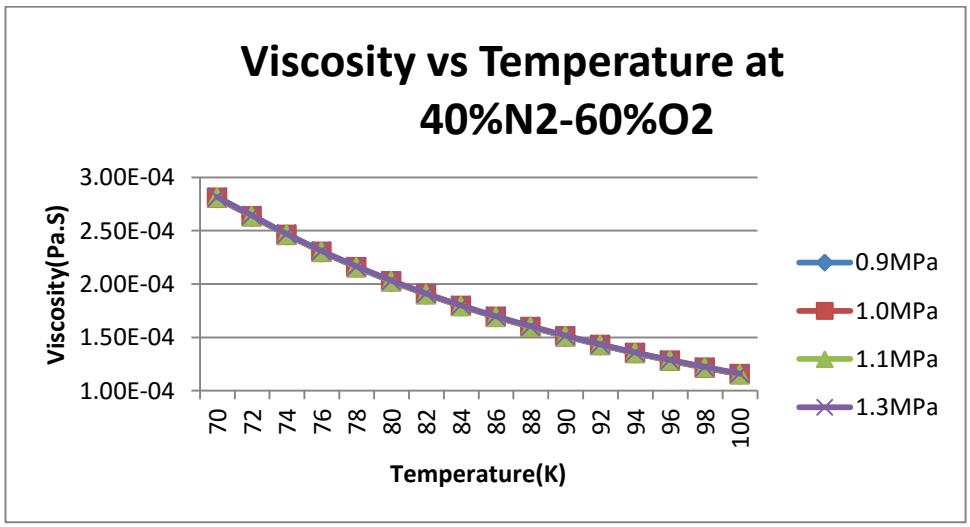

Figure 41Viscosity vs Temperature at 40%N2-60%O2

Figure41 represents the variation of viscosity as the function of temperature at various pressures. It is observed that viscosity decreases with the increase in temperature. It is also seen that there is no significant change in viscosity with the increase in pressure.

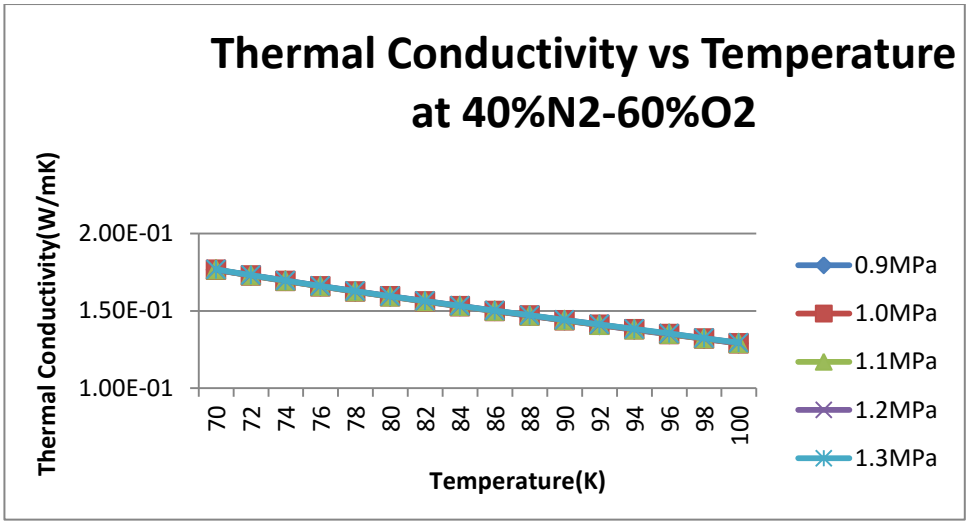

Figure 42Thermal Conductivity vs Temperature at 40%N2-60%O2

Figure42 represents the variation in thermal conductivity with respect to temperature at various pressures. It is observed that with the increase in temperature, thermal conductivity decreases. It is also observed that there is no significant change in thermal conductivity with the increase in pressure.

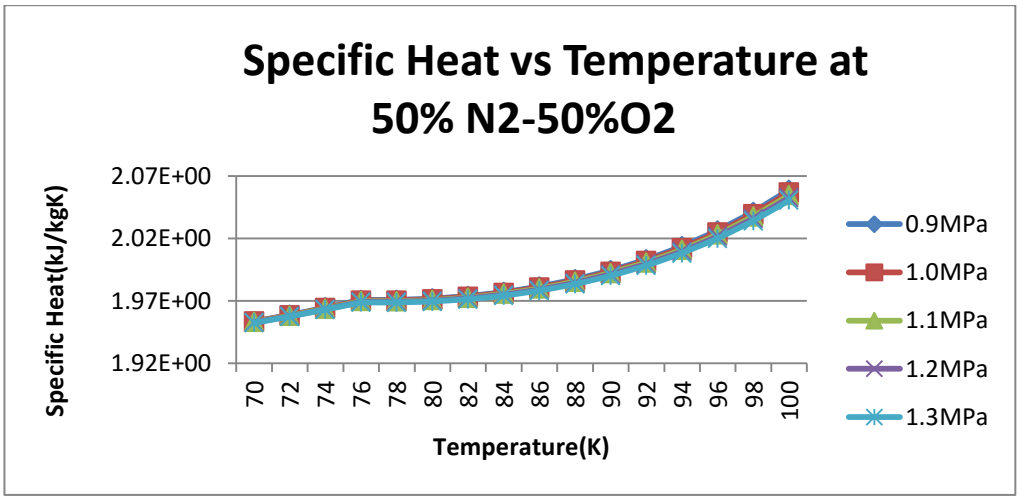

Figure 43Specific Heat vs Temperature at 50% N2-50%O2

Figure43 represents the variation of specific heat as the function of temperature at various pressures. It is observed that as temperature increases, specific heat also increases. It is also observed with increase in pressure, there is no significant change in specific heat.

`

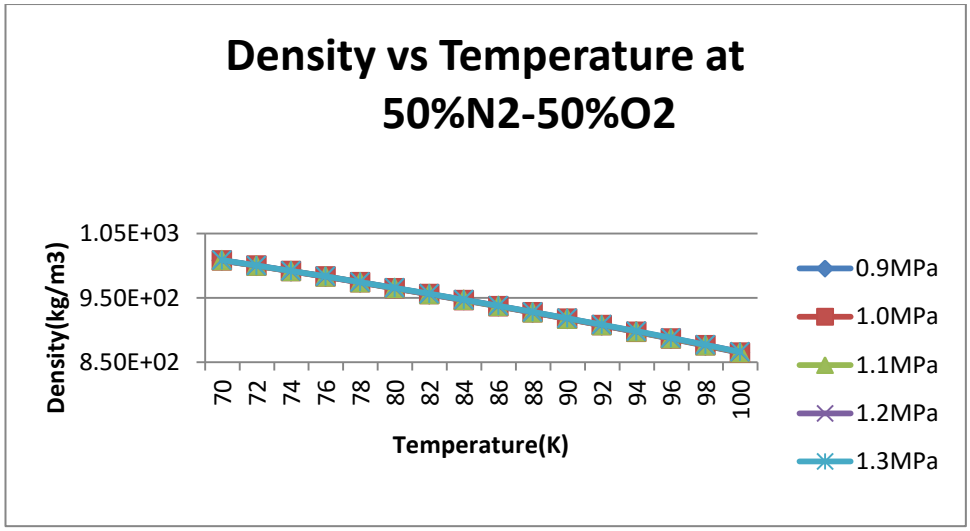

Figure 44Density vs Temperature at 50%N2-50%O2

Figure44 represents the variation of density with respect to temperature at various pressures. It is observed that with the increase in temperature, density decreases gradually. It is also seen that with increase in pressure, there is no significant change in density.

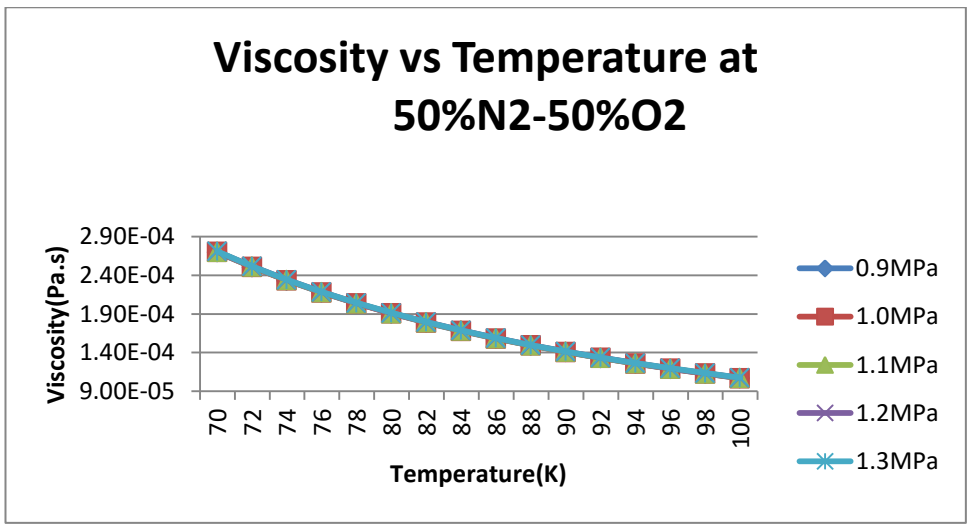

Figure 45Viscosity vs Temperature at 50%N2-50%O2

Figure45 represents the variation of viscosity with respect to temperature at various pressures. It is observed that viscosity decreases with the increase in temperature. It is also seen that there is no significant change in viscosity with the increase in pressure.

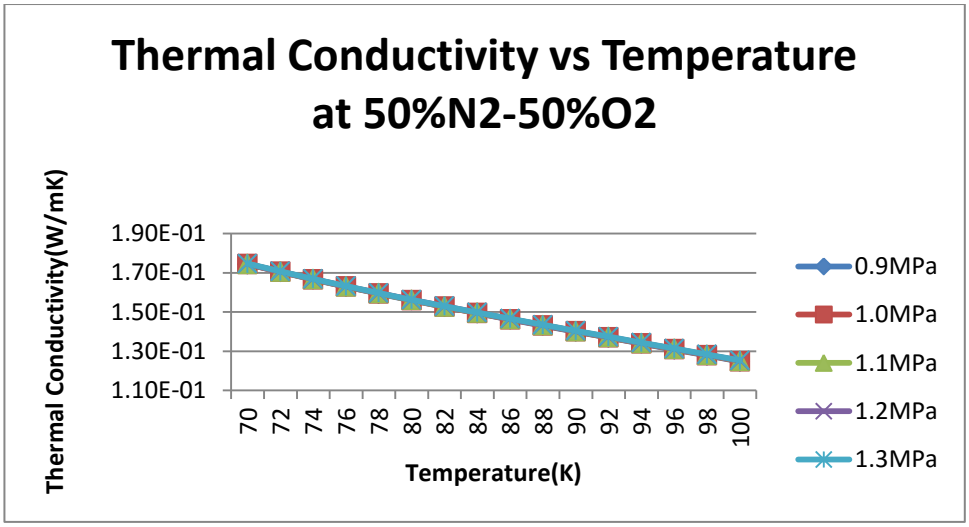

Figure 46Thermal Conductivity vs Temperature at 50%N2-50%O2

Figure46 represents the variation in thermal conductivity with respect to temperature at various pressures. It is observed that with the increase in temperature, thermal conductivity decreases. It is also observed that there is no significant change in thermal conductivity with the increase in pressure.

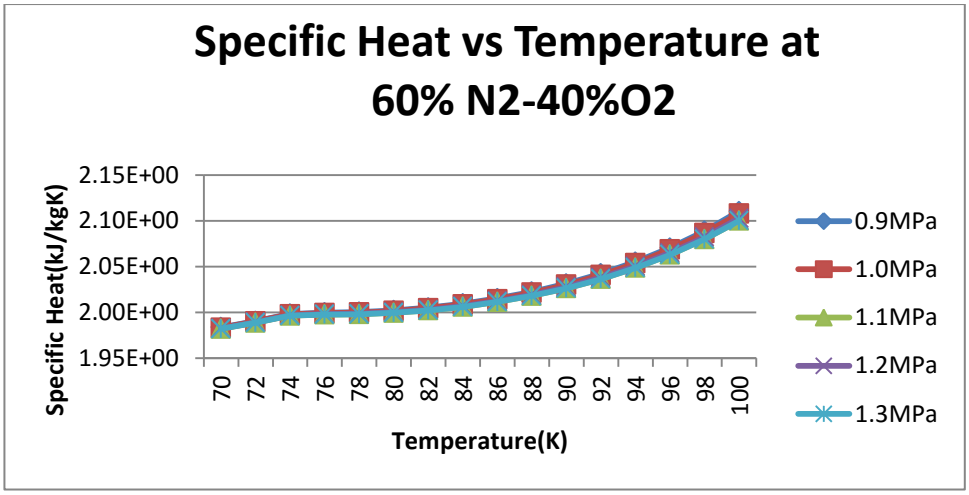

Figure 47Specific Heat vs Temperature at 60% N2-40%O2

Figure47 represents the variation of specific heat as the function of temperature at various pressures. It is observed that as temperature increases, specific heat also increases. It is also observed with increase in pressure, there is no significant change in specific heat.

`

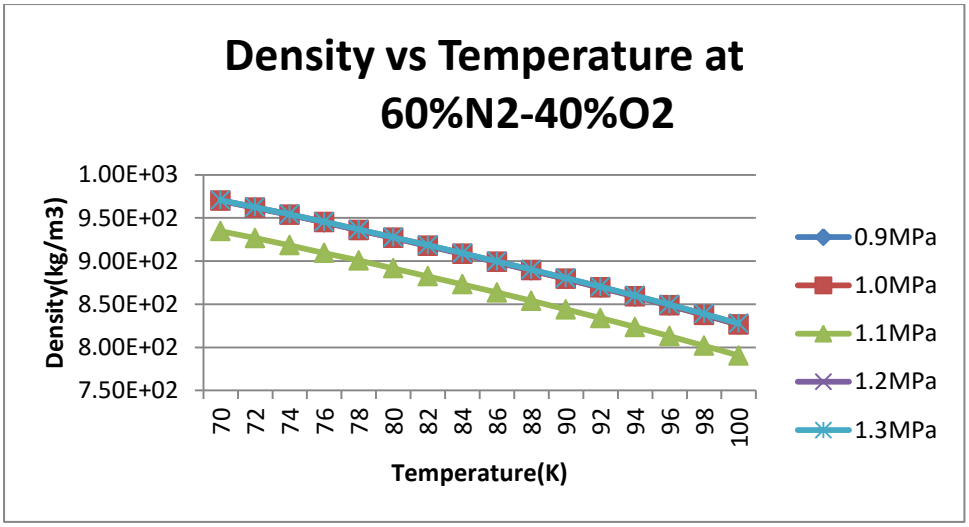

Figure 48Density vs Temperature at 60%N2-40%O2

Figure48 represents the variation of density with respect to temperature at various pressures. It is observed that with the increase in temperature, density decreases gradually. It is also seen that with increase in pressure, there is a change in density.

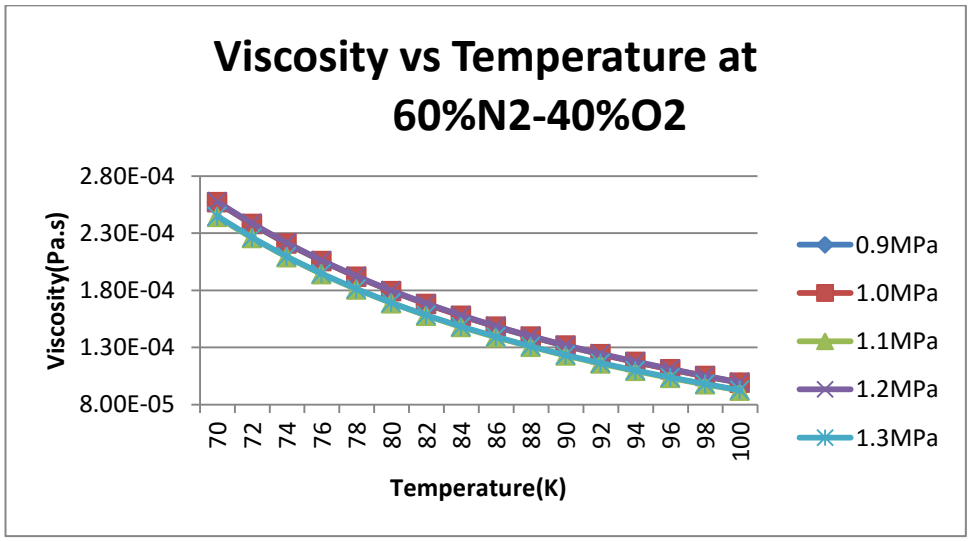

Figure 49Viscosity vs Temperature at 60%N2-40%O2

Figure49 represents the variation of viscosity as the function of temperature at various pressures. It is observed that viscosity decreases with the increase in temperature. It is also seen that there is no significant change in viscosity with the increase in pressure.

`

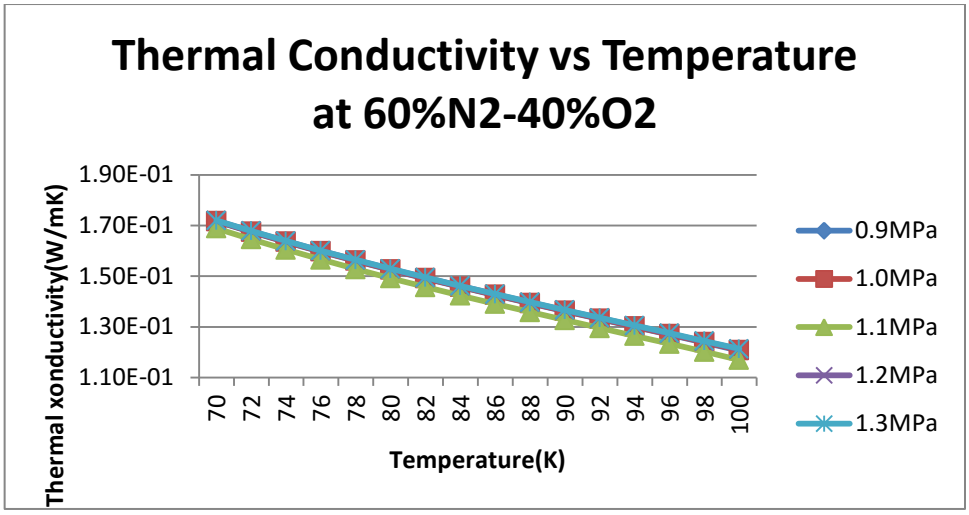

Figure 50Thermal Conductivity vs Temperature at 60%N2-40%O2

Figure50 represents the variation in thermal conductivity as a function of temperature at various pressures. It is observed that with the increase in temperature, thermal conductivity decreases. It is also observed that with the increase in pressurethere is change in thermal conductivity at 1.1 MPa.

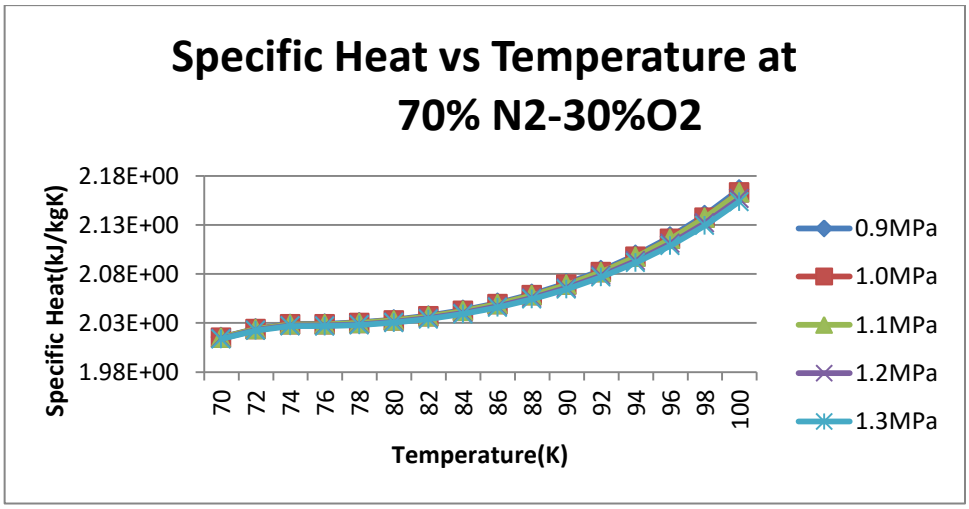

Figure 51Specific Heat vs Temperature at 70% N2-30%O2

Figure51 represents the variation of specific heat as the function of temperature at various pressures. It is observed that as temperature increases, specific heat also increases. It is also observed with increase in pressure, there is no significant change in specific heat.

`

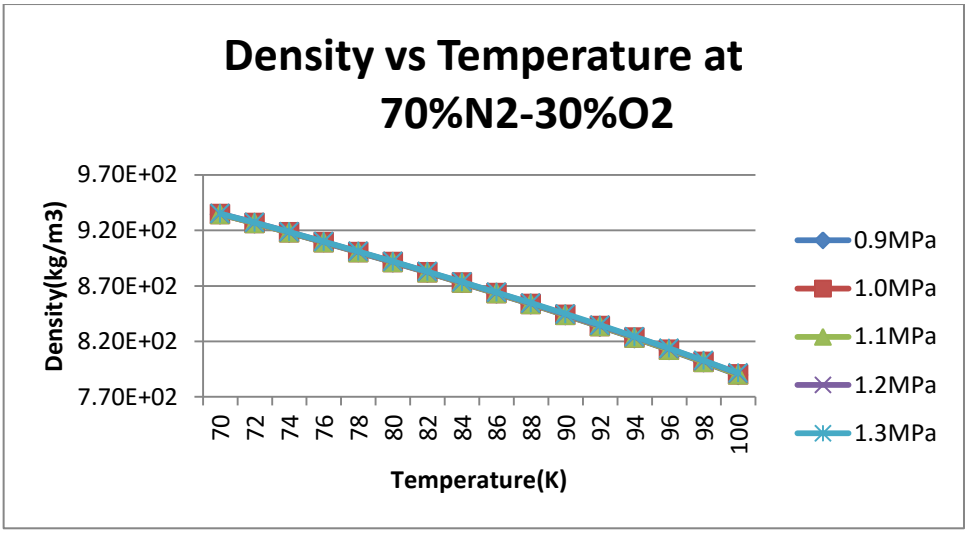

Figure 52Density vs Temperature at 70%N2-30%O2

Figure52 represents the variation of density with respect to temperature at various pressures. It is observed that with the increase in temperature, density decreases gradually. It is also seen that with increase in pressure, there is no significant change in density.

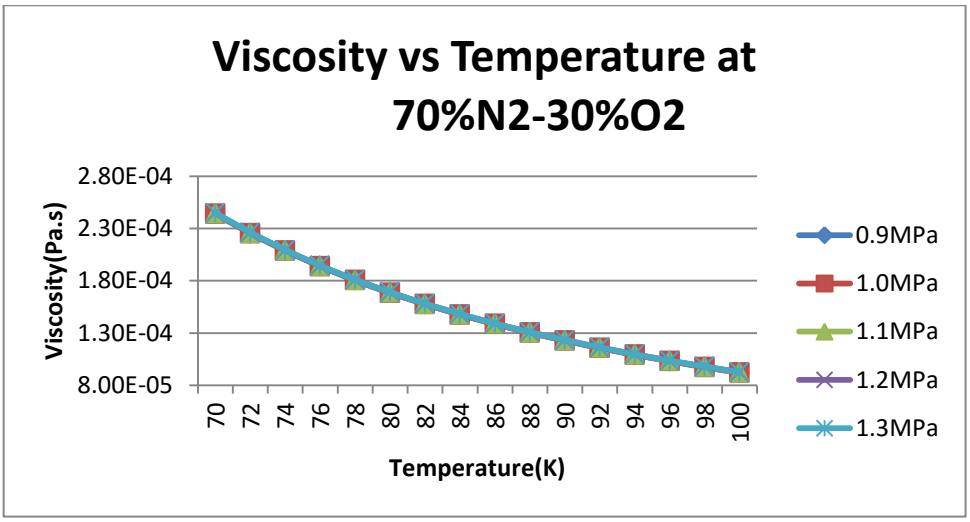

Figure 53Viscosity vs Temperature at 70%N2-30%O2

Figure53 represents the variation of viscosity as the function of temperature at various pressures. It is observed that viscosity decreases with the increase in temperature. It is also seen that there is no significant change in viscosity with the increase in pressure.

`

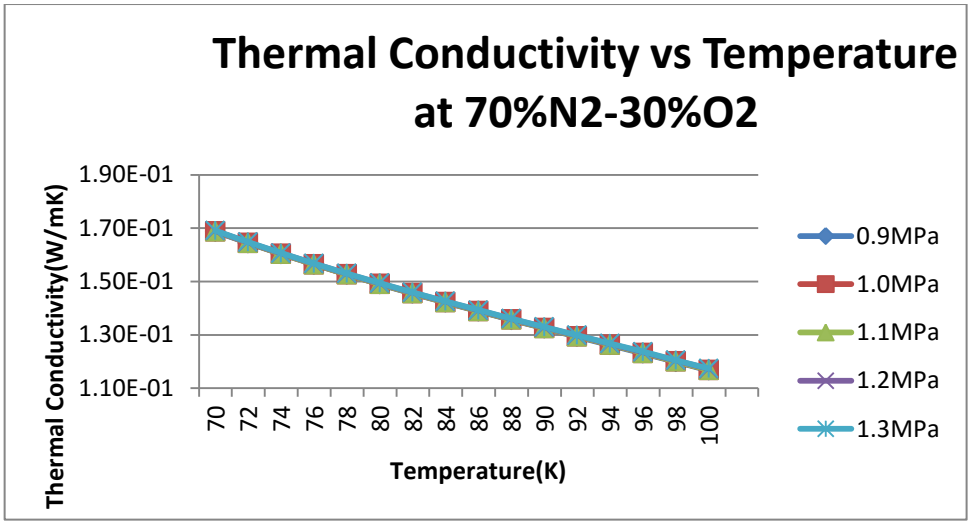

Figure 54Thermal Conductivity vs Temperature at 70%N2-30%O2

Figure54 represents the variation in thermal conductivity with respect to temperature at various pressures. It is observed that with the increase in temperature, thermal conductivity decreases. It is also observed that there is no significant change in thermal conductivity with the increase in pressure.

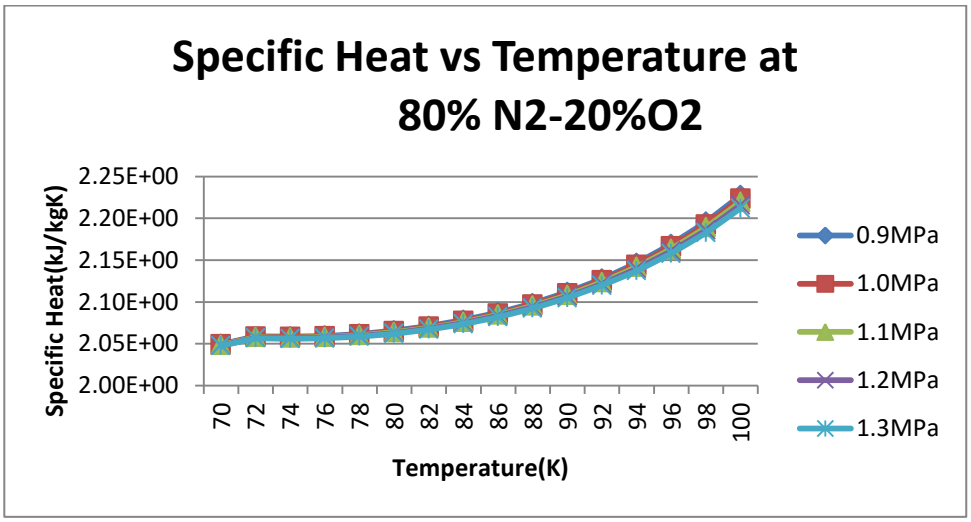

Figure 55Specific Heat vs Temperature at 80% N2-20%O2

Figure55 represents the variation of specific heat as the function of temperature at various pressures. It is observed that as temperature increases, specific heat also increases. It is also observed with increase in pressure, there is no significant change in specific heat.

`

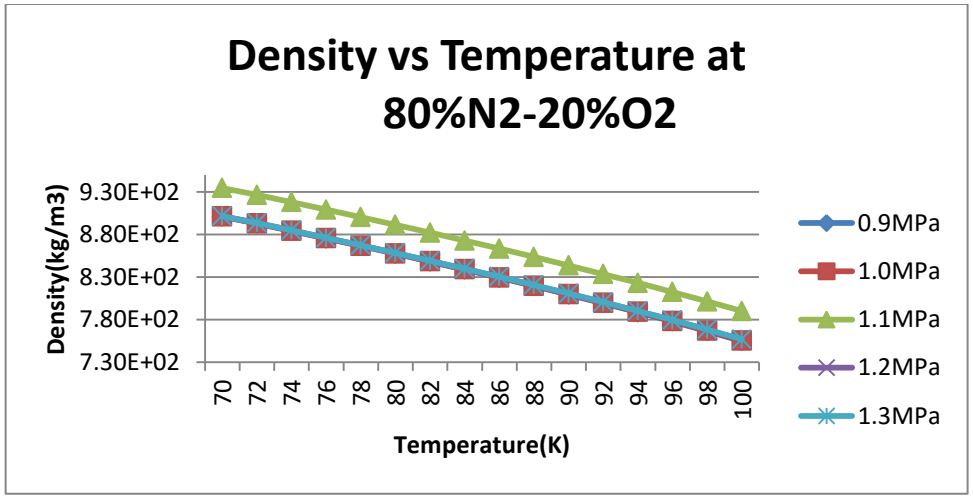

Figure 56Density vs Temperature at 80%N2-20%O2

Figure56 represents the variation of density with respect to temperature at various pressures. It is observed that with the increase in temperature, density decreases gradually. It is also seen that with increase in pressure, density changes.

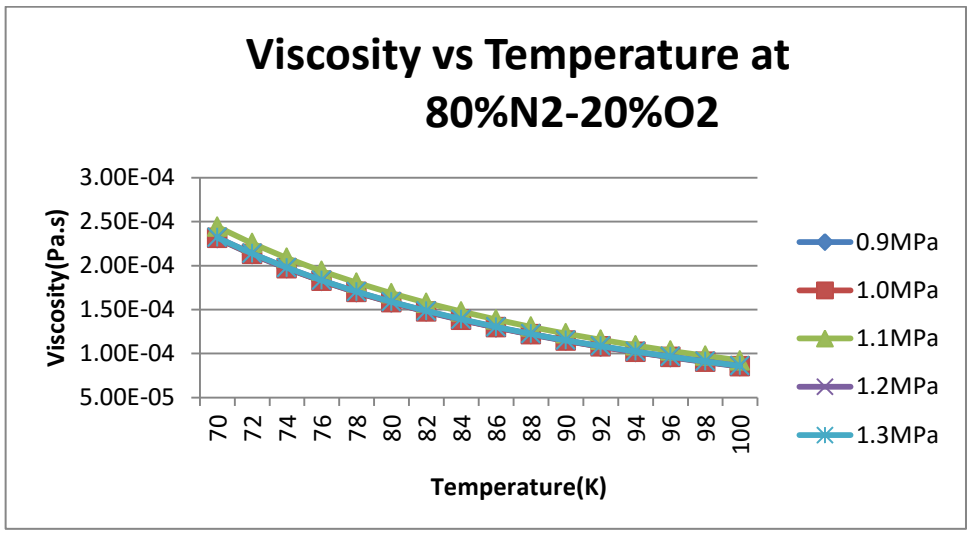

Figure 57Viscosity vs Temperature at 80%N2-20%O2

Figure57 represents the variation of viscosity as the function of temperature at various pressures. It is observed that viscosity decreases with the increase in temperature. It is also seen that there is no significant change in viscosity with the increase in pressure.

`

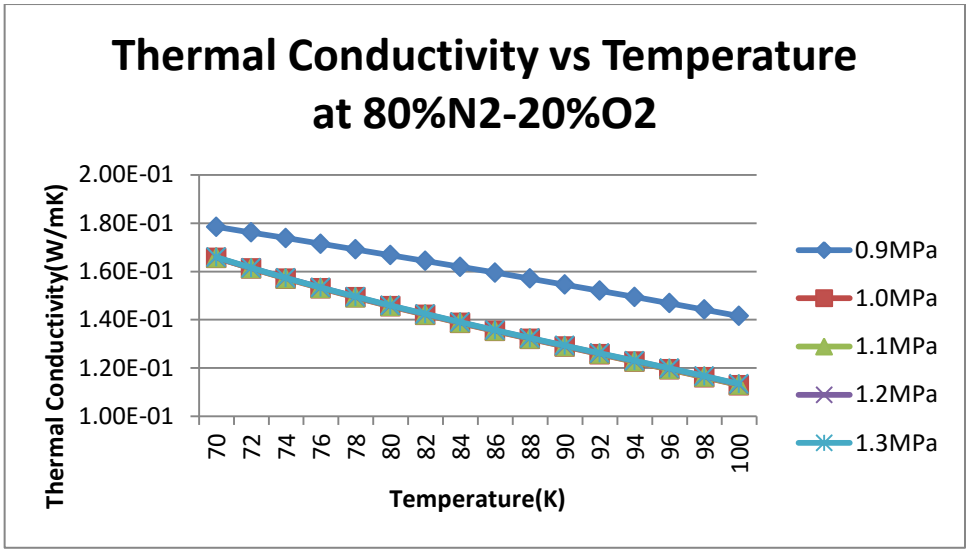

Figure 58Thermal Conductivity vs Temperature at 80%N2-20%O2

Figure58 represents the variation in thermal conductivity with respect to temperature at various pressures. It is observed that with the increase in temperature, thermal conductivity decreases. It is also observed that thermal conductivity changes with the increase in pressure.

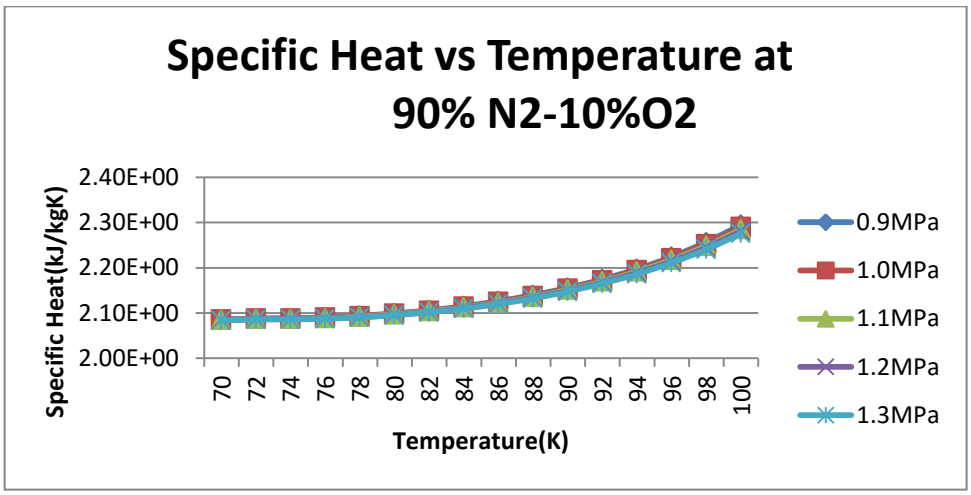

Figure 59Specific Heat vs Temperature at 90% N2-10%O2

Figure59 represents the variation of specific heat as the function of temperature at various pressures. It is observed that as temperature increases, specific heat also increases. It is also observed with increase in pressure, there is no significant change in specific heat.

`

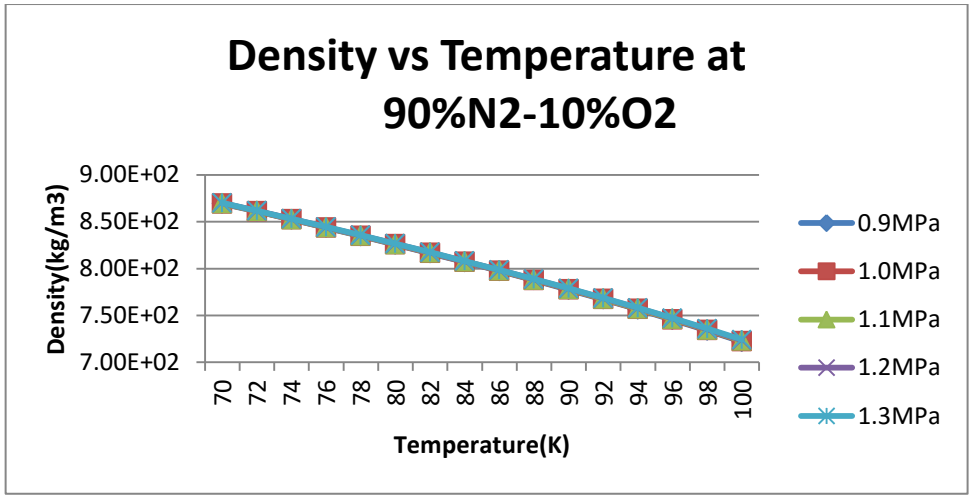

Figure 60Density vs Temperature at 90%N2-10%O2

Figure60 represents the variation of density with respect to temperature at various pressures. It is observed that with the increase in temperature, density decreases gradually. It is also seen that with increase in pressure, there is no significant change in density.

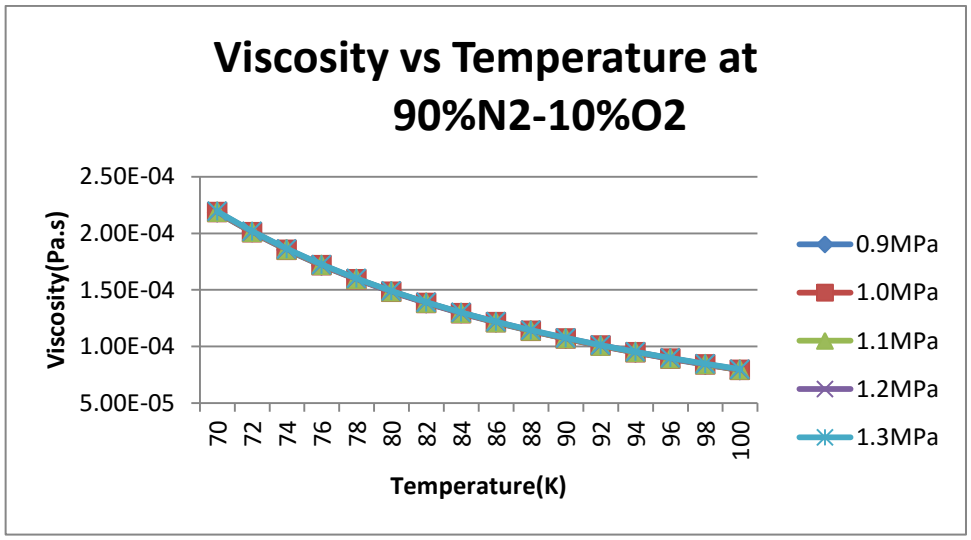

Figure 61Viscosity vs Temperature at 90%N2-10%O2

Figure61 represents the variation of viscosity as the function of temperature at various pressures. It is observed that viscosity decreases with the increase in temperature. It is also seen that there is no significant change in viscosity with the increase in pressure.

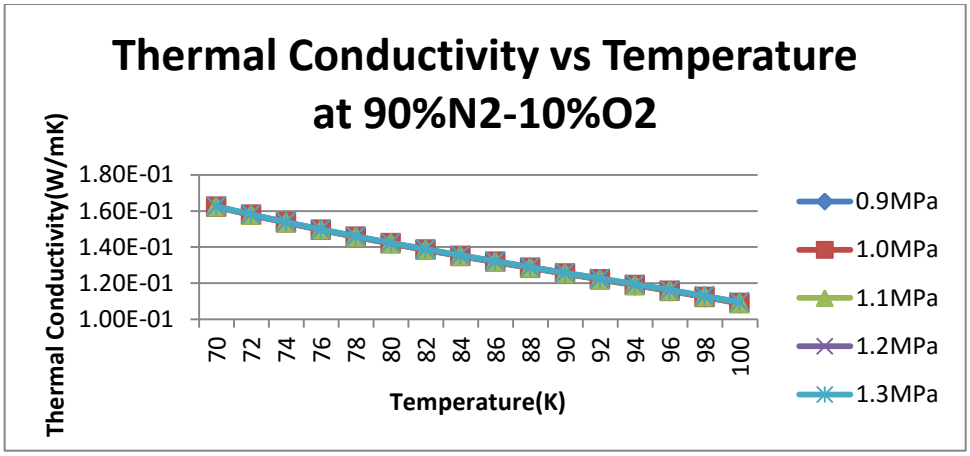

Figure 62Thermal Conductivity vs Temperature at 90%N2-10%O2

Figure 62 represents the variation in thermal conductivity with respect to temperature at various pressures. It is observed that with the increase in temperature, thermal conductivity decreases. It is also observed that there is no significant change in thermal conductivity with the increase in pressure.

7.2 Thermophysical properties of mixed cryogen with nanoparticles

After the dispersion of oxide nanoparticles such as Al_2O_3 and CuO nanoparticles in base fluids, the thermophysical properties are investigated.

7.2.1 Effective Thermal Conductivity using Maxwell Co-relation

For the estimation of effective thermal conductivity, Maxwell Correlation is being used for investigation

7.2.1.1 Effective Thermal Conductivity for Al_2O_3 (Sapphire) Nanoparticle

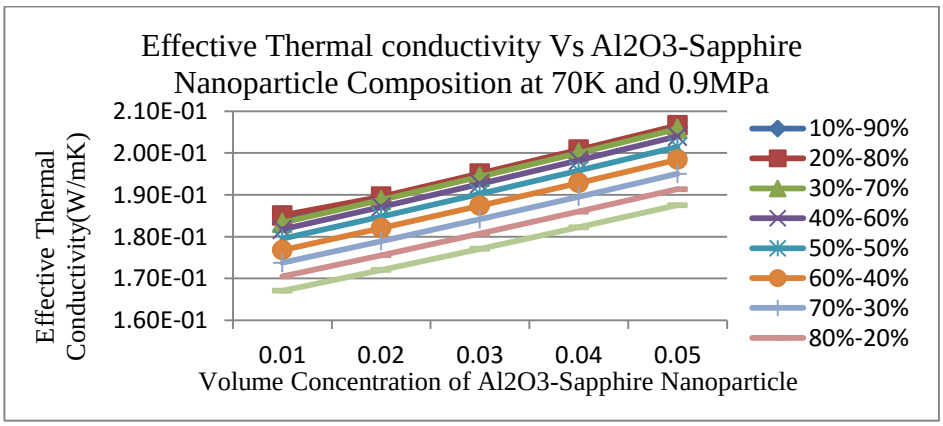

Figure 63 Effective Thermal conductivity Vs Al2O3-Sapphire at 70K and 0.9 MPa

`

Figure63 represents the variation in thermal conductivity with respect to volume concentration of Al2O3- Sapphire nanoparticle at various composition of mixed cryogen. It is observed that with the increase in volume concentration of Al2O3 nanoparticle, thermal conductivity increases. It is also observed that with decrease in liquid oxygen composition in mixed cryogen thermal conductivity increases.

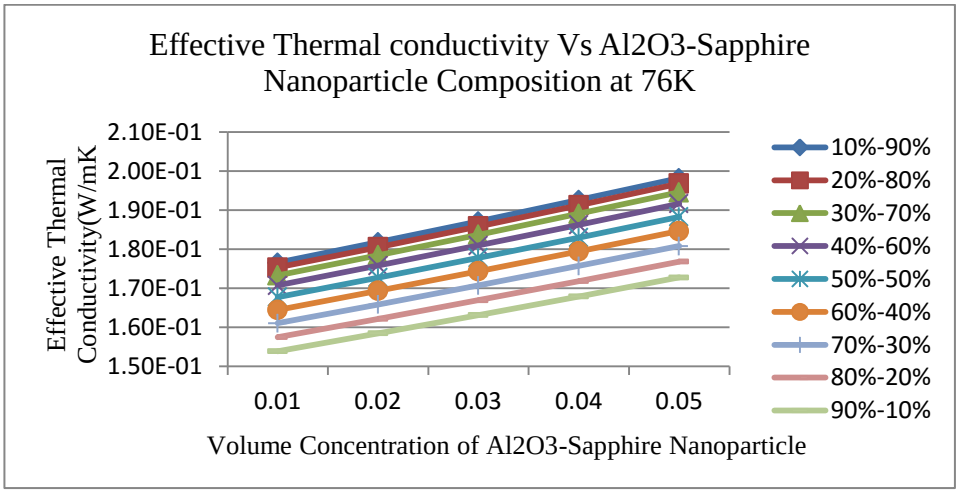

Figure 64 Effective Thermal conductivity Vs Al2O3-Sapphire at 76K and 0.9MPa

Figure64 represents the variation in effective thermal conductivity with respect to volume concentration of Al2O3- Sapphire nanoparticle at various composition of mixed cryogen. It is observed that with the increase in volume concentration of Al2O3 nanoparticle, thermal conductivity increases. It is also observed that with decrease in liquid oxygen composition in mixed cryogen thermal conductivity increases.

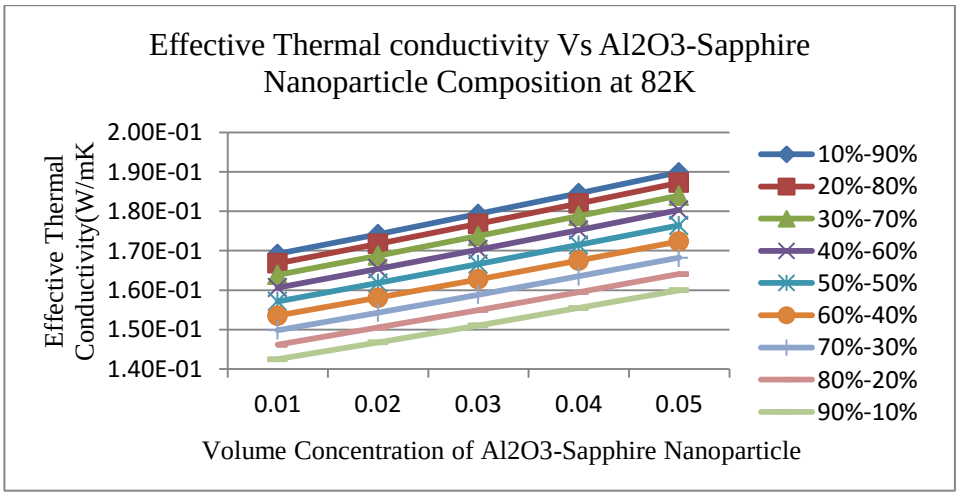

Figure 65Effective Thermal conductivity Vs Al2O3-Sapphire at 76K and 0.9 MPa

`

Figure65 represents the variation in effective thermal conductivity with respect to volume concentration of Al2O3- Sapphire nanoparticle at various composition of mixed cryogen. It is observed that with the increase in volume concentration of Al2O3 nanoparticle, thermal conductivity increases. It is also observed that with decrease in liquid oxygen composition in mixed cryogen thermal conductivity increases.

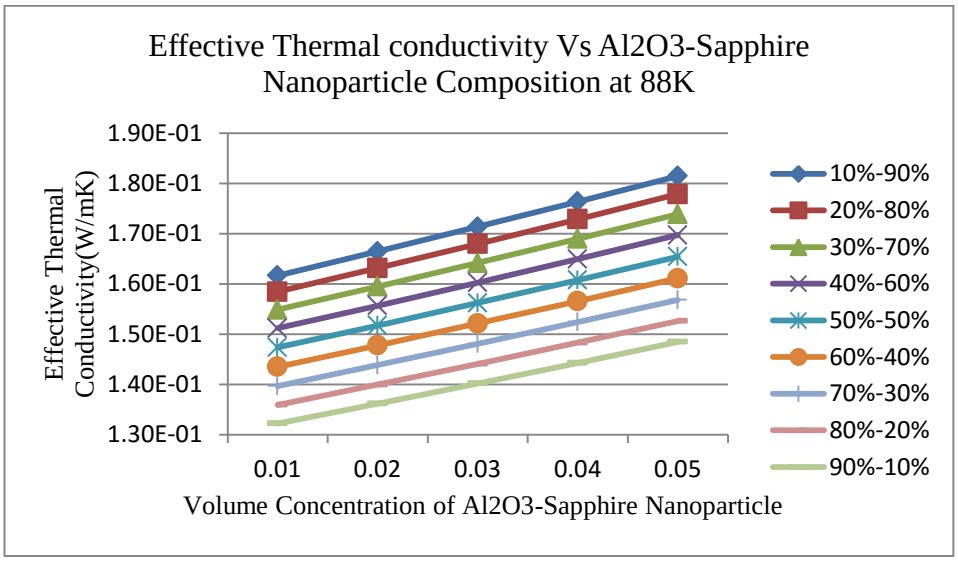

Figure 66 Effective Thermal conductivity Vs Al2O3-Sapphire at 88K and 0.9MPa

Figure 66 represents the variation in effective thermal conductivity with respect to volume concentration of Al2O3- Sapphire nanoparticle at various composition of mixed cryogen. It is observed that with the increase in volume concentration of Al2O3 nanoparticle, thermal conductivity increases. It is also observed that with decrease in liquid oxygen composition in mixed cryogen thermal conductivity increases.

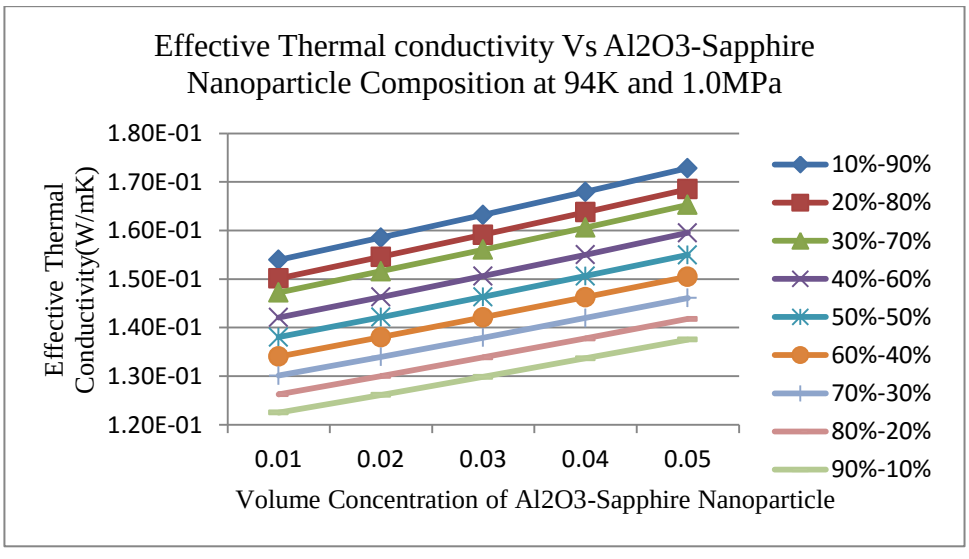

`

Figure 67Effective Thermal conductivity Vs Al2O3-Sapphire at 94K and 0.9MPa

Figure67 represents the variation in effective thermal conductivity with respect to volume concentration of Al2O3- Sapphire nanoparticle at various composition of mixed cryogen. It is observed that with the increase in volume concentration of Al2O3 nanoparticle, thermal conductivity increases. It is also observed that with decrease in liquid oxygen composition in mixed cryogen thermal conductivity increases.

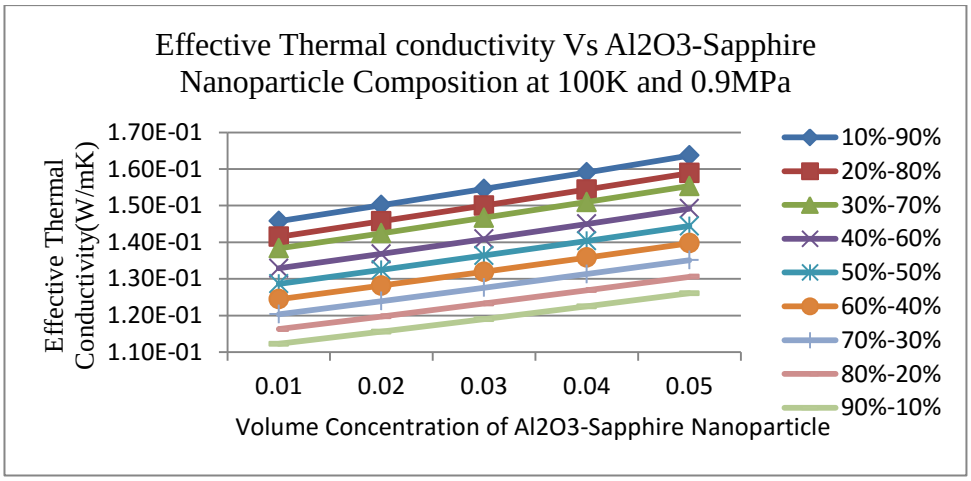

Figure 68Effective Thermal conductivity Vs Al2O3-Sapphire at 100K and 0.9MPa

Figure68 represents the variation in effective thermal conductivity with respect to volume concentration of Al2O3- Sapphire nanoparticle at various composition of mixed cryogen. It is observed that with the increase in volume concentration of Al2O3 nanoparticle, thermal conductivity increases. It is also observed that with decrease in liquid oxygen composition in mixed cryogen thermal conductivity increases.

`

7.2.1.2 Effective Thermal Conductivity for CuO Nanoparticle

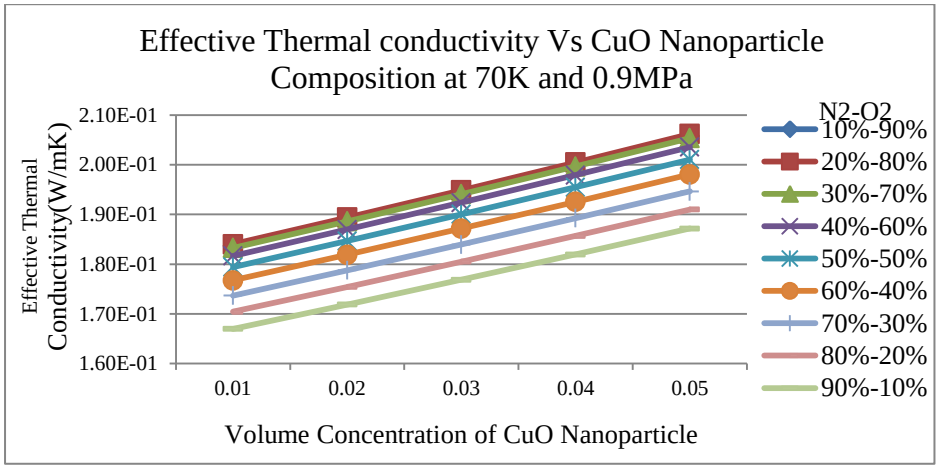

Figure 69 Effective Thermal conductivity Vs CuO at 70K and 0.9MPa

Figure69 represents the variation in effective thermal conductivity with respect to volume concentration of CuO nanoparticle at various composition of mixed cryogen. It is observed that with the increase in volume concentration of CuO nanoparticle, thermal conductivity increases. It is also observed that with decrease in liquid oxygen composition in mixed cryogen thermal conductivity increases.

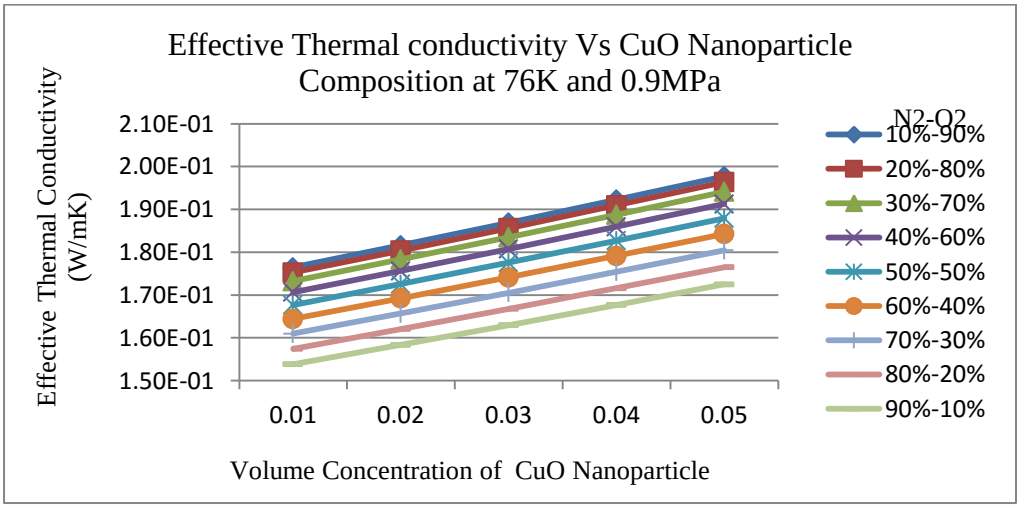

Figure 70 Effective Thermal conductivity Vs CuO at 76K and 0.9MPa

Figure70 represents the variation in effective thermal conductivity with respect to volume concentration of CuO nanoparticle at various composition of mixed cryogen. It is observed that with the increase in volume concentration of CuO nanoparticle, thermal conductivity increases. It is also observed that with decrease in liquid oxygen composition in mixed cryogen thermal conductivity increases.

`

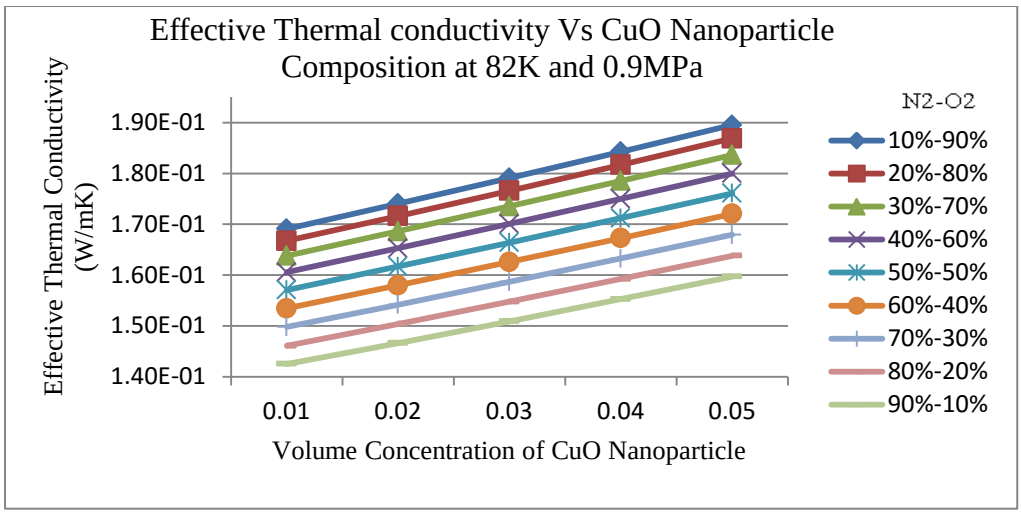

Figure 71 Effective Thermal conductivity Vs CuO at 82K and 0.9MPa

Figure71 represents the variation in effective thermal conductivity with respect to volume concentration of CuO nanoparticle at various composition of mixed cryogen. It is observed that with the increase in volume concentration of CuO nanoparticle, thermal conductivity increases. It is also observed that with decrease in liquid oxygen composition in mixed cryogen thermal conductivity increases.

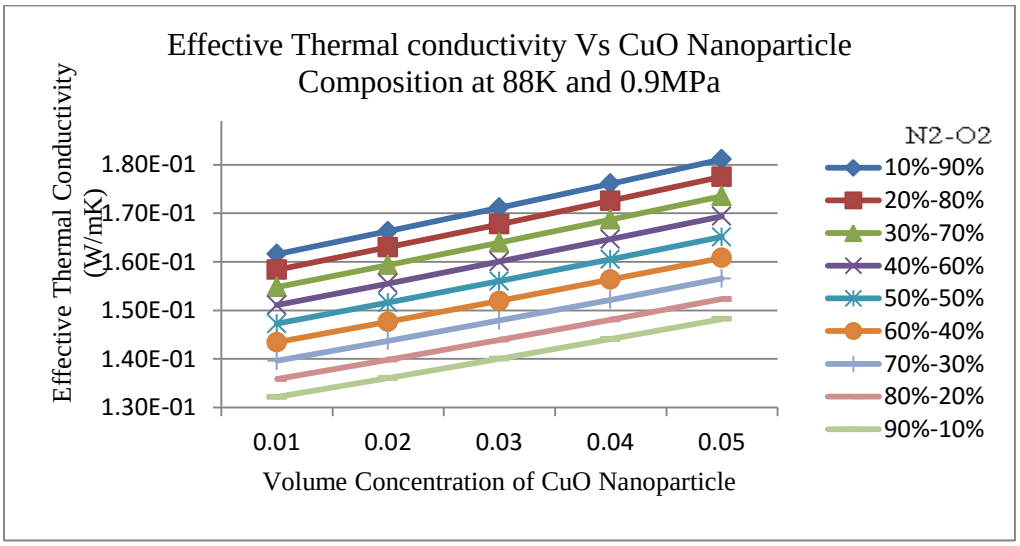

Figure 72 Effective Thermal conductivity Vs CuO at 88K and 0.9MPa

Figure72 represents the variation in effective thermal conductivity with respect to volume concentration of CuO nanoparticle at various composition of mixed cryogen. It is observed that with the increase in volume concentration of CuO nanoparticle, thermal conductivity increases. It is also observed that with decrease in liquid oxygen composition in mixed cryogen thermal conductivity increases.

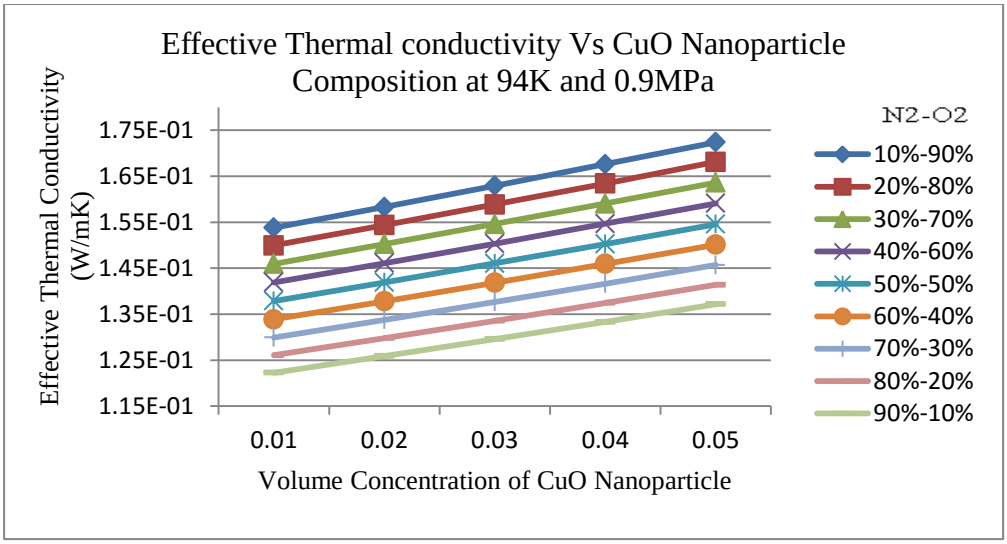

Figure 73 Effective Thermal conductivity Vs CuO at 94K and 0.9MPa

Figure73 represents the variation in effective thermal conductivity with respect to volume concentration of CuO nanoparticle at various composition of mixed cryogen. It is observed that with the increase in volume concentration of CuO nanoparticle, thermal conductivity increases. It is also observed that with decrease in liquid oxygen composition in mixed cryogen thermal conductivity increases.

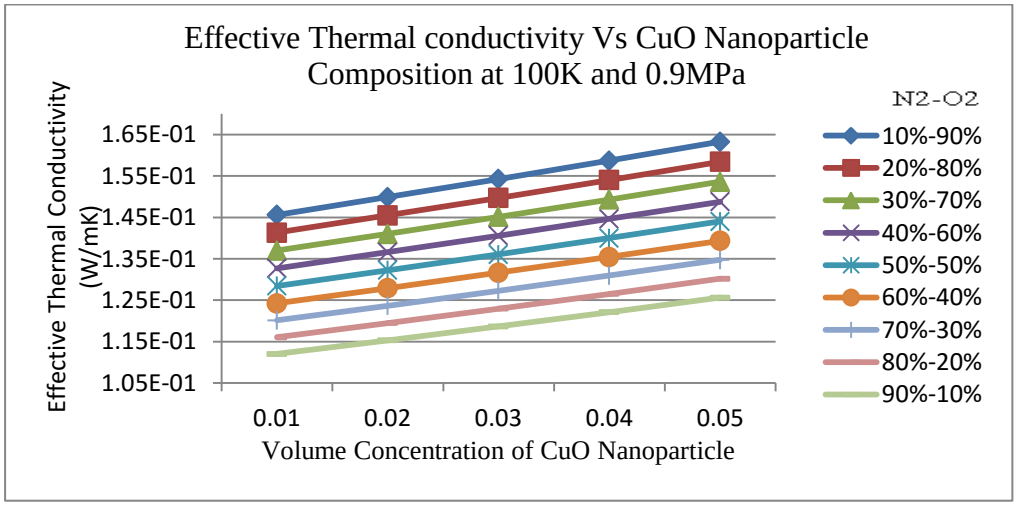

Figure 74 Effective Thermal conductivity Vs CuO at 100K and 0.9MPa

Figure74 represents the variation in effective thermal conductivity with respect to volume concentration of CuO nanoparticle at various composition of mixed cryogen. It is observed that with the increase in volume concentration of CuO nanoparticle, thermal conductivity increases. It is also observed that with decrease in liquid oxygen composition in mixed cryogen thermal conductivity increases.

`

7.2.2 Effective Viscosity using Drew and Passman Co-relation

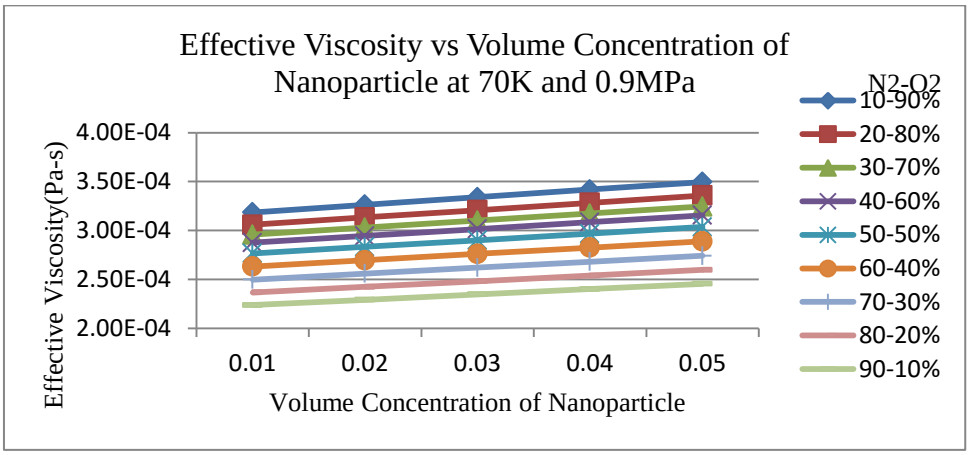

Figure 75Effective Viscosity vs Nanoparticle at 70K and 0.9MPa

Figure75 represents the variation in effective viscosity with respect to volume concentration of nanoparticle at various composition of mixed cryogen. It is observed that with the increase in volume concentration of nanoparticle, viscosity increases. It is also observed that with decrease in liquid oxygen composition in mixed cryogen effective viscosity increases.

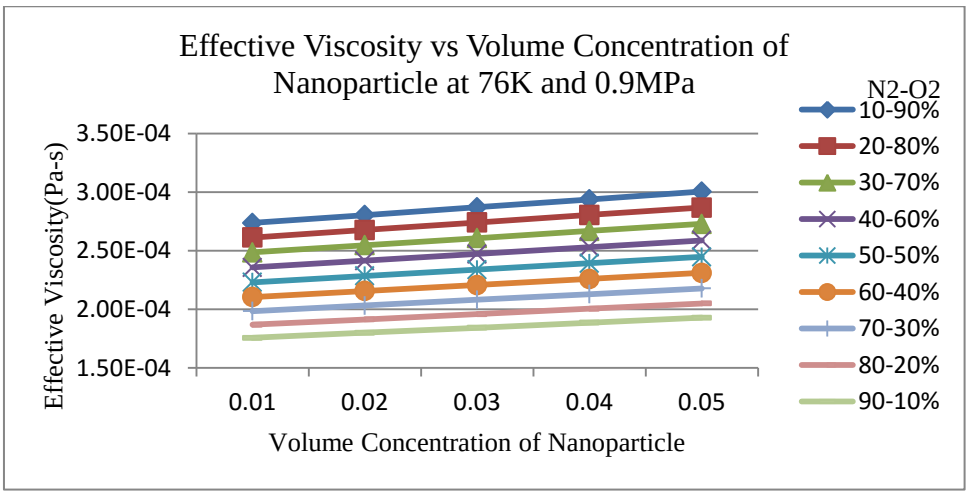

Figure 76Effective Viscosity vs Nanoparticle at 70K and 0.9MPa

Figure76 represents the variation in effective viscosity with respect to volume concentration of nanoparticle at various composition of mixed cryogen. It is observed that with the increase in volume concentration of nanoparticle, viscosity increases. It is also observed that with decrease in liquid oxygen composition in mixed cryogen effective viscosity increases.

`

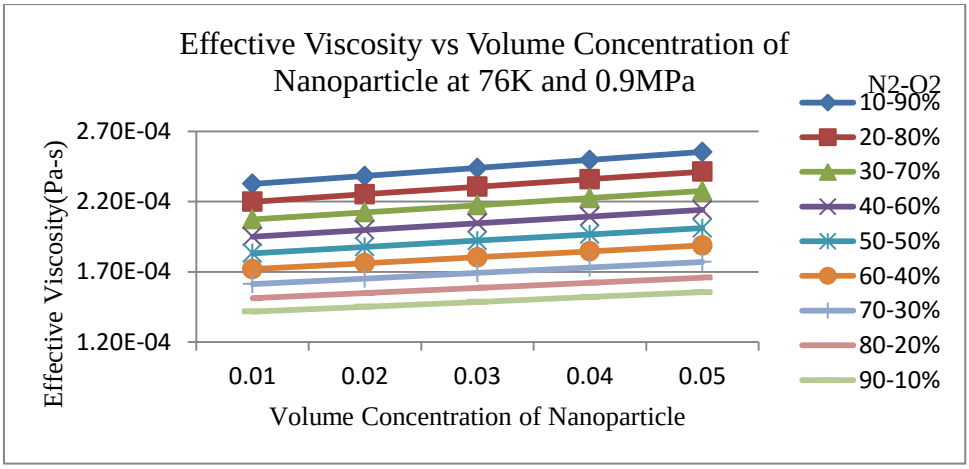

Figure 77Effective Viscosity vs Nanoparticle at 76K and 0.9MPa

Figure77 represents the variation in effective viscosity with respect to volume concentration of nanoparticle at various composition of mixed cryogen. It is observed that with the increase in volume concentration of nanoparticle, viscosity increases. It is also observed that with decrease in liquid oxygen composition in mixed cryogen effective viscosity increases.

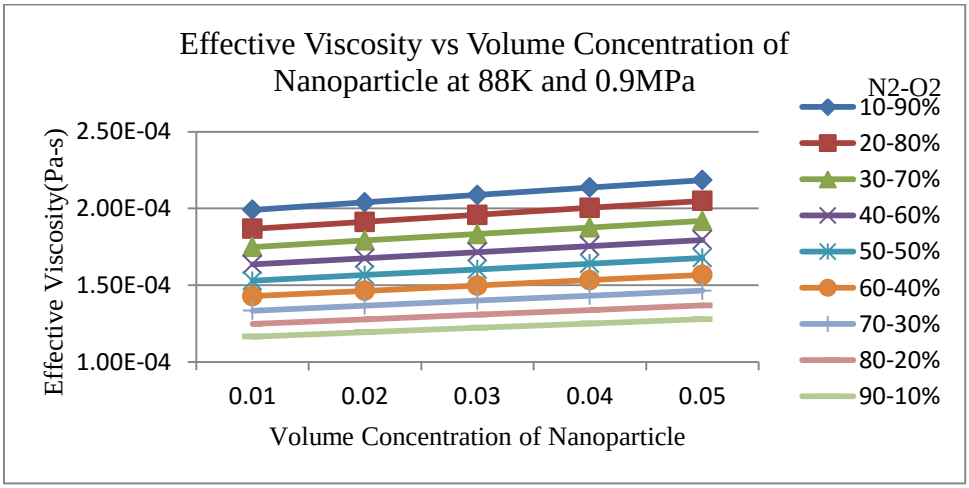

Figure 78Effective Viscosity vs Nanoparticle at 88K and 0.9MPa

Figure78 represents the variation in effective viscosity with respect to volume concentration of nanoparticle at various composition of mixed cryogen. It is observed that with the increase in volume concentration of nanoparticle, viscosity increases. It is also observed that with decrease in liquid oxygen composition in mixed cryogen effective viscosity increases.

`

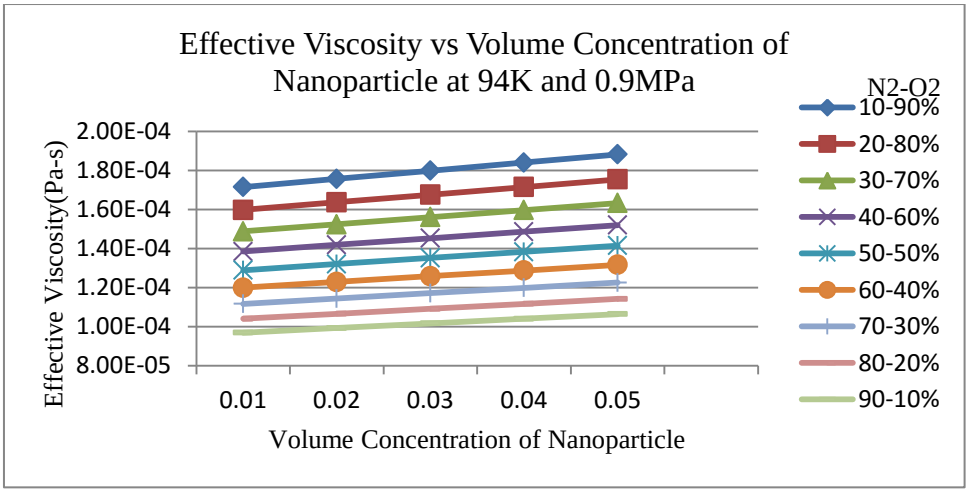

Figure 79Effective Viscosity vs Nanoparticle at 94K and 0.9MPa

Figure79 represents the variation in effective viscosity with respect to volume concentration of nanoparticle at various composition of mixed cryogen. It is observed that with the increase in volume concentration of nanoparticle, viscosity increases. It is also observed that with decrease in liquid oxygen composition in mixed cryogen effective viscosity increases.

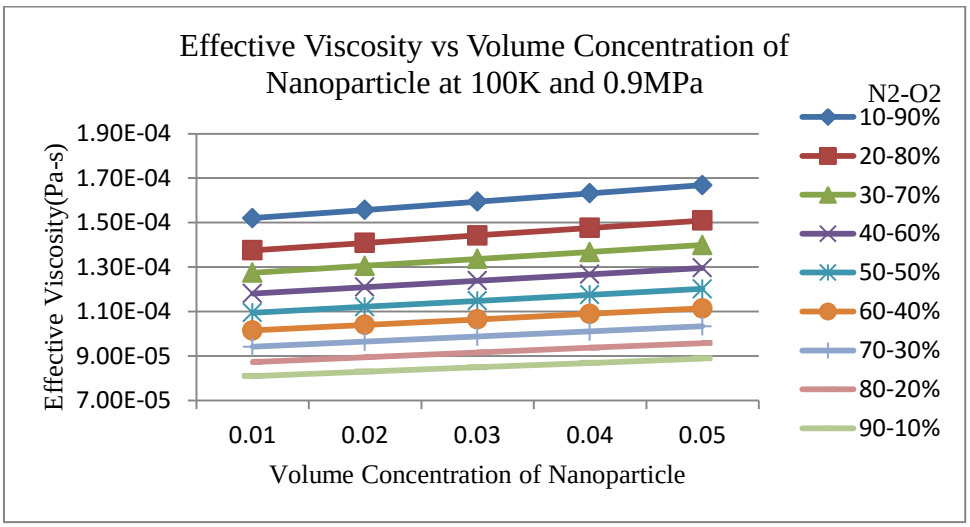

Figure 80Effective Viscosity vs Nanoparticle at 100K and 0.9MPa

Figure80 represents the variation in effective viscosity with respect to volume concentration of nanoparticle at various composition of mixed cryogen. It is observed that with the increase in volume concentration of nanoparticle, viscosity increases. It is also observed that with decrease in liquid oxygen composition in mixed cryogen effective viscosity increases.

`

7.2.3 Effective Density

Effective density is being calculated for various nanoparticles as following

7.2.3.1 Effective Density for Al_2O_3 (Sapphire) Nanoparticle

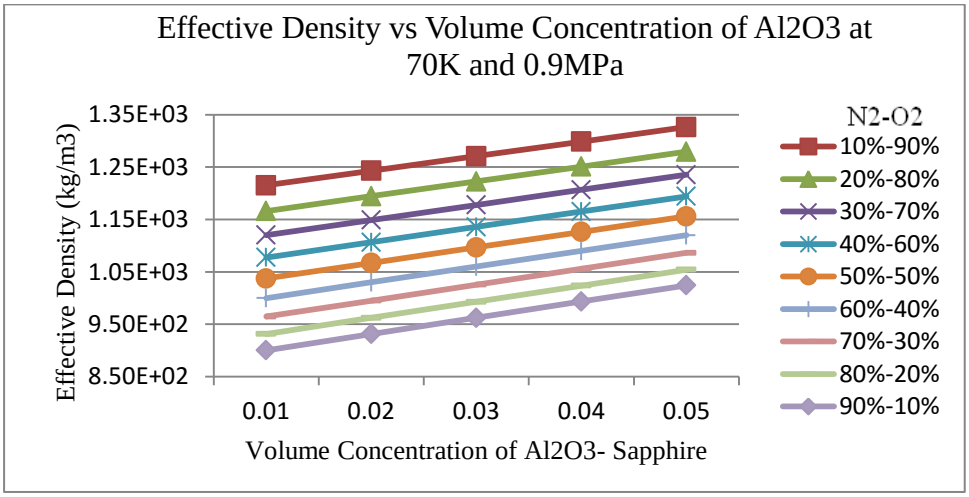

Figure 81Effective Density vs Al2O3 at 70K and 0.9MPa

Figure77 represents the variation in effective density with respect to volume concentration of Al2O3- Sapphire nanoparticle at various composition of mixed cryogen. It is observed that with the increase in volume concentration of Al2O3- Sapphire nanoparticle, effective density increases. It is also observed that with decrease in liquid oxygen composition in mixed cryogen effective density increases.

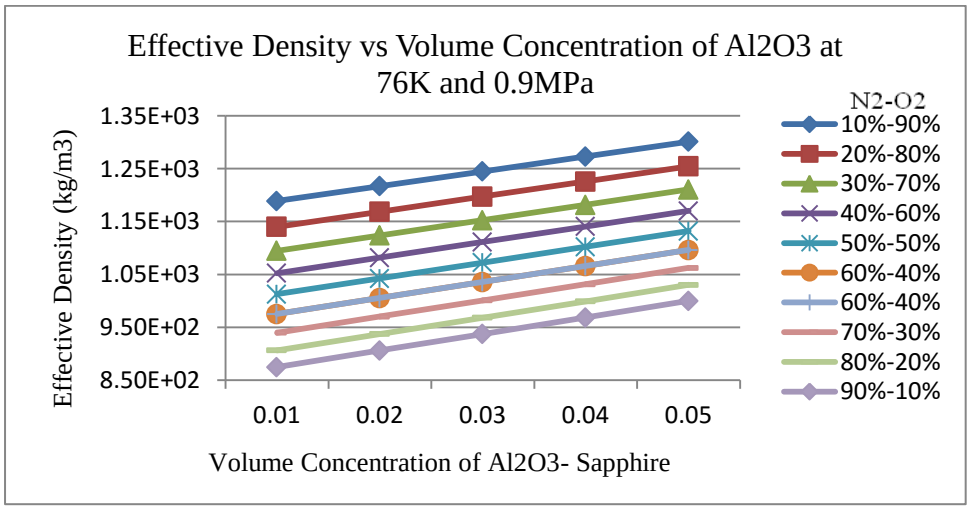

Figure 82Effective Density vs Al2O3 at 76K and 0.9MPa

`

Figure82 represents the variation in effective density with respect to volume concentration of Al2O3- Sapphire nanoparticle at various composition of mixed cryogen. It is observed that with the increase in volume concentration Al2O3- Sapphire of nanoparticle, effective density increases. It is also observed that with decrease in liquid oxygen composition in mixed cryogen effective density increases.

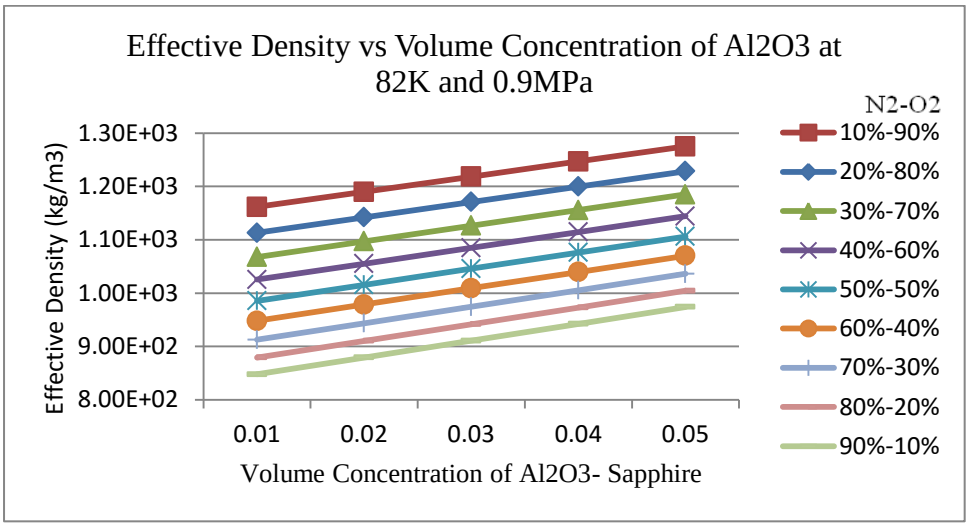

Figure 83Effective Density vs Al2O3 at 82K and 0.9MPa

Figure83 represents the variation in effective density with respect to volume concentration of Al2O3- Sapphire nanoparticle at various composition of mixed cryogen. It is observed that with the increase in volume concentration of Al2O3- Sapphire nanoparticle, effective density increases. It is also observed that with decrease in liquid oxygen composition in mixed cryogen effective density increases.

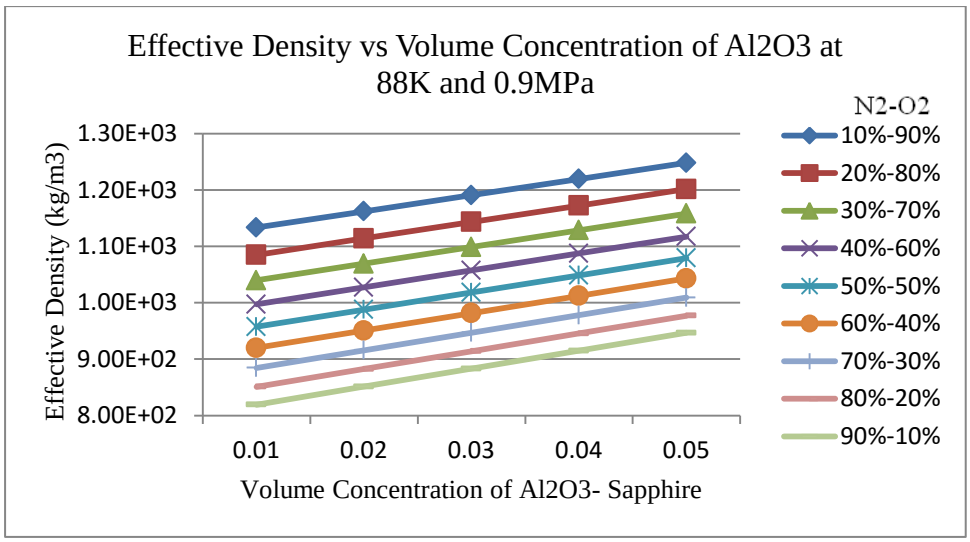

Figure 84Effective Density vs Al2O3 at 88K and 0.9MPa

`

Figure84 represents the variation in effective density with respect to volume concentration of Al2O3- Sapphire nanoparticle at various composition of mixed cryogen. It is observed that with the increase in volume concentration of Al2O3- Sapphire nanoparticle, effective density increases. It is also observed that with decrease in liquid oxygen composition in mixed cryogen effective density increases.

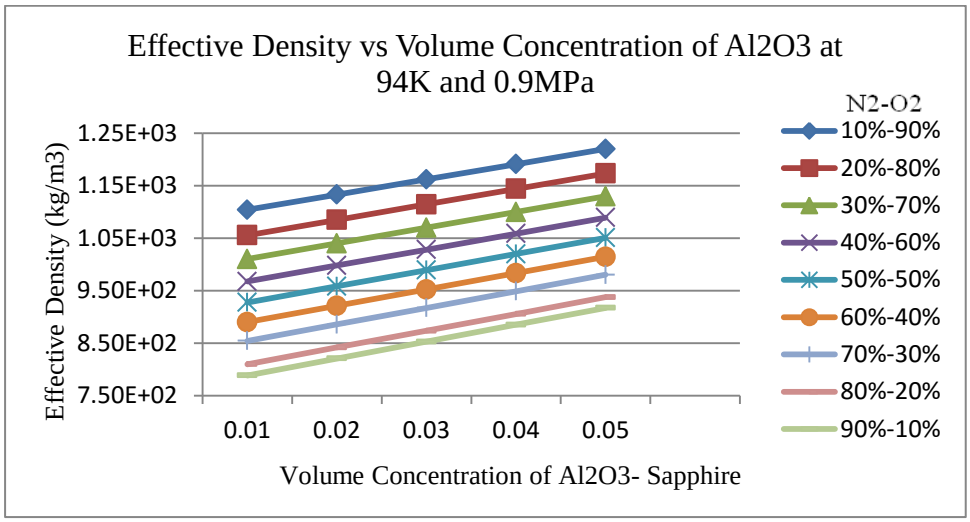

Figure 85Effective Density vs Al2O3 at 94K and 0.9MPa

Figure85 represents the variation in effective density with respect to volume concentration of Al2O3- Sapphire nanoparticle at various composition of mixed cryogen. It is observed that with the increase in volume concentration of Al2O3- Sapphire nanoparticle, effective density increases. It is also observed that with decrease in liquid oxygen composition in mixed cryogen effective density increases.

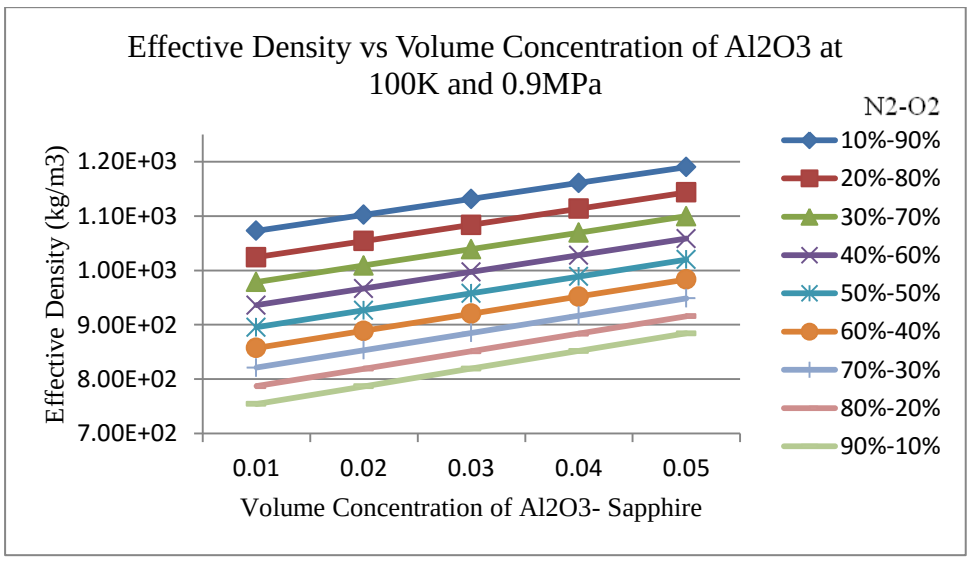

Figure 86Effective Density vs Al2O3 at 100K and 0.9MPa

`

Figure86 represents the variation in effective density with respect to volume concentration of Al2O3- Sapphire nanoparticle at various composition of mixed cryogen. It is observed that with the increase in volume concentration of Al2O3- Sapphire nanoparticle, effective density increases. It is also observed that with decrease in liquid oxygen composition in mixed cryogen effective density increases.

7.2.3.1 Effective Density for CuO Nanoparticle

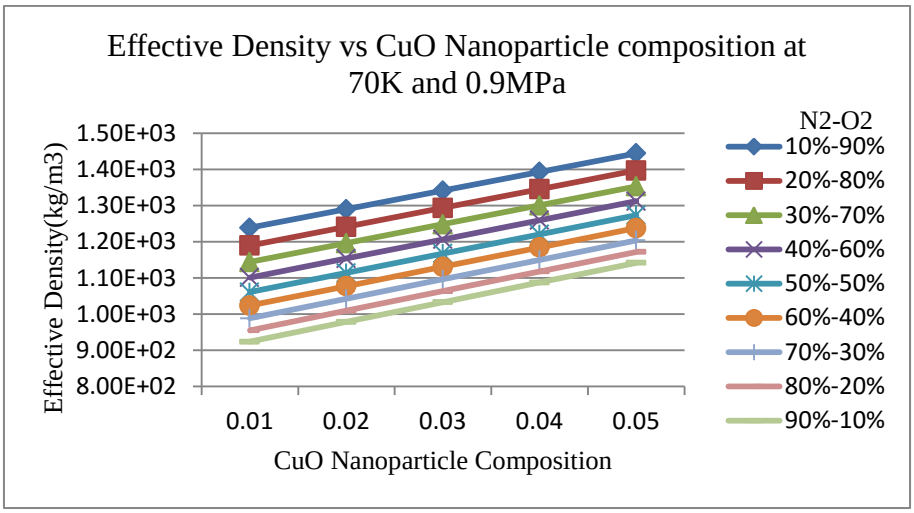

Figure 87 Effective Density vs CuO at 70K and 0.9MPa

Figure87 represents the variation in effective density with respect to volume concentration of CuO nanoparticle at various composition of mixed cryogen. It is observed that with the increase in volume concentration of CuO nanoparticle, effective density increases. It is also observed that with decrease in liquid oxygen composition in mixed cryogen effective density increases.

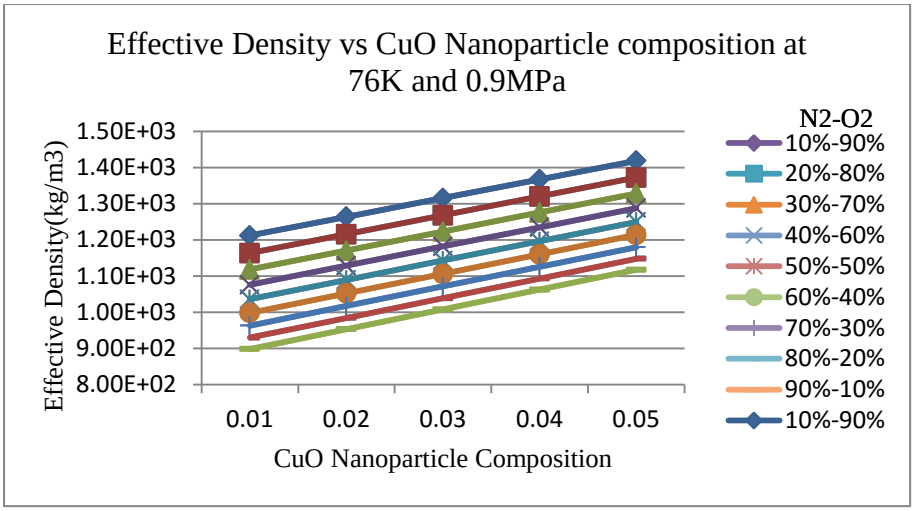

Figure 88 Effective Density vs CuO at 76K and 0.9MPa

Figure88 represents the variation in effective density with respect to volume concentration of CuO nanoparticle at various composition of mixed cryogen. It is observed that with the increase in volume concentration of CuO nanoparticle, effective density increases. It is also observed that with decrease in liquid oxygen composition in mixed cryogen effective density increases.

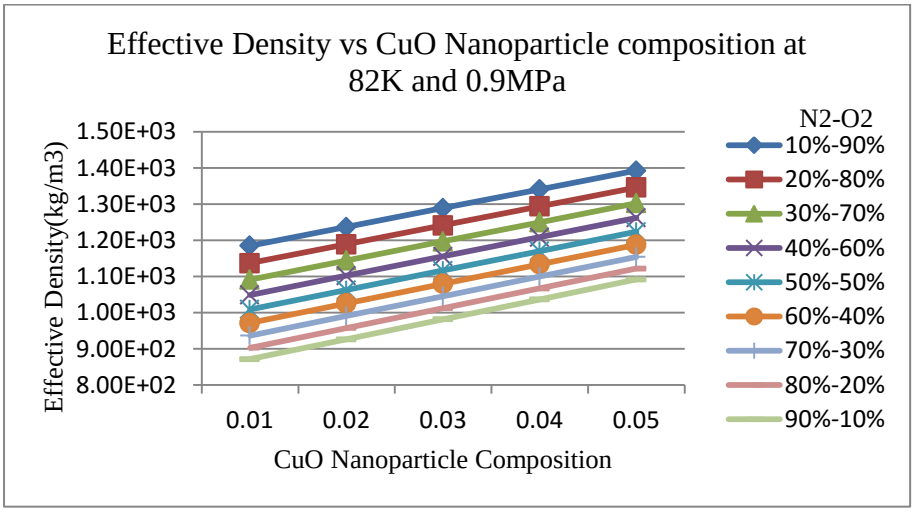

Figure 89 Effective Density vs CuO at 82K and 0.9MPa

Figure89 represents the variation in effective density with respect to volume concentration of CuO nanoparticle at various composition of mixed cryogen. It is observed that with the increase in volume concentration of CuO nanoparticle, effective density increases. It is also observed that with decrease in liquid oxygen composition in mixed cryogen effective density increases.

`

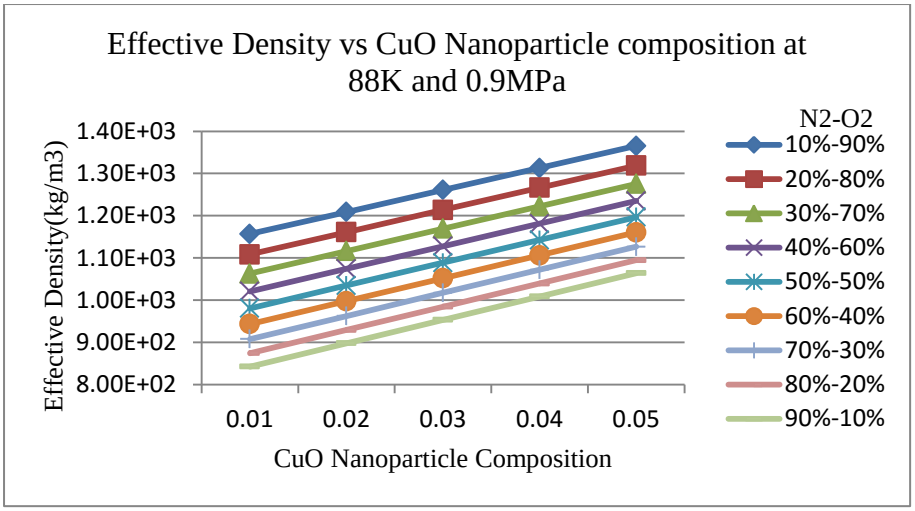

Figure 90 Effective Density vs CuO at 88K and 0.9MPa

Figur90 represents the variation in effective density with respect to volume concentration of CuO nanoparticle at various composition of mixed cryogen. It is observed that with the increase in volume concentration of CuO nanoparticle, effective density increases. It is also observed that with decrease in liquid oxygen composition in mixed cryogen effective density increases.

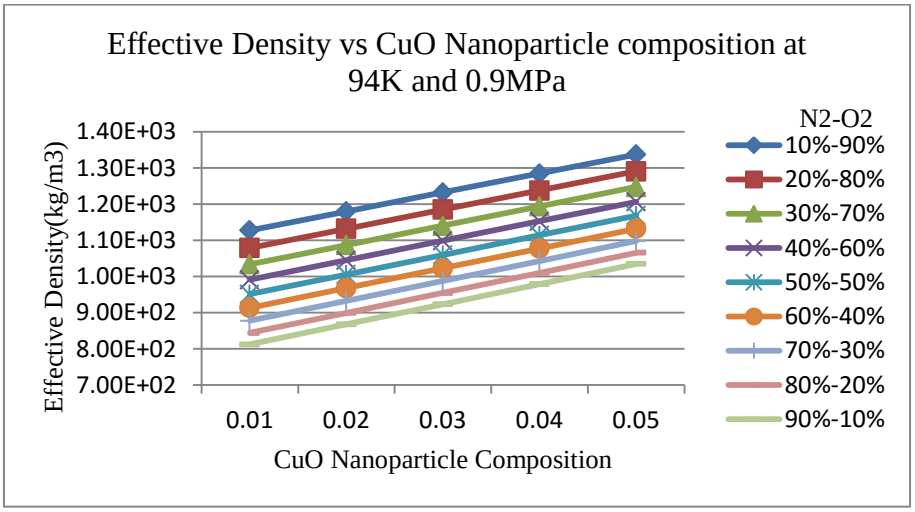

Figure 91 Effective Density vs CuO at 94K and 0.9MPa

Figure91 represents the variation in effective density with respect to volume concentration of CuO nanoparticle at various composition of mixed cryogen. It is observed that with the increase in volume concentration of CuO nanoparticle, effective density increases. It is also observed that with decrease in liquid oxygen composition in mixed cryogen effective density increases.

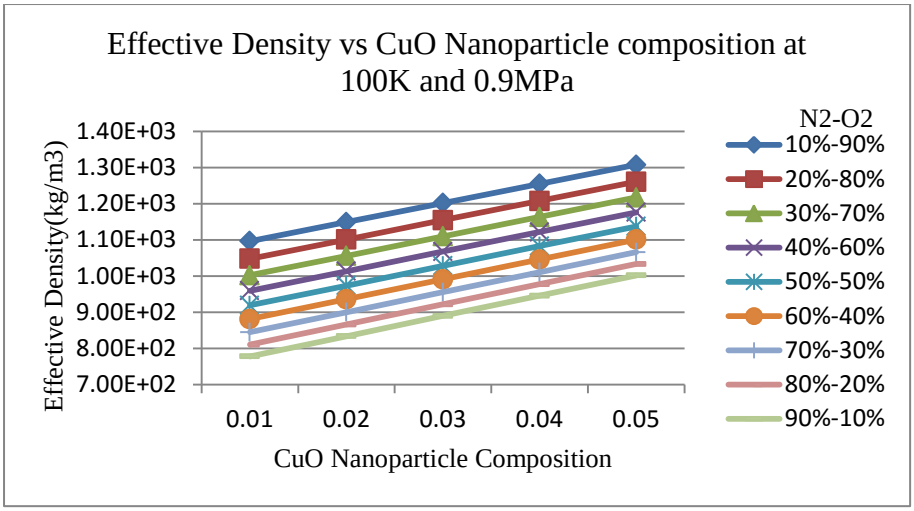

Figure 92 Effective Density vs CuO at 100K and 0.9MPa

Figure92 represents the variation in effective density with respect to volume concentration of CuO nanoparticle at various composition of mixed cryogen. It is observed that with the increase in volume concentration of CuO nanoparticle, effective density increases. It is also observed that with decrease in liquid oxygen composition in mixed cryogen effective density increases.

7.2.4 Effective Specific Heat

Various nanoparticles are used for investigation of effective specific heat

7.2.4.1 Effective Specific Heat for Al_2O_3 (Sapphire) Nanoparticle

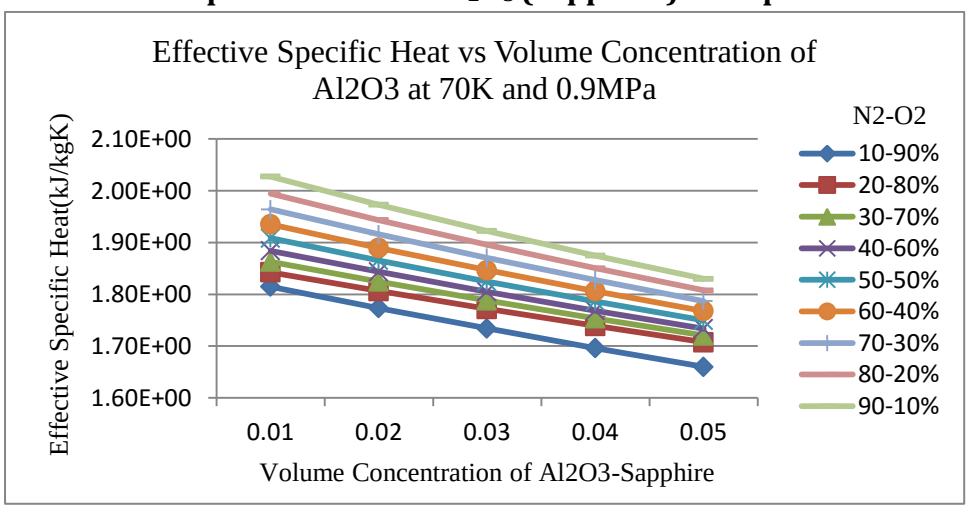

Figure 93Effective Specific Heat vs Al2O3 at 70K and 0.9MPa

Figure93 represents the variation in effective specific heat with respect to volume concentration of Al2O3-Sapphire nanoparticle at various composition of mixed cryogen. It

`

is observed that with the increase in volume concentration of Al2O3-Sapphire nanoparticle, effective specific heat decreases. It is also observed that with increase in liquid oxygen composition in mixed cryogen effective specific heat decreases.

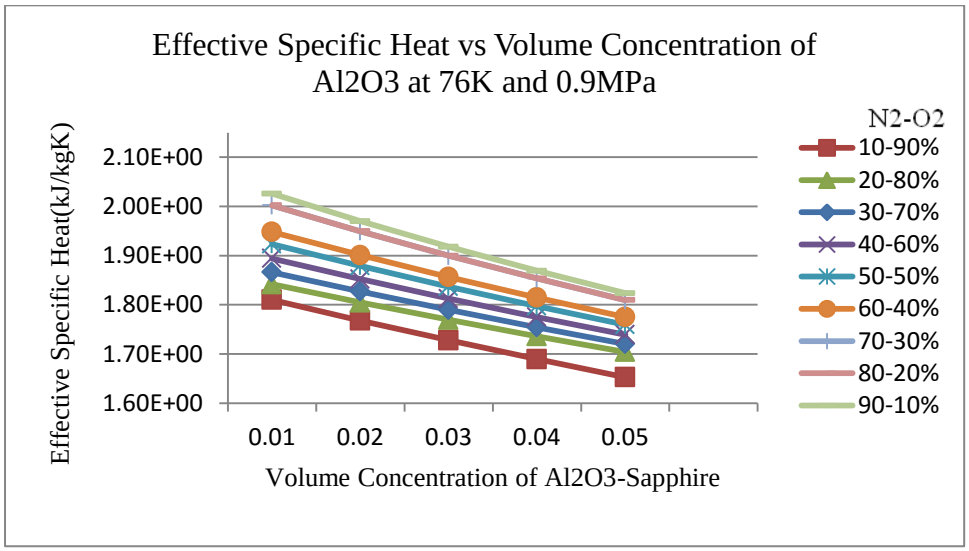

Figure 94Effective Specific Heat vs Al2O3 at 76K and 0.9MPa

Figure94 represents the variation in effective specific heat with respect to volume concentration of Al2O3-Sapphire nanoparticle at various composition of mixed cryogen. It is observed that with the increase in volume concentration of Al2O3-Sapphire nanoparticle, effective specific heat decreases. It is also observed that with increase in liquid oxygen composition in mixed cryogen effective specific heat decreases.

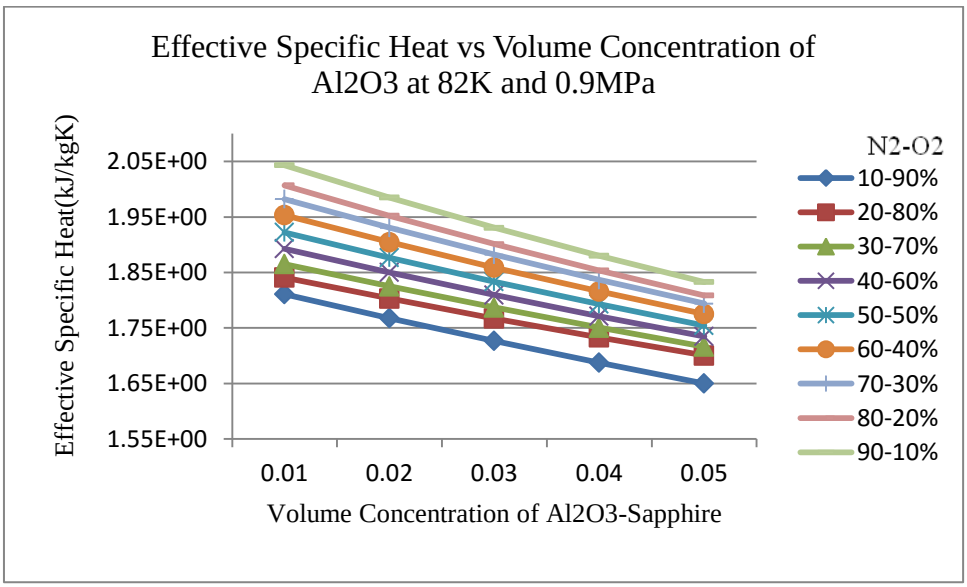

Figure 95Effective Specific Heat vs Al2O3 at 82K and 0.9MPa

`

Figure95 represents the variation in effective specific heat with respect to volume concentration of Al2O3-Sapphire nanoparticle at various composition of mixed cryogen. It is observed that with the increase in volume concentration of Al2O3-Sapphire nanoparticle, effective specific heat decreases. It is also observed that with increase in liquid oxygen composition in mixed cryogen effective specific heat decreases.

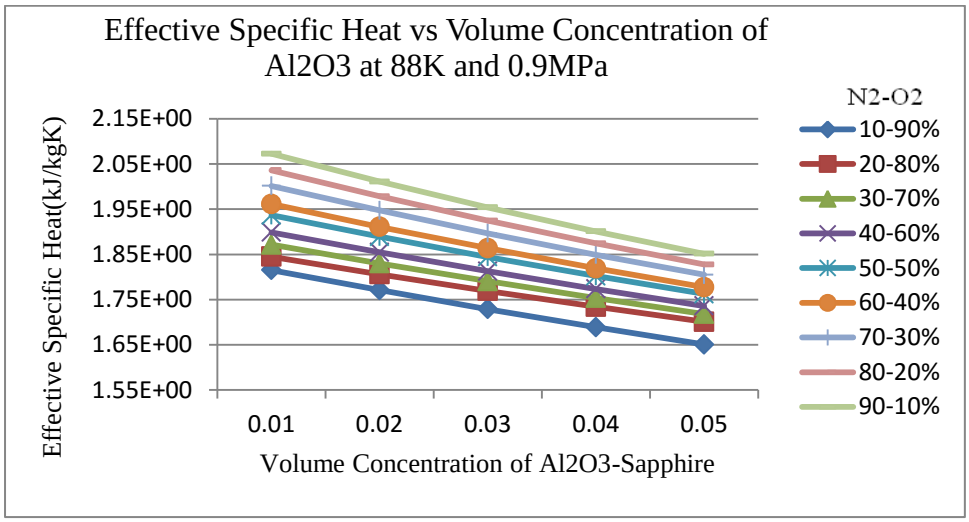

Figure 96Effective Specific Heat vs Al2O3 at 88K and 0.9MPa

Figure96 represents the variation in effective specific heat with respect to volume concentration of Al2O3-Sapphire nanoparticle at various composition of mixed cryogen. It is observed that with the increase in volume concentration of Al2O3-Sapphire nanoparticle, effective specific heat decreases. It is also observed that with increase in liquid oxygen composition in mixed cryogen effective specific heat decreases.

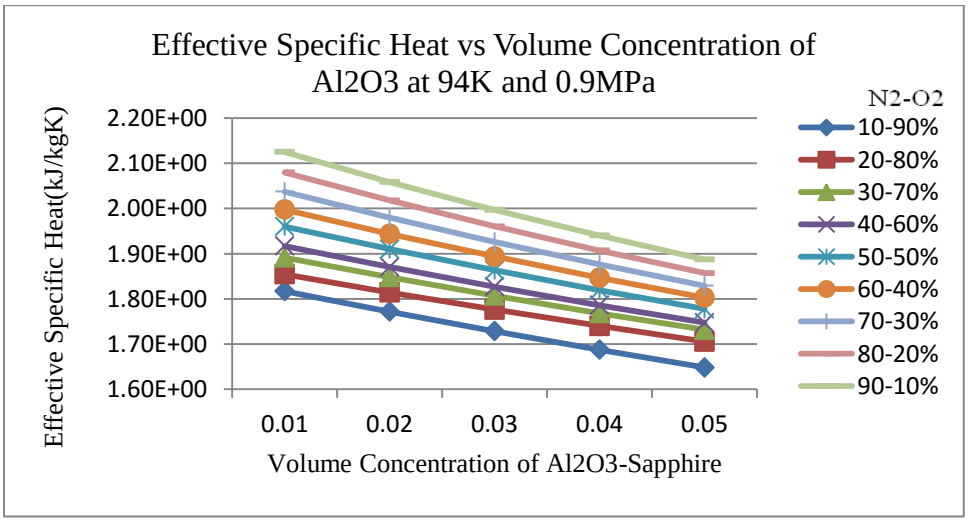

Figure 97Effective Specific Heat vs Al2O3 at 94K and 0.9MPa

`

Figure97 represents the variation in effective specific heat with respect to volume concentration of Al2O3-Sapphire nanoparticle at various composition of mixed cryogen. It is observed that with the increase in volume concentration of Al2O3-Sapphire nanoparticle, effective specific heat decreases. It is also observed that with increase in liquid oxygen composition in mixed cryogen effective specific heat decreases.

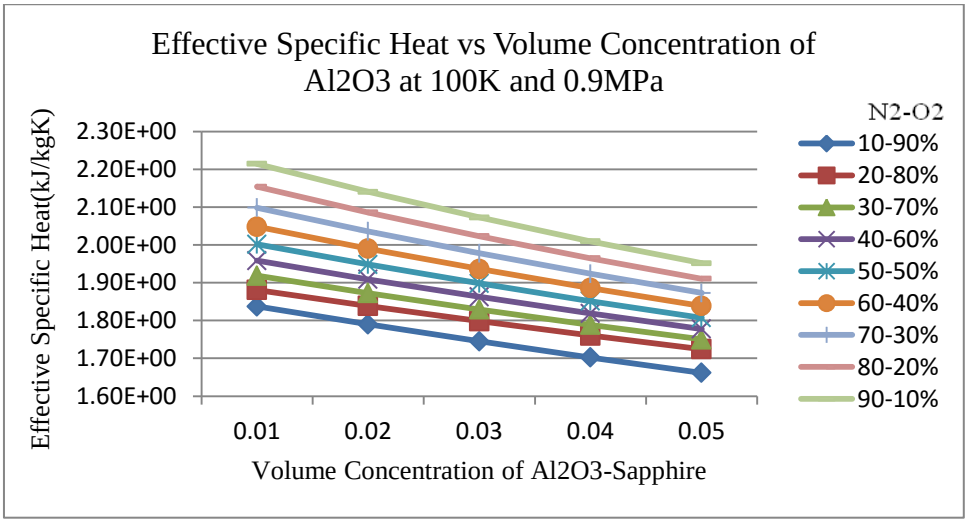

Figure 98Effective Specific Heat vs Al2O3 at 100K and 0.9MPa

Figure98 represents the variation in effective specific heat with respect to volume concentration of Al2O3-Sapphire nanoparticle at various composition of mixed cryogen. It is observed that with the increase in volume concentration of Al2O3-Sapphire nanoparticle, effective specific heat decreases. It is also observed that with increase in liquid oxygen composition in mixed cryogen effective specific heat decreases.

`

7.2.4.2 Effective Specific Heat for CuO Nanoparticle

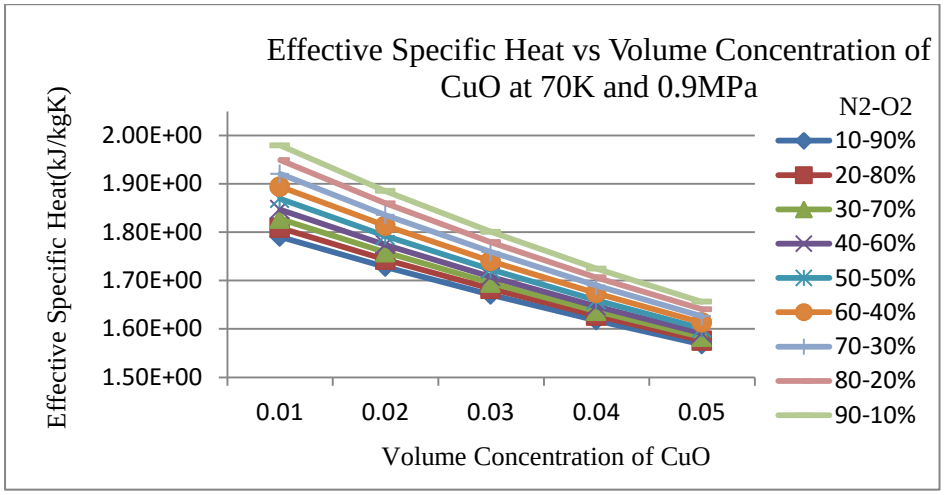

Figure 99 Effective Specific Heat vs CuO at 70K and 0.9MPa

Figure99 represents the variation in effective specific heat with respect to volume concentration of CuO nanoparticle at various composition of mixed cryogen. It is observed that with the increase in volume concentration of CuO nanoparticle, effective specific heat decreases. It is also observed that with increase in liquid oxygen composition in mixed cryogen effective specific heat decreases.

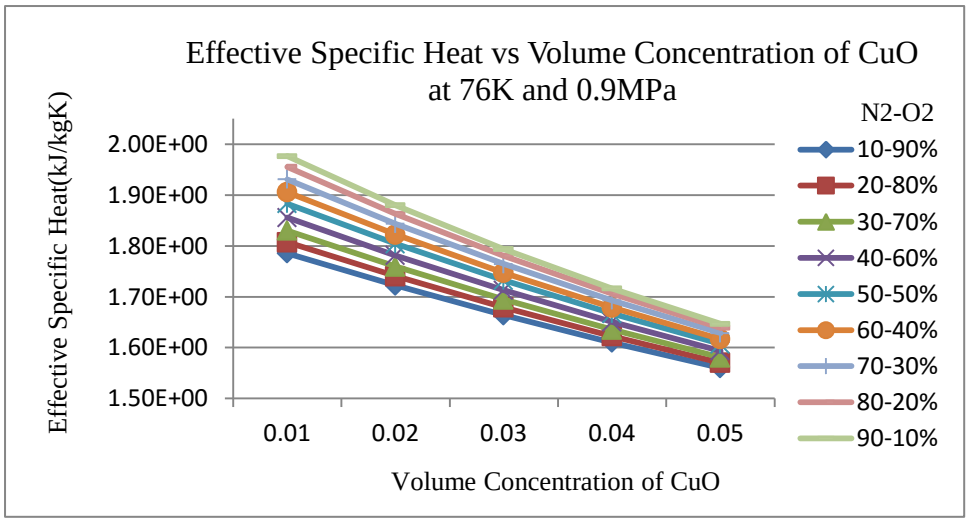

Figure 100Effective Specific Heat vs CuO at 76K and 0.9MPa

Figure101 represents the variation in effective specific heat with respect to volume concentration of CuO nanoparticle at various composition of mixed cryogen. It is observed that with the increase in volume concentration of CuO nanoparticle, effective specific heat decreases. It is also observed that with increase in liquid oxygen composition in mixed cryogen effective specific heat decreases.

`

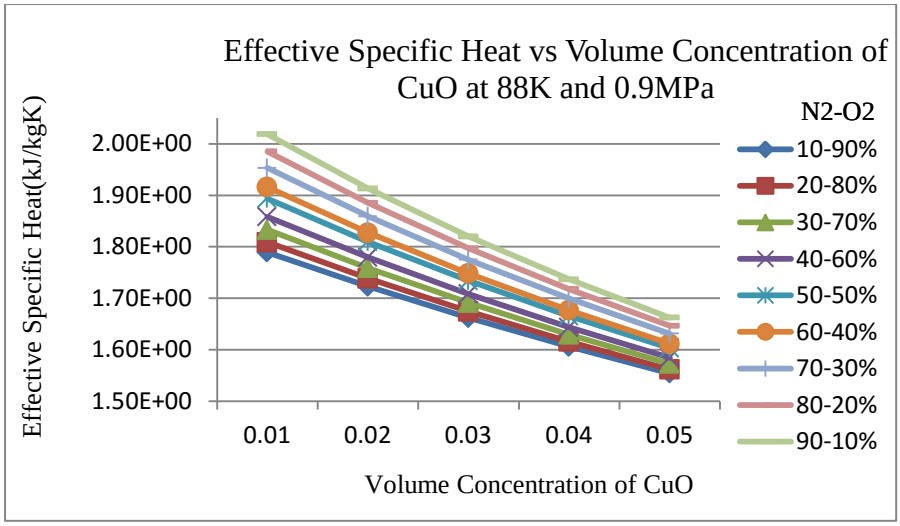

Figure 101Effective Specific Heat vs CuO at 88K and 0.9MPa

Figure101 represents the variation in effective specific heat with respect to volume concentration of CuO nanoparticle at various composition of mixed cryogen. It is observed that with the increase in volume concentration of CuO nanoparticle, effective specific heat decreases. It is also observed that with increase in liquid oxygen composition in mixed cryogen effective specific heat decreases.

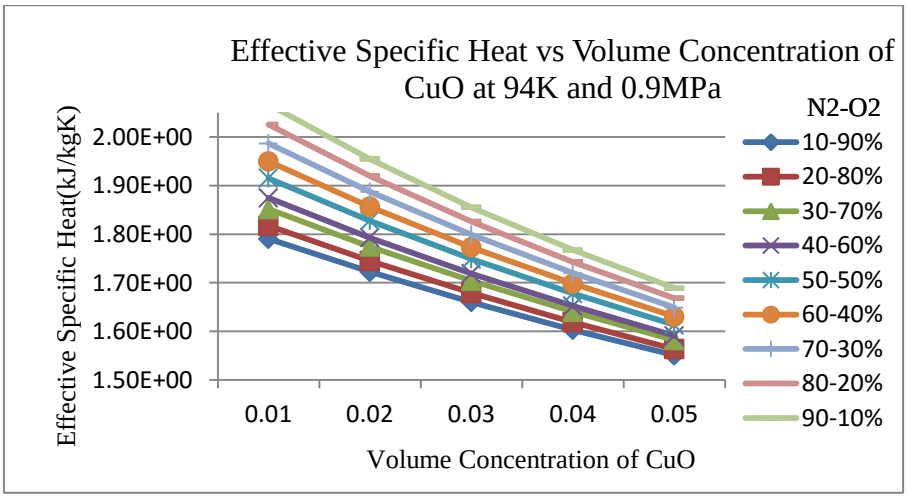

Figure 102Effective Specific Heat vs CuO at 94K and 0.9MPa

Figure102 represents the variation in effective specific heat with respect to volume concentration of CuO nanoparticle at various composition of mixed cryogen. It is observed that with the increase in volume concentration of CuO nanoparticle, effective specific heat decreases. It is also observed that with increase in liquid oxygen composition in mixed cryogen effective specific heat decreases.

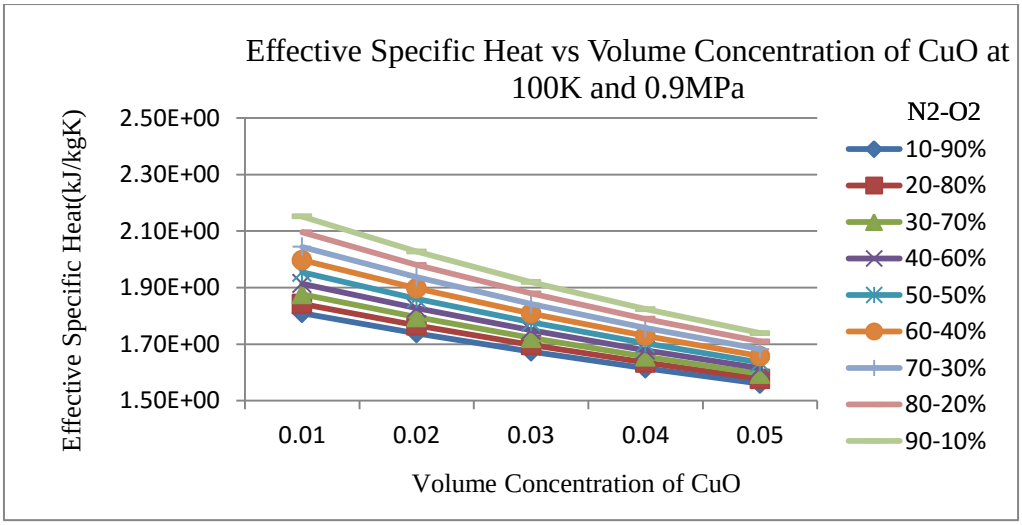

Figure 103Effective Specific Heat vs CuO at 100K and 0.9MPa

Figure103 represents the variation in effective specific heat with respect to volume concentration of CuO nanoparticle at various composition of mixed cryogen. It is observed that with the increase in volume concentration of CuO nanoparticle, effective specific heat decreases. It is also observed that with increase in liquid oxygen composition in mixed cryogen effective specific heat decreases.

7.3 Evaluation of Thermohydraulic Performance

Thermohydraulic performance of HTS cable is measured evaluating pressure drop, heat transfer and Nusselt number for various nanoparticles.

7.3.1 Pressure Drop Analysis of Mixed Cryogen without Nanoparticles

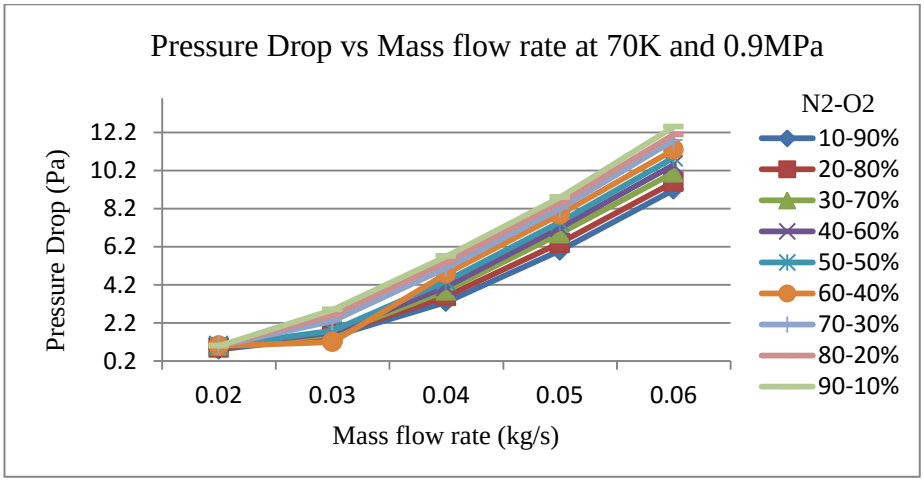

Figure 104 Pressure Drop vs Mass flow rate at 70K and 0.9MPa

`

Figure104 represents the pressure drop as function of mass flow rate ranging from 0.02kg/s-0.06kg/s with mixture combination range of 10-90% to 90-10% by volume of LN2-LO2 at constant temperature of 70K . It is observed that with increase in mass flow rate, pressure drop increases. Likewise, with increase of LN2 in mixed cryogen significant increase in pressure drop is marked.

7.3.2 Pressure Drop Analysis of Mixed Cryogen with Nanoparticles

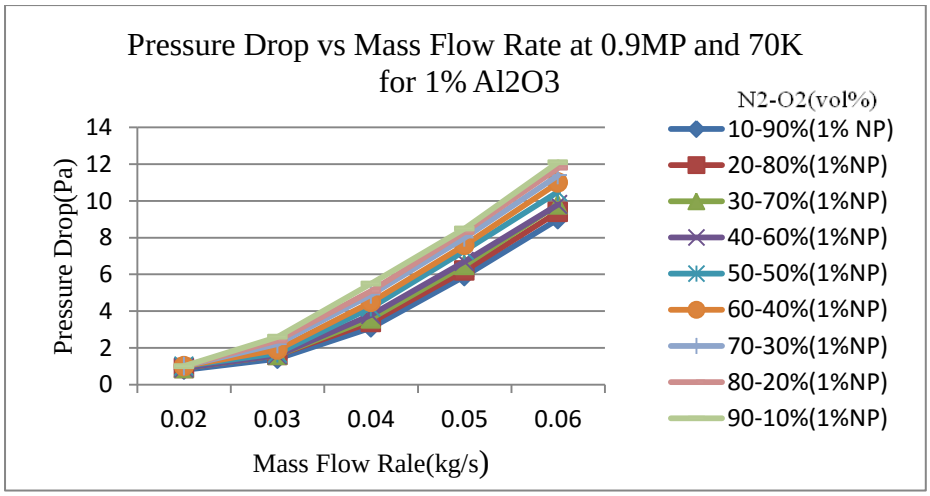

Figure 105 Pressure Drop vs Mass Flow Rate at 0.9MP and 70K for 1% Al2O3

Figure105 represents the pressure drop as function of mass flow rate ranging from 0.02kg/s-0.06kg/s, with mixture combination range of 10-90% to 90-10% of LN2-LO2 suspended with 1% Al_2O_3 by volume concentration at constant temperature of 70K . It is observed that with increase in mass flow rate, pressure drop increases. Likewise, with increase of LN2 in mixed cryogen significant increase in pressure drop is marked. Moreover, mixed cryogen with 1% Al_2O_3provides more pressure drop than 5%.

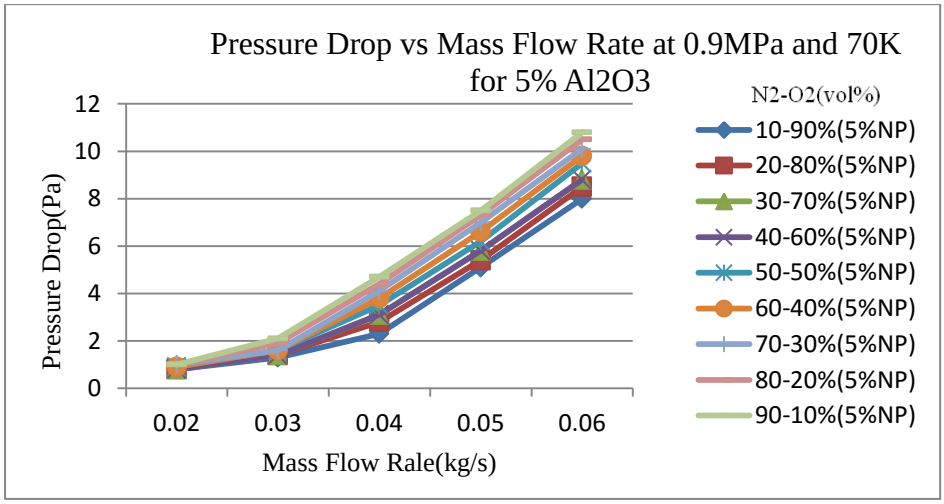

Figure 106 Pressure Drop vs Mass Flow Rate at 0.9MP and 70K for 5% Al2O3

`

Figure106 represents the pressure drop as function of mass flow rate ranging from 0.02kg/s-0.06kg/s, with mixture combination range of 10-90% to 90-10% of LN2-LO2 suspended with 5% Al_2O_3 by volume concentration at constant temperature of 70K . It is observed that with increase in mass flow rate, pressure drop increases. Likewise, with increase of LN2 in mixed cryogen significant increase in pressure drop is marked. Moreover, mixed cryogen with 5% Al_2O_3 provides lesser pressure drop than 1%.

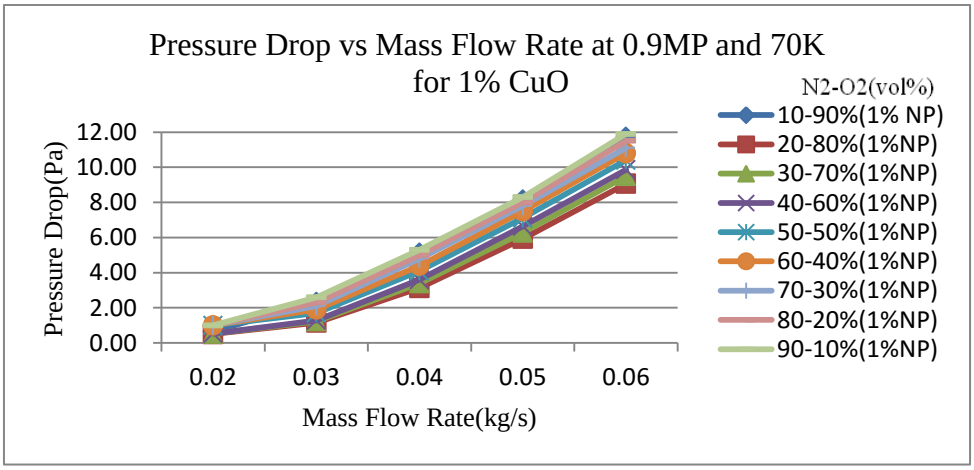

Figure 107 Pressure Drop vs Mass Flow Rate at 0.9MP and 70K for 1% CuO

Figure107 represents the pressure drop as function of mass flow rate ranging from 0.02kg/s-0.06kg/s, with mixture combination range of 10-90% to 90-10% of LN2-LO2 suspended with 1% CuO by volume concentration at constant temperature of 70K . It is observed that with increase in mass flow rate, pressure drop increases. Likewise, with increase of LN2 in mixed cryogen significant increase in pressure drop is marked. Moreover, mixed cryogen with 1% nanoparticle provides more pressure drop than 5%.

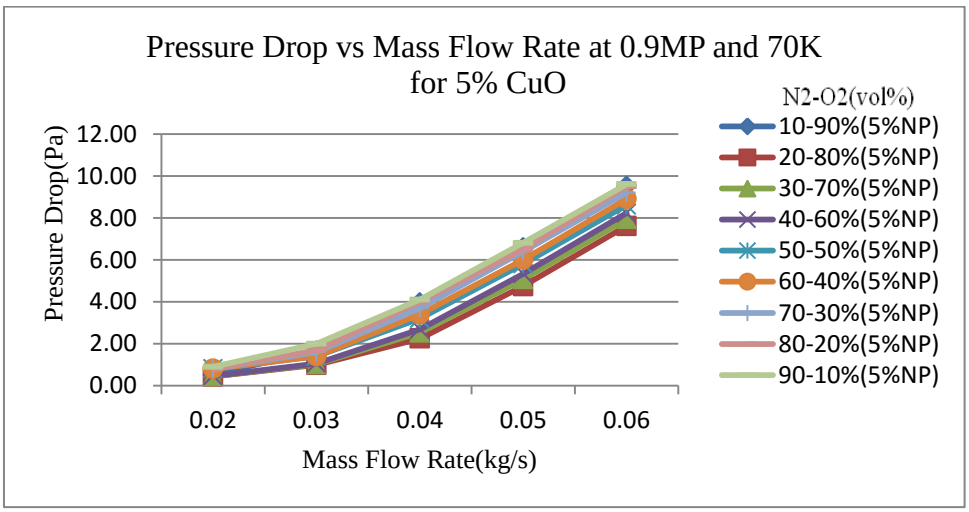

Figure 108 Pressure Drop vs Mass Flow Rate at 0.9MP and 70K for 5% CuO

`

Figure108 represents the pressure drop as function of mass flow rate ranging from 0.02kg/s-0.06kg/s, with mixture combination range of 10-90% to 90-10% of LN2-LO2 suspended with 5% CuO by volume concentration at constant temperature of 70K . It is observed that with increase in mass flow rate, pressure drop increases. Likewise, with increase of LN2 in mixed cryogen significant increase in pressure drop is marked. Moreover, mixed cryogen with 5% nanoparticle provides lesser pressure drop than 1%.

7.3.3 Heat Transfer Analysis of Mixed Cryogen without Nanoparticles

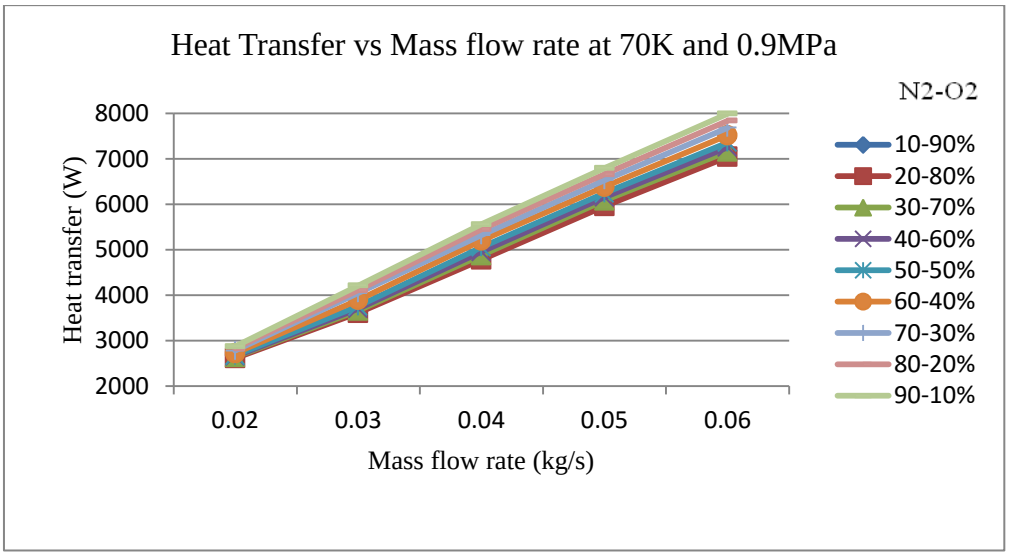

Figure 109 Heat Transfer vs Mass flow rate at 70K and 0.9MPa

Figure 109 represents the heat transfer as function of mass flow rate ranging from 0.02kg/s-0.06kg/s with mixture combination range of 10-90% to 90-10% by volume of LN2-LO2 at constant temperature of 70K . It is observed that with increase in mass flow rate, heat transfer increases. Likewise, with increase of LN2 in mixed cryogen significant increase in heat transfer is marked.

`

7.3.4 Heat Transfer Analysis of Mixed Cryogen with Nanoparticles

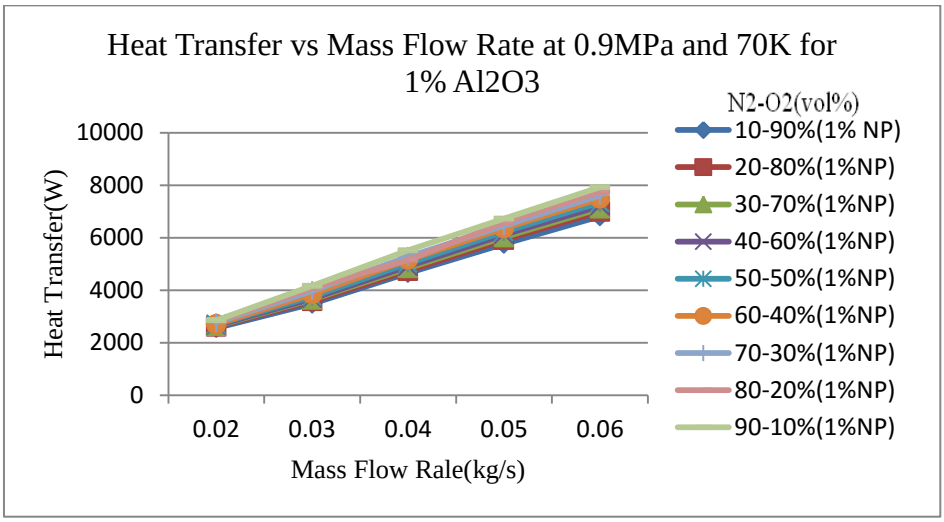

Figure 110 Heat Transfer vs Mass Flow Rate at 0.9MPa and 70K for 1% Al2O3

Figure 110 represents the heat transfer as function of mass flow rate ranging from 0.02kg/s-0.06kg/s with mixture combination range of 10-90% to 90-10% of LN2-LO2 with 1% Al_2O_3 by volume at constant temperature of 70K . It is observed that with increase in mass flow rate, heat transfer increases. Likewise, with increase of LN2 in mixed cryogen significant increase in heat transfer is marked. Moreover, higher heat transfer rate is obtained with 1% Al_2O_3 than 5%.

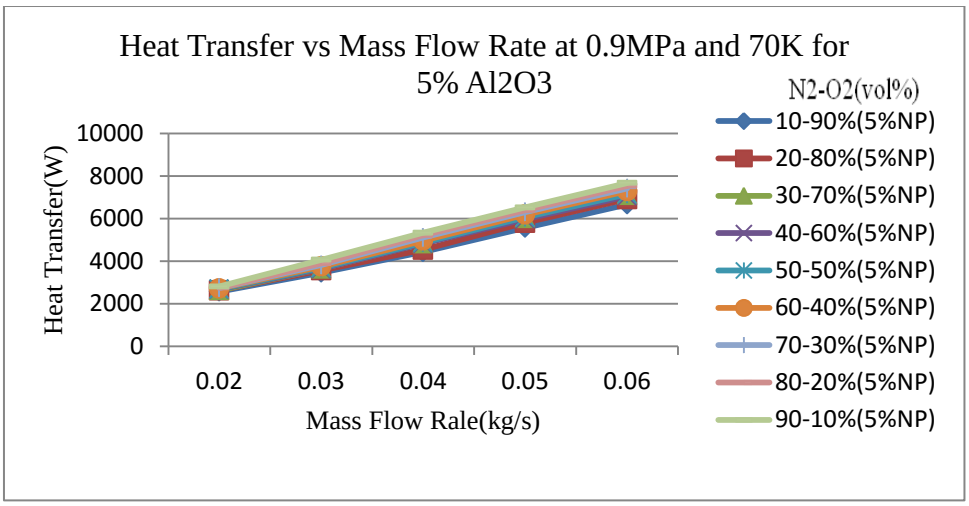

Figure 111 Heat Transfer vs Mass Flow Rate at 0.9MPa and 70K for 5% Al2O3

Figure 111 represents the heat transfer as function of mass flow rate ranging from 0.02kg/s-0.06kg/s with mixture combination range of 10-90% to 90-10% of LN2-LO2 with 5% Al_2O_3 by volume at constant temperature of 70K . It is observed that with

`

increase in mass flow rate, heat transfer increases. Likewise, with increase of LN2 in mixed cryogen significant increase in heat transfer is marked. Moreover, lesser heat transfer rate is obtained with 5% Al_2O_3 than 1%.

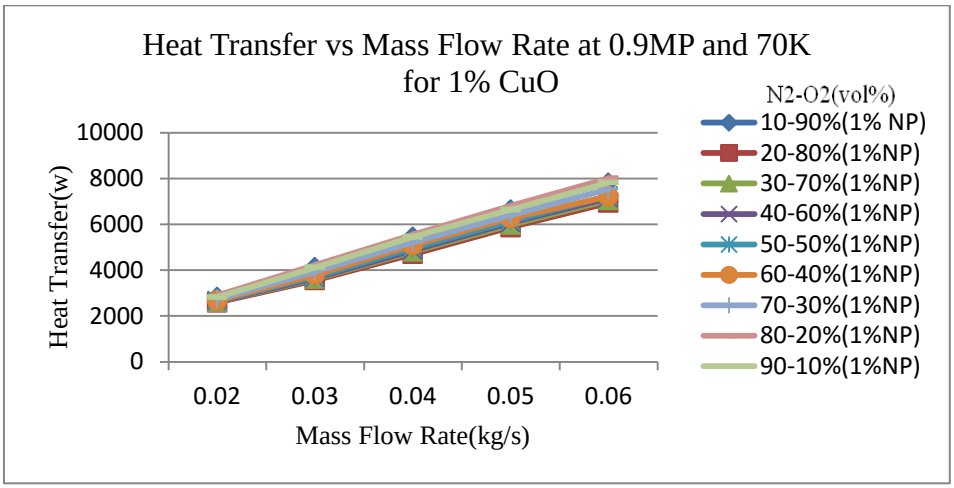

Figure 112 Heat Transfer vs Mass Flow Rate at 0.9MPa and 70K for 1% CuO

Figure 112 represents the heat transfer as function of mass flow rate ranging from 0.02kg/s-0.06kg/s with mixture combination range of 10-90% to 90-10% of LN2-LO2 with 1% CuO by volume at constant temperature of 70K . It is observed that with increase in mass flow rate, heat transfer increases. Likewise, with increase of LN2 in mixed cryogen significant increase in heat transfer is marked. Moreover, higher heat transfer rate is obtained with 1% CuO than 5%.

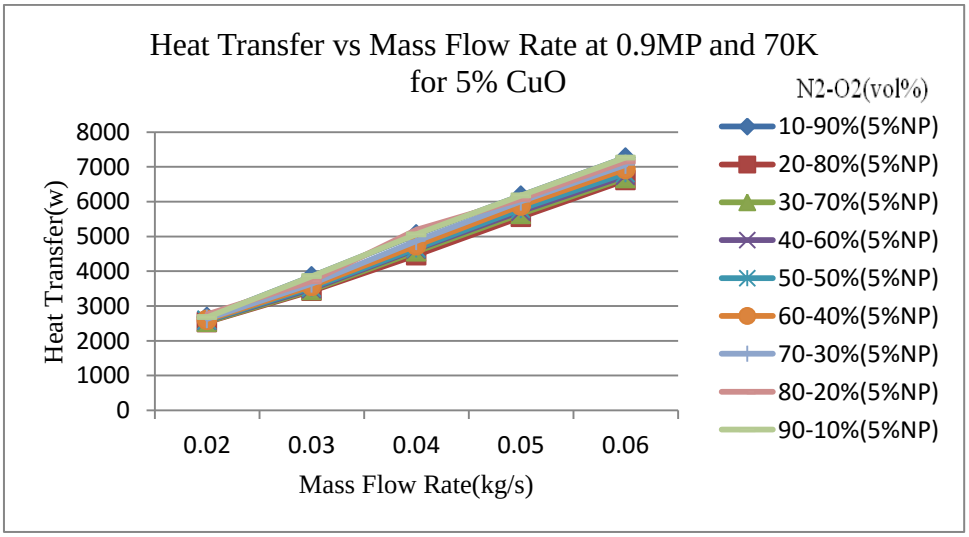

Figure 113 Heat Transfer vs Mass Flow Rate at 0.9MPa and 70K for 5% CuO

Figure 113 represents the heat transfer as function of mass flow rate ranging from 0.02kg/s-0.06kg/s with mixture combination range of 10-90% to 90-10% of LN2-LO2

with 5% CuO by volume at constant temperature of 70K . It is observed that with increase in mass flow rate, heat transfer increases. Likewise, with increase of LN2 in mixed cryogen significant increase in heat transfer is marked. Moreover, lesser heat transfer rate is obtained with 5% CuO than 1%.

7.3.5 Nusselt Number Analysis of Mixed Cryogen without Nanoparticles

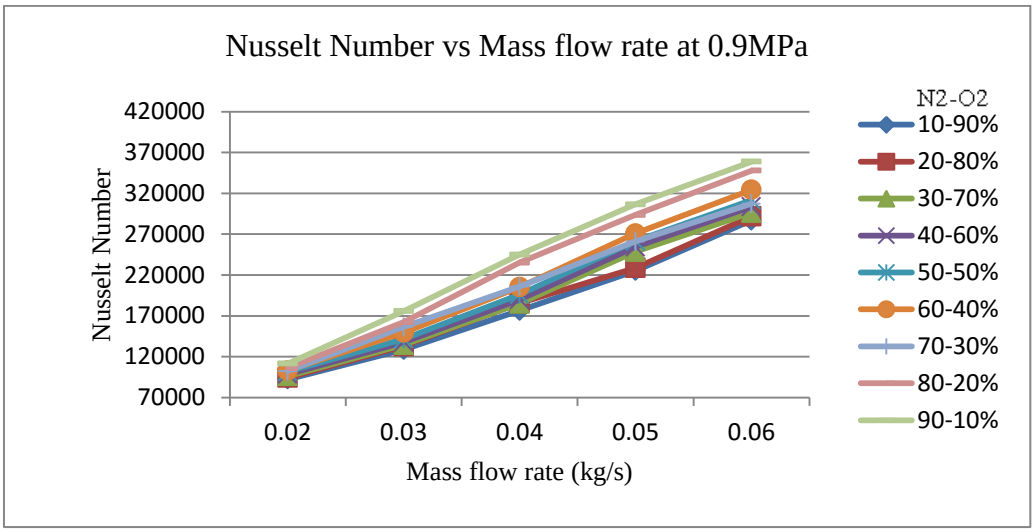

Figure 114 Nusselt Number vs Mass flow rate at 0.9MPa

Figure114 represents the Nusselt number as function of mass flow rate ranging from 0.02kg/s-0.06kg/s with mixture combination range of 10-90% to 90-10% by volume of LN2-LO2 with Al_2O_3 at constant temperature of 70K . The result indicates that with increase in mass flow rate, Nusselt number increases. Likewise, with increase of LN2 in mixture significant increase in Nusselt number is marked.

`

7.3.6 Nusselt Number Analysis of Mixed Cryogen with Nanoparticles

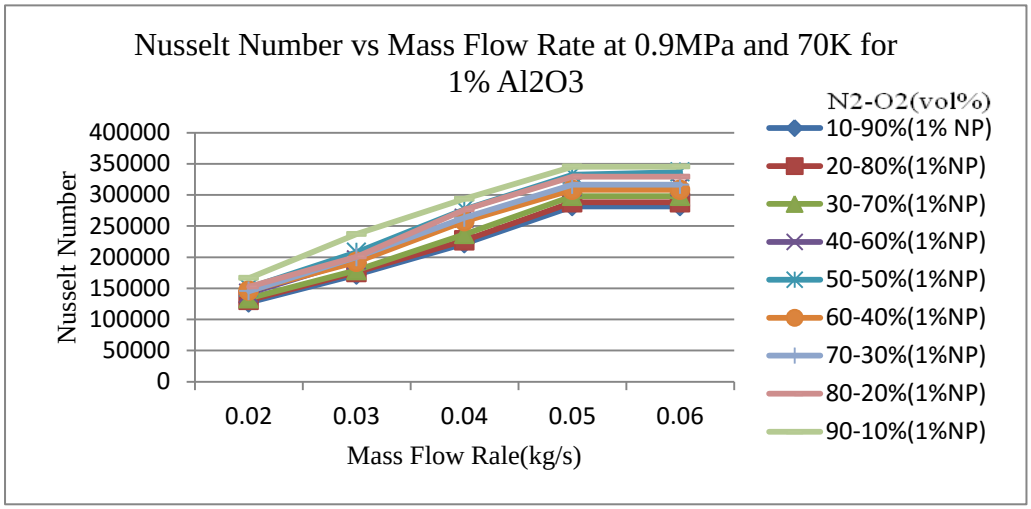

Figure 115 Nusselt Number vs Mass Flow Rate at 0.9MPa and 70K for 1% Al2O3

Figure115 represents the Nusselt number as function of mass flow rate ranging from 0.02kg/s-0.06kg/s with mixture combination range of 10-90% to 90-10% of LN2-LO2 with 1%Al_2O_3 by volume at constant temperature of 70K . The result indicates that with increase in mass flow rate, Nusselt number increases. Likewise, with increase of LN2 in mixture significant increase in Nusselt number is marked. Moreover, with 1% Al_2O_3 higher Nusselt number is obtained.

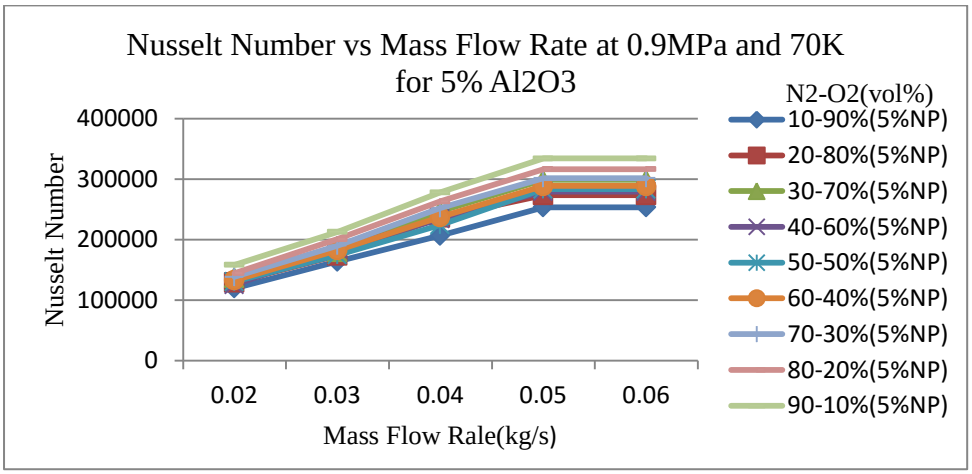

Figure 116 Nusselt Number vs Mass Flow Rate at 0.9MPa and 70K for 5% Al2O3

Figure116 represents the Nusselt number as function of mass flow rate ranging from 0.02kg/s-0.06kg/s with mixture combination range of 10-90% to 90-10% of LN2-LO2 with 5%Al_2O_3 by volume at constant temperature of 70K . The result indicates that with increase in mass flow rate, Nusselt number increases. Likewise, with increase of LN2 in

`

mixture significant increase in Nusselt number is marked. Moreover, with 5% Al_2O_3 lesser Nusselt number is obtained.

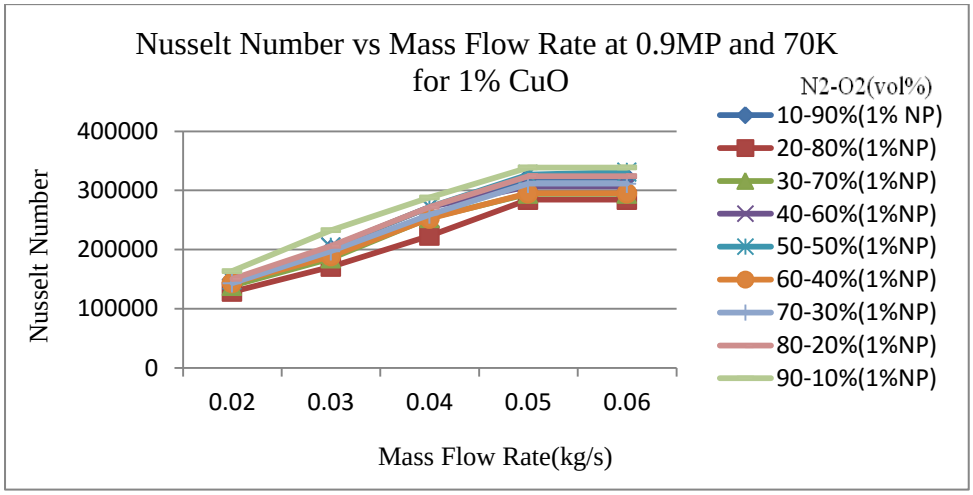

Figure 117 Nusselt Number vs Mass Flow Rate at 0.9MP and 70K for 1% CuO

Figure117 represents the Nusselt number as function of mass flow rate ranging from 0.02kg/s-0.06kg/s with mixture combination range of 10-90% to 90-10% of LN2-LO2 with 1%CuO by volume at constant temperature of 70K . The result indicates that with increase in mass flow rate, Nusselt number increases. Likewise, with increase of LN2 in mixture significant increase in Nusselt number is marked. Moreover, with 1% CuO higher Nusselt number is obtained.

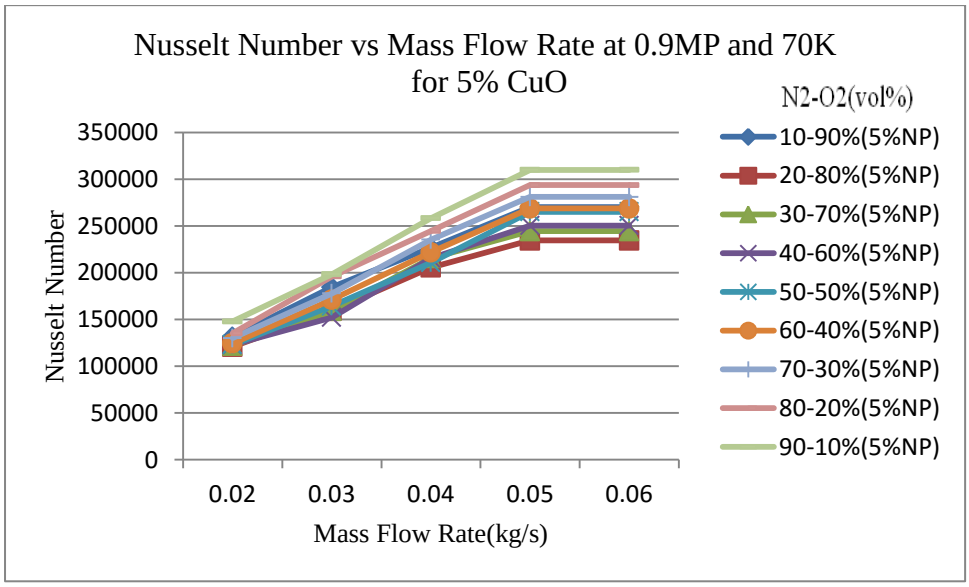

Figure 118 Nusselt Number vs Mass Flow Rate at 0.9MP and 70K for 5% CuO

Figure118 represents the Nusselt number as function of mass flow rate ranging from 0.02kg/s-0.06kg/s with mixture combination range of 10-90% to 90-10% of LN2-LO2

`

with 5%CuO by volume at constant temperature of 70K . The result indicates that with increase in mass flow rate, Nusselt number increases. Likewise, with increase of LN2 in mixture significant increase in Nusselt number is marked. Moreover, with 5% CuO lesser Nusselt number is obtained.

`

CHAPTER-VIII

8 CONCLUSION AND FUTURE SCOPE

In the present research work, thermophysical properties of mixed cryogens such as LN_2+LO_x under specified pressure of 0.9MPa-1.3Mpa and temperature of 70K-100K is investigated. Further, Al_2O_3 and CuO nanoparticle is dispersed in basefluid with volume concentration of 1% and 5%. Again thermophysical properties are evaluated using correlations. Furthermore, thermohydraulic performance is being checked using ANSYS® (FLUENT). Pressure drop, Heat transfer and Nusselt number is being calculated at varying mass flow rates. It can be concluded that specific heat increases whereas density, viscosity and thermal conductivity decreases with increase in pressure. Moreover, with respect to volume fraction of nanoparticle specific heat decreases whereas density, viscosity and thermal conductivity increases. Hence these thermophysical properties are dependent on temperature and volume fraction. With the enhancement in thermophysical properties better heat transfer rate is obtained. Also, after suspension of nanoparticles less pressure drop and high heat transfer is achieved. Al_2O_3 nanoparticle with 1% vol. conc provides lesser pressure drop and maximum heat transfer for mixed cryogen. Thus power transmission in HTS cables can work more efficiently with suspension of 1% Al_2O_3 nanoparticle which concludes the feasibility of nano cryogens in futuristic HTS cables.

Further studies can be done on various other superconducting devices such as superconducting motors, SMES. Different types of hybrid cryogens can be used as coolant with two or more Nanofluids.

`

CHAPTER-IX

9 LIST OF REFERENCES

[1]. Wei, B., Zou, C., Yuan, X., & Li, X. (2017). Thermo-physical property evaluation of diathermic oil based hybrid nanofluids for heat transfer applications. *International Journal of Heat and Mass Transfer*, *107*, 281–287. https://doi.org/10.1016/j.ijheatmasstransfer.2016.11.044

[2]. Bang, S. S., Lee, G. S., Kwon, G.-Y., Lee, Y. H., Chang, S. J., Lee, C.-K., … Shin, Y.-J. (2016). Modeling and simulation of HTS cables for scattering parameter analysis. *Physica C: Superconductivity and Its Applications*, *530*, 142–146. https://doi.org/10.1016/j.physc.2016.07.013

[3]. Huminic, G., & Huminic, A. (2016). Heat transfer and flow characteristics of conventional fluids and nanofluids in curved tubes: A review. *Renewable and Sustainable Energy Reviews*, *58*, 1327–1347. https://doi.org/10.1016/j.rser.2015.12.230

[4]. Dondapati, R. S., Ravula, J., Thadela, S., & Usurumarti, P. R. (2015). Analytical approximations for thermophysical properties of supercritical nitrogen (SCN) to be used in futuristic high temperature superconducting (HTS) cables. *Physica C: Superconductivity and Its Applications*, *519*, 53–59. https://doi.org/10.1016/j.physc.2015.08.005

[5]. Liu, Y., Olewski, T., & Véchot, L. N. (2015). Modeling of a cryogenic liquid pool boiling by CFD simulation. *Journal of Loss Prevention in the Process Industries*, *35*, 125–134. https://doi.org/10.1016/j.jlp.2015.04.006

[6]. Vyas, G., Dondapati, R. S., & Usurumarti, P. R. (2015). Parametric evaluation of AC losses in 500 MVA/1.1 kA high temperature superconducting (HTS) cable for efficient power transmission: Self field analysis. *Proceedings - UKSim-AMSS 8th European Modelling Symposium on Computer Modelling and Simulation, EMS 2014*, 315–319. https://doi.org/10.1109/EMS.2014.95

[7]. Chang, H. M., & Lee, S. I. (2014). Conduction-Cooling System for Superconducting Magnets at 20-30 K. *IEEE Transactions on Applied Superconductivity*, *24*(3), 3–6. https://doi.org/10.1109/TASC.2013.2286680

[8]. Xing, M., Yu, J., & Wang, R. (2015). Thermo-physical properties of water-based single-walled carbon nanotube nanofluid as advanced coolant. *Applied Thermal Engineering*, *87*, 344–351. https://doi.org/10.1016/j.applthermaleng.2015.05.033

`

[9]. Iwai, S., Takahashi, M., Miyazaki, H., Tosaka, T., Tasaki, K., Hanai, S. Oguro, H. (2015). Concept of a cryogenic system for a cryogen-free 25 T superconducting magnet. *Physics Procedia*, *67*, 326–330. https://doi.org/10.1016/j.phpro.2015.06.095

[10]. Dondapati, R. S., & Rao, V. V. (2013). Long Length Internally Cooled HTS Cables, *23*(3), 2–5.

[11]. Kole, M., & Dey, T. K. (2013). Enhanced thermophysical properties of copper nanoparticles dispersed in gear oil. *Applied Thermal Engineering*, *56*(1–2), 45–53. https://doi.org/10.1016/j.applthermaleng.2013.03.022

[12]. Javadi, F. S., Sadeghipour, S., Saidur, R., BoroumandJazi, G., Rahmati, B., Elias, M. M., & Sohel, M. R. (2013). The effects of nanofluid on thermophysical properties and heat transfer characteristics of a plate heat exchanger. *International Communications in Heat and Mass Transfer*, *44*, 58–63. https://doi.org/10.1016/j.icheatmasstransfer.2013.03.017

[13]. Song, J. Bin, & Lee, H. (2012). Mixed cryogen cooling systems for HTS power applications: A status report of progress in Korea University. *Cryogenics*, *52*(12), 648–655. https://doi.org/10.1016/j.cryogenics.2012.06.013

[14]. Saidur, R., Leong, K. Y., & Mohammad, H. A. (2011). A review on applications and challenges of nanofluids. *Renewable and Sustainable Energy Reviews*, *15*(3), 1646–1668. https://doi.org/10.1016/j.rser.2010.11.035

[15]. Li, Y., Chen, H., & Ding, Y. (2010). Fundamentals and applications of cryogen as a thermal energy carrier: A critical assessment. *International Journal of Thermal Sciences*, *49*(6), 941–949. https://doi.org/10.1016/j.ijthermalsci.2009.12.012

[16]. Higashikawa, K., & Nakamura, T. (2009). Cooling performance of hybrid refrigerant of solid nitrogen and small amount of neon for the purpose of HTS power applications. *Physica C: Superconductivity and Its Applications*, *469*(21), 1910–1914. https://doi.org/10.1016/j.physc.2009.06.007

[17]. Hwang, Y., Lee, J. K., Lee, J. K., Jeong, Y. M., Cheong, S. ir, Ahn, Y. C., & Kim, S. H. (2008). Production and dispersion stability of nanoparticles in nanofluids. *Powder Technology*, *186*(2), 145–153. https://doi.org/10.1016/j.powtec.2007.11.020

[18]. Iancu, C. V., Wright, E. R., Heymann, J. B., & Jensen, G. J. (2006). A comparison of liquid nitrogen and liquid helium as cryogens for electron cryotomography. *Journal of Structural Biology*, *153*(3), 231–240. https://doi.org/10.1016/j.jsb.2005.12.004

`

[19]. Suzuki, Y., Yoshida, S., & Kamioka, Y. (2003). Subcooled liquid nitrogen refrigerator for HTS power systems. *Cryogenics*, *43*(10–11), 597–602. https://doi.org/10.1016/S0011-2275(03)00169-3

[20]. Masur, L. J., Buczek, D., Harley, E., Kodenkandath, T., Li, X., Lynch, J.Kellers, J. (2003). The status of commercial and developmental HTS wires. *Physica C: Superconductivity and Its Applications*, *392–396*(PART 2), 989–997. https://doi.org/10.1016/S0921-4534(03)00729-9

[21]. Kellers, J., & Masur, L. J. (2002). Reliable commercial HTS wire for power applications. *Physica C: Superconductivity and Its Applications*, *372–376*(PART 2), 1040–1045. https://doi.org/10.1016/S0921-4534(02)00966-8

[22]. J. C. Thermodynamics, V. Antón, H. Artigas, J. Muñoz-embid, M. Artal, and C. Lafuente, "Thermophysical properties of two binary aqueous mixtures containing a pyridinium-based ionic liquid," vol. 99, pp. 116–123, 2016.

[23]. Y. Xuan and W. Roetzel, "Conceptions for heat transfer correlation of nano ‒ uids," vol. 43, pp. 3701–3707, 2000.

[24]. Y. B. Tao, Y. W. Liu, F. Gao, X. Y. Chen, and Y. L. He, "Numerical analysis on pressure drop and heat transfer performance of mesh regenerators used in cryocoolers," *Cryogenics (Guildf).*, vol. 49, no. 9, pp. 497–503, 2009.

[25]. H. Chen, Y. Ding, and A. Lapkin, "Rheological behaviour of nano fl uids containing tube / rod-like nanoparticles," *Powder Technol.*, vol. 194, no. 1–2, pp. 132–141, 2009.

[26]. H. Chen, S. Witharana, Y. Jin, C. Kim, and Y. Ding, "Predicting thermal conductivity of liquid suspensions of nanoparticles (nanofluids) based on rheology," vol. 7, pp. 151–157, 2009.

[27]. K. Mahanpour, S. Sarli, M. Saghi, B. Asadi, R. Aghayari, and H. Maddah, "Investigation on Physical Properties of Al 2 O 3 / Water Nano Fluid," vol. 2, no. 2, pp. 114–119, 2015.

[28]. M. F. Nabil, W. H. Azmi, K. A. Hamid, N. N. M. Zawawi, G. Priyandoko, and R. Mamat, "Thermo-physical properties of hybrid nano fl uids and hybrid nanolubricants : A comprehensive review on performance," *Int. Commun. Heat Mass Transf.*, vol. 83, pp. 30–39, 2017.

[29]. N. Begum, S. Siddiqa, and M. A. Hossain, "Nanofluid Bioconvection with Variable Thermophysical Properties," *J. Mol. Liq.*, 2017.

`

[30]. P. Lü, K. Zhou, X. Cai, and H. P. Wang, “Thermophysical properties of undercooled liquid Ni-Zr alloys : Melting temperature, density, excess volume and thermal expansion,” vol. 135, pp. 22–28, 2017.

[31]. M. Gupta, V. Singh, R. Kumar, and Z. Said, “A review on thermophysical properties of nano fl uids and heat transfer applications,” *Renew. Sustain. Energy Rev.*, vol. 74, no. February, pp. 638–670, 2017.

[32]. G. Huminic, A. Huminic, C. Fleaca, F. Dumitrache, and I. Morjan, “applications,” *Int. Commun. Heat Mass Transf.*, vol. 84, pp. 94–101, 2017.

[33]. J. Shah, S. K. Gupta, Y. Sonvane, and V. Davariya, “Review : Enhancing e ffi ciency of solar thermal engineering systems by thermophysical properties of a promising nano fl uids,” no. February, 2017.

[34]. I. M. Mahbubul, R. Saidur, and M. A. Amalina, “Heat transfer and pressure drop characteristics of Al 2 O 3 -R141b nanorefrigerant in horizontal smooth circular tube,” *Procedia Eng.*, vol. 56, pp. 323–329, 2013.

[35]. Y. Xu, J. Chen, B. Zheng, Y. Ren, J. Zheng, and Z. Deng, “SC,” *Vacuum*, 2016.

[36]. X. Bin and S. Yumei, “International Journal of Heat and Mass Transfer Investigation on the pressure drop during flow boiling of liquefied natural gas in a vertical micro-fin tube,” *HEAT MASS Transf.*, vol. 90, pp. 159–166, 2015.

[37]. Y. Kim *et al.*, “The application of the cryogenic system on the HTS power cable circuit in actual grid,” *Cryogenics (Guildf).*, vol. 52, no. 12, pp. 661–666, 2012.

[38]. D. Kim, H. Park, S. Kim, H. Jang, and Y. Kim, “Dynamic Characteristics of Pressure Build Up Tank for HTS Power Cable Refrigeration System,” *Phys. Procedia*, vol. 58, pp. 334–337, 2014.

[39]. L. H. T. S. Cables, J. A. Demko, and R. C. Duckworth, “Cooling Configuration Design Considerations for,” vol. 19, no. 3, pp. 1752–1755, 2009.

[40]. R. S. Dondapati, G. S. Member, and V. V Rao, “CFD Analysis of Cable-In-Conduit Conductors (CICC) for Fusion Grade Magnets,” vol. 22, no. 3, 2012.

[41]. O. Maruyama, T. Ohkuma, and T. Izumi, “Numerical analysis of heat transfer and fluid characteristics in long distance HTS cable,” *Phys. Procedia*, vol. 45, pp. 285–288, 2013.

[42]. D. R. Sekhar and V. V Rao, “Three dimensional CFD analysis of Cable-in-Conduit Conductors (CICCs) using porous medium approach,” *Cryogenics (Guildf).*, vol. 54, pp. 20–29, 2013.

`

[43]. J. Song and H. Lee, “Mixed cryogen cooling systems for HTS power applications : A status report of progress in Korea University,” *Cryogenics (Guildf).*, vol. 52, no. 12, pp. 648–655, 2012.

[44]. H. Afrianto, R. Tanshen, B. Munkhbayar, U. T. Suryo, H. Chung, and H. Jeong, “International Journal of Heat and Mass Transfer A numerical investigation on LNG flow and heat transfer characteristic in heat exchanger,” *Int. J. Heat Mass Transf.*, vol. 68, pp. 110–118, 2014.

[45]. R. S. Dondapati and V. V Rao, “Influence of mass flow rate on Turbulent Kinetic Energy (TKE) distribution in Cable-in-Conduit Conductors (CICCs) used for fusion grade magnets,” *Fusion Eng. Des.*, vol. 88, no. 5, pp. 341–349, 2013.

[46]. H. Chang, K. Nam, and H. Suk, “Integrated design of cryogenic refrigerator and liquid-nitrogen circulation loop for HTS cable,” *Cryogenics (Guildf).*, vol. 1, pp. 1–10, 2016.

[47]. G. Huminic and A. Huminic, “Application of nanofluids in heat exchangers : A review,” *Renew. Sustain. Energy Rev.*, vol. 16, no. 8, pp. 5625–5638, 2012.

[48]. T. M. Kochenburger and L. R. Oellrich, “Evaluation of a two-stage mixed refrigerant cascade for HTS cooling below 60 K,” vol. 67, pp. 227–232, 2015.

[49]. J. Lee, G. Hwang, S. Jeong, B. Jun, and Y. Hee, “Design of high efficiency mixed refrigerant Joule – Thomson refrigerator for cooling HTS cable,” *Cryogenics (Guildf).*, vol. 51, no. 7, pp. 408–414, 2011.

[50]. Y. Suzuki, S. Yoshida, and Y. Kamioka, “Subcooled liquid nitrogen refrigerator for HTS power systems,” vol. 43, pp. 597–602, 2003.